ISSN 0494-7304 0207-4478

ARTU ÜLIKOOLI
TOIMETISED
CTA ET COMMENTATIONES UNIVERSITATIS TARTUENSIS

950

METHODS OF STUDY OF ELECTRICAL PROCESSES IN CASES AND AEROSOLS

Методы исследования электрических процессов в газах и аэрозолях

IONIZATION, AEROSOLS, ELECTROMETRY

TARTU 1992

TARTU ÜLIKOOLI TOIMETISED
ACTA ET COMMENTATIONES UNIVERSITATIS TARTUENSIS
ALUSTATUD 1893. a. VIHIK 950

METHODS OF STUDY OF ELECTRICAL PROCESSES IN CASES AND AEROSOLS

Методы исследования электрических процессов в газах и аэрозолях

IONIZATION, AEROSOLS, ELECTROMETRY

TARTU 1992

Contents

M. AINTS, A. HALJASTE, K. KUDU, and V. SOBEK Breakdown dynamics in uniform HF electric field 5
M. LAAN and P. PARIS Streamer initiation by *X*-ray pulse 14
E. PROTASEVICH Air-discharge peculiarities at variable humidity and pressure 1-20 Torr (Self-organisation of supercooled HF-discharge plasma) 23
J. SALM Electrostatic dispersion of air ions with a normal mobility distribution 33
A. LUTS Chemical kinetics of tropospheric ions at higher ionization rates 39
T. PARTS The effect of some alkylamines on mobility spectra of small air ions 59
J. SALM The dependence of ion mobility on the mass (in Russian)..... 66
Ü. KIKAS The identification of particle sources by aerosol spectra measurements 73
L. LANGUS and E. TAMM The neutralization of aerosol.. 80
J. SALM and I.Ya. SERGEEV Measurement of size spectra of fine aerosol particles (in Russian) 89
V. TAMME Practical operational problems of vibrating orifice aerosol generator 97
M. KAASIK, L. VISNAPUU and R. PRIIMAN Deposition of electrically charged and uncharged aerosols in chamber 101
M. KAASIK Electrostatic dispersion of air ions generated by a pneumatic sprayer in a chamber 110
R. MATISEN and F. MILLER Air ion meters of small air ions UT-9007 115
M. ROOS and O. SAKS Fast picoammeter UT-9003 (in Russian)..... 118
O. SAKS and J. HÄMMALOV Measurement of disturbances caused by the operation of the needle-contact on electrometer input 124
J. HÄMMALOV Dependence of surface noise on the number of adsorbed gas molecules 131

Содержание

М.Х. АЙНТС, А.Я. ХАЛЬЯСТЕ, К.Ф. КУДУ, В. СОБЕК
Динамика пробоя в однородном ВЧ поле 5
М.Р. ЛААН, П.П. ПАРИС Инициирование стримера импульсом рентгеновского излучения 14
Е.Т. ПРОТАСЕВИЧ Особенности разряда в воздухе при переменной влажности и давлениях 1-20 торр (самоорганизация переохлажденной плазмы высокочастотного разряда)..... 23
Я.Й. САЛЬМ Электростатическое рассеивание аэроионов с нормальным распределением подвижностей 33
А.М. ЛУТС Кинетика тропосферных легких ионов при повышенной интенсивности ионообразования 39
Т.М. ПАРТС Влияние некоторых алкиламинов на спектры подвижности легких аэроионов 59
Я.Й. САЛЬМ Зависимость подвижности иона от его массы 66
Ю.Э. КИКАС О возможности определения источников частиц по измерениям спектра аэрозолей 73
Л.Э. ЛАНГУС, Э.И. ТАММ Нейтрализация аэрозолей 80
Я.Й. САЛЬМ, И.Я. СЕРГЕЕВ Измерения распределения высокодисперсных аэрозольных частиц по размерам 89
В.Б. ТАММЕ К проблеме эксплуатации генератора аэрозолей с вибрирующим отверстием 97
М.А.-Х. КААЗИК, Л.Ю. ВИСНАПУУ, Р.Э. ПРИЙМАН Рассеяние электрически заряженного и незаряженного аэрозоля в камере 101
М.А.-Х. КААЗИК Электростатическое рассеяние аэроионов при постоянной ионизации воздуха 110
Р.Л. МАТИЗЕН, Ф.Г. МИЛЛЕР Аэроионометр легких аэроионов UT-9007 115
М.Э. РООС, О.В. САКС Быстродействующий измеритель малого тока УТ-9003 118
О.В. САКС, Ю.А. ХЯММАЛОВ Исследование помех, вызванных действием игольчатого контакта на входе электрометра 124
Ю.А. ХЯММАЛОВ Зависимость поверхностного шума от числа адсорбируемых на поверхности молекул газа 131

BREAKDOWN DYNAMICS IN UNIFORM HF ELECTRIC FIELD

M. Aints, A. Haljaste, K. Kudu, V. Sobek

Abstract. In the present paper the origin and development of the breakdown in high frequency (HF) electric field in air at atmospheric pressure has been investigated experimentally. The breakdown voltage dependence on the distance between parallel plate electrodes (0.1 - 9 mm) was measured at frequencies of 3.333 MHz, 10 MHz and 20 MHz. The formation time of the HF breakdown initiated by radiation of a N_2 laser was investigated as a function of an overvoltage in the 4 mm discharge gap. An image converter-intensifier camera (ICI camera) as well a high-speed photomultiplier (PM) were used in the investigation of the dynamics of light phenomena accompanying the breakdown. The model of HF breakdown has been developed, where a significant role is given to attachment and detachment of electrons.

Introduction. The lowering of electric strength of the air insulation in HF electric fields in comparison with the strength in DC electric fields is a well known empirical fact [1]. At small distances between the electrodes the HF breakdown voltage increases monotonously with the gap distance, and its value equals with that at DC voltage. From the certain gap distance the breakdown voltage in HF fields becomes lower than in DC fields. This gap length is known as a critical length at the given frequency, and the frequency as a critical one for given gap length. The lowering of breakdown voltage in discharge gaps longer than the critical, or at the frequencies higher than the critical, is explained by the oscillation and accumulation of ions in the discharge gap during the dark current stage. As the result of a further increase in frequency or in gap length the so-called second critical gap length is reached. Here a new steep decrease of the HF breakdown voltage compared to the DC breakdown voltage starts. It is caused by the oscillation of both ions and electrons in the interelectrode space. In the region between the first and second critical frequencies the relative reduction of the HF breakdown voltage is less than 10-15 %. At frequencies higher than the second critical, relative reduction reaches some tens per cent.

The spatio-temporal development of the breakdown at HF voltages has been examined in some experiments in strongly nonuniform fields only. Breakdown phenomena in uniform fields at frequencies higher than critical have not been dealt with.

The present work was carried out to investigate the HF breakdown in the air at atmospheric pressure in the case of uniform HF field. Systematical measurements of the breakdown voltage were expanded towards the longer distances between electrodes so that at used frequencies the both critical gap lengths remained into region under study. The methods of high-speed photography and oscillography were used to study the spatio-temporal development of the breakdown channel at frequencies below and upon the second critical frequency.

Experimental setup. The scheme of experimental setup is presented in Fig. 1. The discharge gap consists of two parallel Rogowsky profile brass plate electrodes 93 mm in

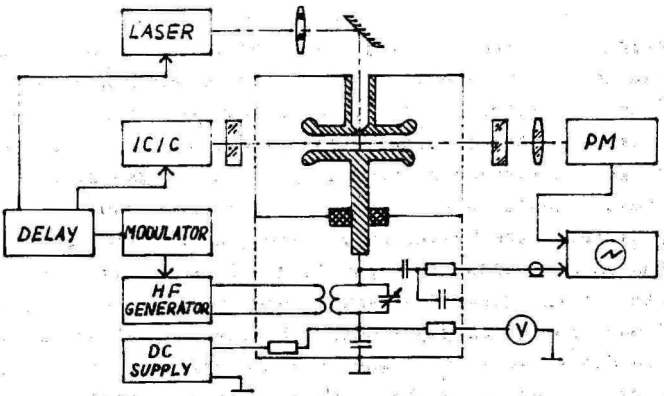

Fig. 1. Experimental setup.

diameter. The distance between electrodes was controlled with accuracy of 0.01 mm. The HF voltage was measured by means of capacitive voltage divider and oscilloscope with accuracy of ± 5 %. The DC voltage between the electrodes was measured with accuracy of ± 2 %. The spatio-temporal distribution of radiation of the breakdown was registered by ICI camera in streak mode. ICI camera had a multialkaline photocathode, sensitive in spectral range of 250-860 nm. The quartz ob-

jective, f = 200 mm, aperture ratio 1:4, was used. The radiation of the discharge was registered in the region of 360 - 400 nm cut out with help of colour filters. This region includes the spectral bands 0-1, 0-2, 0-3, 1-2, 1-3, 1-4 of the second positive system of N_2. The radiation was recorded also by means of a high-speed PM. The laser initiation of the breakdown was used to obtain the synchronization of the recording apparatus with the breakdown. The hole, 0.5 mm in diameter was drilled in the center of the grounded electrode. The radiation of N_2 laser was driven through this hole. The laser pulse had a duration less than 10 ns, the wavelength of 337 nm and energy 10^{-6} J per pulse. The laser radiation produced initial electrons in the discharge gap. The laser initiation was applied after the switching-on fluctuations of HF voltage had been vanished. The laser pulse was not synchronized with the phase of HF voltage. The development of breakdown was investigated in 4 mm gap at frequencies of 10 and 20 MHz. The first of them lies lower, and the second one higher of the second critical frequency for the gap length of 4 mm (Fig. 2).

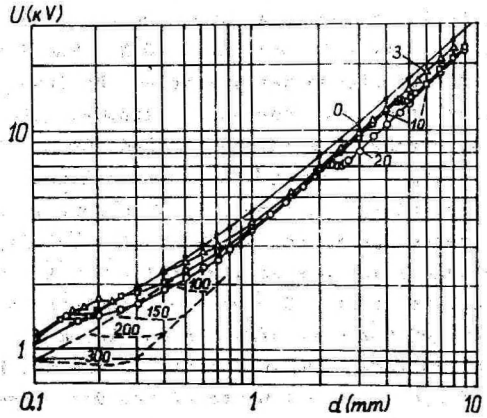

Fig. 2. HF breakdown voltages *vs.* distance between plate electrodes in air at normal pressure. Parameter - frequency in MHz. Dotted curves - Pim's results [2]. U - peak value of HF voltage.

Results and discussion. In Fig. 2 breakdown voltages are plotted against the distance between parallel-plate electrodes. The curves with measured points are obtained in present study. The dotted curves present Pim's results [2]. The frequency serves as a parameter. When in Pim's results one can see the existence of the second critical gap length only, the present results for 10 MHz and 20 MHz show the existence of both critical lengths. It is seen that in gaps, which length is longer than the second critical one, the breakdown voltage gradient limit decreases slowly with increasing the gap length. The minimum gradient found out in the experiment is $2.54 \cdot 10^6$ V/m.

For the investigation of rapid breakdown processes with high time resolution the information about the statistical distribution in formation times of the breakdown is needed. In Fig. 3 the breakdown probability (curves 1 and 2) and formation time (curves 3 and 4) as a function of overvoltage in the 4 mm gap at carrier frequencies of 20 MHz and 10 MHz are presented. The repetition rate of HF pulses was 5 Hz in these experiments. Duration of HF pulses exceeded most probable formation time at least 10 times. Curves in Fig. 3 show, that formation time becomes equal to the duration of half-cycle of carrier frequency, when overvoltage reaches the value of 35-50 %. At the same time the probability of breakdown becomes a little higher than 50 %. The last occurence shows that the breakdown was initiated by laser pulse only when the irradiated electrode was a cathode. The onset value of breakdown voltage was not influenced by the laser pulse. When the HF voltage is lower than onset voltage of breakdown at DC, the typical spatio-temporal development of breakdown at 20 MHz goes on just as streak-photo in Fig. 4 shows. Breakdown channel is placed vertically in the photo, scan goes from left to right. One can see, that in initial stages the intensity of the discharge is modulated by double frequency of HF voltage. The luminosity of the discharge arises at every half-cycle in all parts of the discharge channel at the same moment. Intensity of radiation increases from half-cycle to half-cycle.

Duration of this initial stage is longer if overvoltage is lower. For example, at overvoltage of 5 % it lasts about ten half-cycles. Varying the registering sensitivity, it becomes clear from the PM signal, that the velocity of increase of

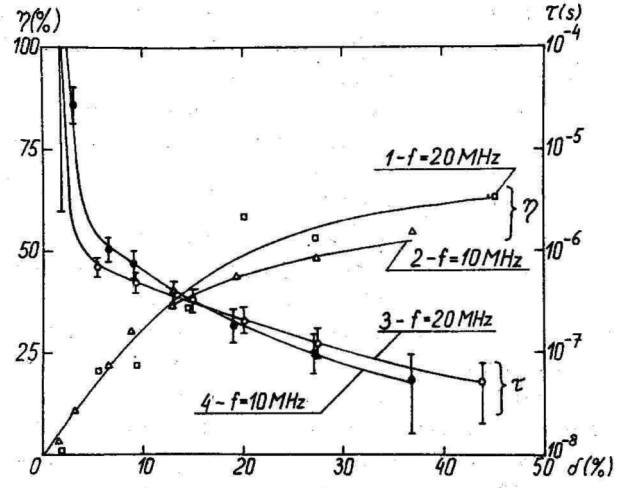

Fig. 3. Probability (η) and formation time (τ) of HF breakdown as a function of overvoltage δ.

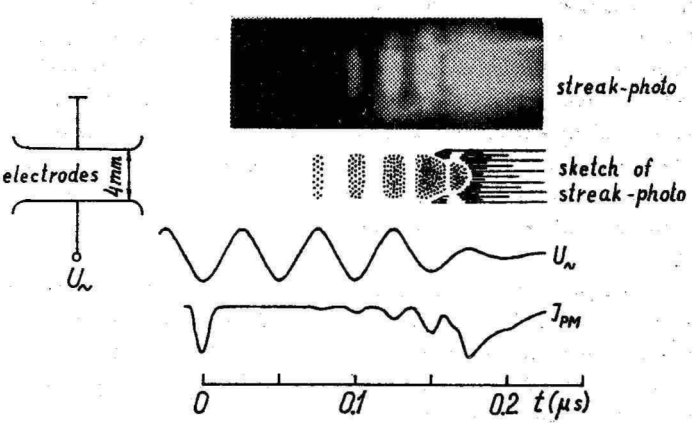

Fig. 4. Streak-photo of HF breakdown at 20 MHz. δ = 28 %, $U_{\sim}$ - HF voltage, I_{pm} - PM signal, the first pulse of PM signal at t = 0 - laser pulse.

light intensity increases towards the final part of this stage. Only this final part is recorded by ICI camera. No light wave propagation in the discharge gap is seen in the initial stage. The oscillation amplitude of electrons in the discharge gap under our conditions is about 1 mm. So we expected to find that near-electrode parts of the discharge channel do not radiate. Really these nonradiating parts are very narrow on streak photos.

The next stage of breakdown formation begins with appearance of intensive waves of luminosity near the both electrodes, and with arising of electrode spots. Near the anode the wave starts from the boundary of dark space and luminous coloumn, and propagates into both directions, towards the anode and cathode. As it seems to be according to streak photos, the another wave starts from the surface of cathode towards the anode at the same time. The initial velocity of the waves is $(0.2 - 1.2) \cdot 10^5$ m/s, and it increases with the wave propagation. With the origin of waves, the HF voltage on the gap begins to decrease. When the waves meet, the HF voltage ($U_\sim$ in Fig. 4) collapses and the modulation of the discharge radiation disappears. The final stage of the breakdown - HF arc - arises.

The propagation of intensive waves lasts, as a rule, two half-cycles. Between half-cycles the light intensity has a minimum. After this minimum at first the part of channel, not passed by waves, radiates most brightly. The region passed by waves radiates significantly fainter. After a certain delay the development of intensive light wave goes on from the place, where it had stopped in the previous half-cycle. At the same moment a new wave starts there in the opposite direction.

The changes in light intensity and in HF voltage peak value show, that propagation of intensive waves is accompanied by fast increase of conductivity of the channel and by redistribution of electric field strength along the discharge channel. This more and more accelerating wave process causes the voltage collapse.

When the value of HF voltage is higher than the onset potential of DC breakdown, the luminosity arises simultaneously in the full length of the channel, as in the case of lower voltages, but the distribution of luminosity along the channel is inhomogeneous. The intensive waves arise at the

same first half-cycle. Arise and propagation of waves is not symmetrical near the electrodes. The conditions for wave arise seem to be better near the electrode with hole.

According to above description, the development mechanism of HF breakdown at frequencies higher than the second critical one, seems to be as follows. A part of initial electrons do not leave the discharge gap and begin to oscillate in HF field, or attach to O_2 molecules constituting negative ions. As the amplitude value of HF field is high enough, the electron impact ionization takes place as well as the detachment of electrons. Concentrations of positive and negative ions and electrons begin to increase. The increase of vibrational temperature, gas temperature and the concentration of metastable molecules starts as well. As a result the growth of electron detachment coefficient follows. When the value of the detachment coefficient exceeds certain critical value, the destruction of negative ions becomes determining in the growth of electron concentration. Relatively homogenous distribution of negative and positive ions along the gap axis guarantees the absence of disturbances of electric field and hence a uniform distribution of radiation intensity. The first light phenomena in streak photos correspond to this stage of the discharge process. The plasma channel is formed as a result of ionization and detachment processes. The growth of electron concentration and gas amplification at the stage of negative ion destruction may be the reason of instabilities and origin of ionization waves, recorded in streak photos as luminosity waves. Ionization growth accompanying the waves, leads to growth of conductivity of the channel and to voltage collapse.

In the case of 4 mm gap length the frequency of 10 MHz is lower than the second critical. So accumulation of positive and negative ions and not electrons is possible in the discharge gap during the initial dark stage. During half-cycles after the laser flash, the initial electrons are generated by destruction of negative ions. The development of the breakdown at lower overvoltages is similar to that at the frequency of 20 MHz at higher overvoltages where the HF voltage amplitude exceeded onset potential of DC breakdown. Ionization waves start from the electrodes and from other points of the discharge channel as well. The waves, arising in the gap, propagate in both directions (Fig. 5). As a rule, the inten-

sive waves and high conductivity discharge channel arise at the same half-cycle, when ICI camera and PM record the first light phenomena in the gap. Streak photos show that development of HF breakdown at lower frequencies acquires the properties similar to that of the breakdown at pulse voltage.

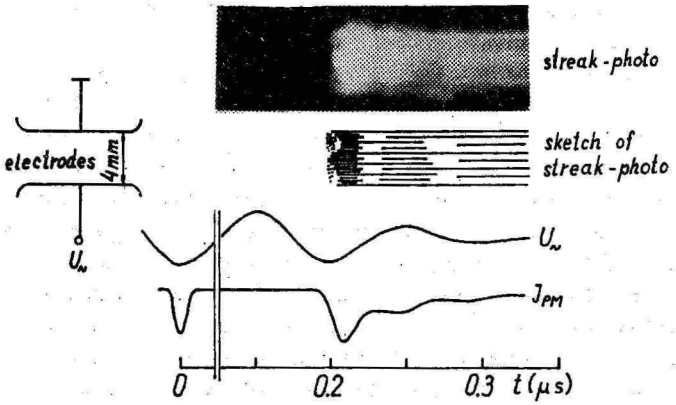

Fig. 5. Streak-photo of HF breakdown at 10 MHz. δ = 19 %.

Conclusions. The results obtained enable us to compare the dynamics of breakdown at pulse and HF voltages. In the development of the HF breakdown one can distinguish following phases: 1) avalanche stage controlled by electron attachment; 2) avalanche stage formed by electron detachment; 3) plasma stage sustained by streamer-like ionization waves; 4) HF arc. The most essential differences between pulse and HF breakdowns arise from the accumulation of positive and negative ions during the first phase of the HF breakdown and from the destruction of negative ions during the second phase.

References

1. Electrical breakdown of gases / Ed. by J.M. Meek and J.D. Craggs, etc.: John Wiley & Sons, 1978. - 878 p.

2. Pim, J.A. The electrical breakdown strength of air at ultra-high frequencies// Proc. IEE.- 1949. - V. 96.- No. 40.- P. 117-129.

ДИНАМИКА ПРОБОЯ В ОДНОРОДНОМ ВЧ ПОЛЕ

М. Айнтс, А. Хальясте, К. Куду, В. Собек

Р е з ю м е

Экспериментально исследовано возникновение и развитие пробоя в однородном высокочастотном электрическом поле в воздухе при атмосферном давлении. Измерена зависимость пробивного напряжения от расстояния в пределах 0,1 - 9 мм между плоскими электродами на частотах 3,33 МГц, 10 МГц и 20 МГц. Измерены времена формирования пробоя, инициированного импульсом N_2 - лазера в 4-х миллиметровом разрядном промежутке. Представлены фоторазвертки разряда. Выдвинута модель развития ВЧ пробоя, в которой существенная роль присвоена процессу прилипания и отлипания электронов.

STREAMER INITIATION BY X-RAY PULSE

M. Laan, P. Paris

For the experimental investigation of a streamer formation the experimental equipment must be well synchronized with the moment of creation of triggering electrons. A good synchronization (which has a nanosecond jitter) in homogeneous field is achieved by liberating the first electrons from the cathode with a short UV pulse. It is impossible to use this method in a positive point-to-plane discharge gap, as the first electrons must be created in a small volume near the positive point. In [1] a streamer was initiated by *XeCl* laser (λ= 308 nm) pulse. Although a good synchronization was achieved, additional difficulties arose in further interpretation since the laser radiation caused a remarkable vaporization of point electrode material.

The aim of this paper is to investigate the streamer formation using the *X*-ray radiation as a source of first electrons.

Experimental set-up. All the experiments were carried out in laboratory air at atmospheric pressure. Positive D.C. corona in a point-to plane discharge gap was investigated. Distance between the electrodes was 4 cm. The point electrode was a hemispherically capped *Pt* wire 1 mm in diameter. Plane electrode was a *Al* disc, 15 cm in diameter, with 4 mm hole in its center, that makes it possible to direct *X*-ray radiation along the discharge gap axis.

The *X*-ray source had a plasma cathode described in [2]. The anode was placed at 4 cm from the cathode. The working pressure was 0.1 Pa. The *X*-ray tube had a lavsan window. 30 kV negative pulse, half-width of which was 110 ns, was supplied to the cathode. *X*-ray pulse had a half-width of 70 ns (Fig. 2). The position of *X*-ray pulse related to the voltage pulse was determined with accuracy of some nanoseconds. 10 pps repetition rate of *X*-ray pulses was used. In absorption measurements for *X*-ray quantum energy determination two different detector systems were used: scintillator + photomultiplier and ionization chamber + electrometer. The mean quantum energy was within limits of 5-6 keV. An *X*-ray pulse originated nearly 10^7 charged particles per cm^3 as

determined by ionization chamber.

Light and current pulses were recorded by a 450 MHz bandwidth oscilloscope. For registration of current pulses a 50 Ω coaxial design of the point electrode connection was used [3]. Light from corona was detected by image intensifier and photomultiplier. Time intervals between the *X*-ray pulse and corresponding corona pulse were registered by the digital timer with a resolution of 10 ns.

Results. Both spontaneous (noninitiated) and initiated positive corona pulses were under observation. In case of positive corona the first observable discharge pulse is a burst pulse which spreads along the electrode surface. With increase in voltage a so-called preonset streamer develops into the discharge gap up to the distance of 10 mm from the point. The voltage region where these streamers exist is about 200 V. The steady state corona will be established at higher voltages [4]. In our case when the *X*-ray radiation is missing, burst pulses are registered ≈ 200 V below the onset potential U_0 of preonset streamers. With increase in voltage their amplitude and duration, as well as their repetition rate also rise. Some tens volts below U_0 the burst pulse current has the duration up to 1 μs and its amplitude achieves 0.1 mA. Corresponding light pulse is considerably shorter (≈ 70 ns) - Fig. 1A. Area covered by the luminous layer on the point electrode is nearly 0.2 mm^2. At the potential U_0, some larger bursts transit to streamer - Fig. 1B. As no attention was paid to the air humidity and the air pressure stabilization, there are variations of ±20 V of U_0 in different days. The burst-to-streamer transition is observable only in the narrow region of voltages: at the onset U_0 the duration of the burst pulse stage of τ = 15 - 20 ns and 50 V above U_0, the burst stage is already not observable.

When the *X*-ray pulse generator is switched on, the initiation of bursts occurs ≈ 400 V below U_0. The current amplitude of these burst pulses about of 100 V below U_0 is eight-fold, compared with the current of spontaneous ones at the same voltage. Area covered by the light of initiated burst is nearly 1 mm^2. In case of initiation the burst-to-streamer transition occurs at 90 V below U_0, corresponding τ = 30 ns, at 10 V higher potential τ = 20 ns and 20 V higher - τ = 10 ns. Near U_0 one *X*-ray pulse initiates more than one

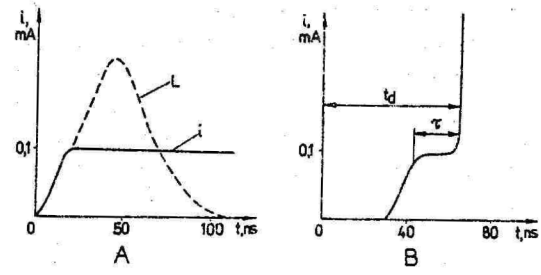

Fig.1. Sketches of burst pulse (A) and burst-to-steamer transition (B). Solid line presents the time dependence of burst pulse current, dashed line - the same dependence of light B - t_d - time interval between the beginning of the *X*-ray pulse and the streamer formation, τ - duration of the burst stage. Transition occurs at U_0 = 7.62 kV.

streamer. The first one is quite well related to the *X*-ray pulse, the next one follows randomly with the delay time of 1 ms and more. At voltages above U_0 exist both initiated and spontaneous streamers. In Fig. 2 delay time distribution of the first initiated streamer for different voltages and mean $\overline{t_d}$ dependence on voltage are presented; in Fig. 3 - t_d and $\overline{t_d}$ dependencies on *X*-ray intensity are presented.

Discussion. It is accepted that in a homogeneous field the formation of a streamer is possible when a number of charged carriers achieve the value of 10^8 in an avalanche [5]. The existence of such a mystic number demands further explanation especially in the case of inhomogeneous point-to-plane geometry where near the onset potential U_0 the magnitude of a single avalanche is several orders less than 10^8 [4].

For that reason another formulation seems to be more preferable: streamer formation occurs at the moment when the ionized gas achieves a plasma density i.e. the Debye length r_D becomes less than the characteristic dimension of ionized gas region d [6,7]. In our case it means that burst-to--streamer transition is possible when the ionized gas density in a thin layer near the point surface achieves the

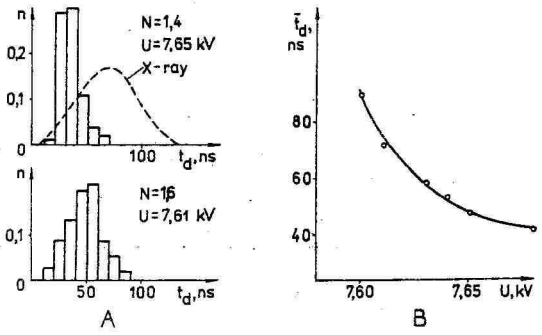

Fig. 2. Delay time t_d dependence on voltage. A : n - relative number of first streamers which have delay time t_d; N - mean number of streamers created by a single X-ray pulse. Onset potential U_0 = 7.62 kV. Dashed line - shape of the X-ray pulse. B : Mean delay time $\bar{t}_d$ dependence on voltage.

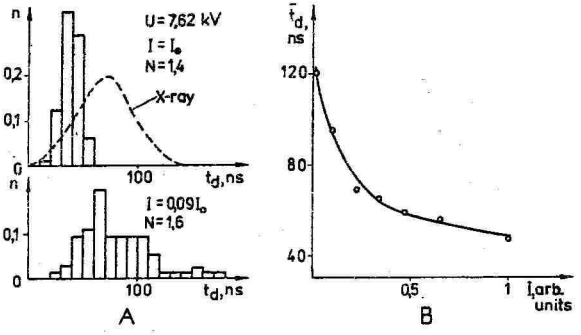

Fig. 3. A : Distribution of delay time t_d for different X-ray intensities. B : Mean delay time $\bar{t}_d$ dependence on X-ray intensity; intensity I_0 corresponds to the charged particles concentration 10^7 cm^{-3} per X-ray pulse. In all cases the jitter of τ is much smaller than that of $(t_d - \tau)$.

plasma density.

To prove the validity of this assumption the electron density in burst pulse must be estimated. Using experimental data for burst current i = 0.1 mA and for area covered by burst $S \approx 0.2$ mm^2, and supposing that drift velocity of electrons $v \leq 2 \cdot 10^7$ cm/s *), from relation $i/S = nev$ the electron concentration $n = 10^{10}$ cm^{-3} is determined. The same order of magnitude was valued for n in avalanche head when streamer formation takes place in homogeneous field [6]. Corresponding value of Debye length r_D for electron temperature $T_e < 5$ eV is less than 10^{-2} cm. The plasma layer thickness can be estimated from the results of [8] where the light distribution for steady state corona was determined. The main part of light was emitted from the layer which thickness < 0.2 mm. The thickness of the region where the main part of charged particles is situated must be close to this value. So the assumption that burst pulse creates a plasma layer near the electrode surface is quite realistic, and all effects characteristic to plasma must occur: electrons are locked to the ions (due to ambipolar diffusion), the field strength in plasma body is low and enhancement of field strength near the cathode side border of plasma takes place (due to separation of positive and negative space charge to the distance of Debye length). A nice presentation of all these effects is given in [9].

The sketches of the burst pulse formation for $U \cong U_0$ are presented in Fig. 4. To trigger the ionization the first electron must appear near the border of ionizing zone (where $\alpha - \eta = 0$; α, η - first Townsend coefficient and attachment coefficient, respectively). An avalanche starting from this electron radiates photons able to ionize gas. If such a photon is absorbed near the border of ionizing zone, it creates a new equivalent avalanche (Fig. 4A), i.e. the role of feedback in this sequence of avalanches is played by photoionization. The site in space where a photon is absorbed is accidental, so the sequence of avalanches will

---

*) This value of v corresponds to reduced field strength E/p = 60 V/cm·Torr. In plasma such a high field can exist only for a short time.

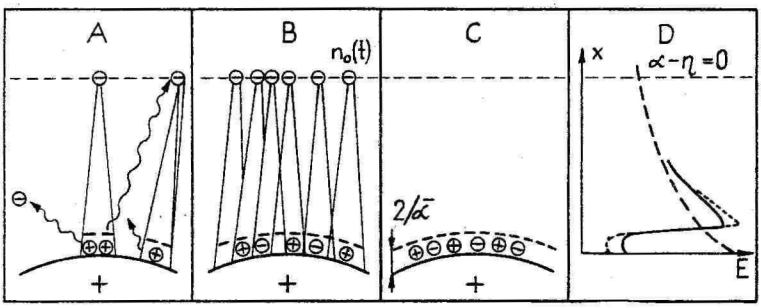

Fig. 4. Different stages of burst pulse development.
A - development of first avalanches; B - stage of overlapping avalanches, $n_0(t)$ - density of electrons created by an *X*-ray pulse; C - plasma layer; D - sketch of distribution. $\bar{\alpha}$ - mean value of α ; dashed line initial field; solid line - burst pulse stage; dotted line - steady state corona.

spread over the electrode surface. The main part of charges are created in a layer of $2/\bar{\alpha}$ thickness. ($\bar{\alpha}$ - mean value of α in ionizing zone). As a drift velocity of ions is low, the accumulation of positive space charge occurs in this layer. At atmospheric pressure and for the used point radius, an extended layer of space charge causes the diminishing of the field [10]. Whereas the concentration of triggering electrons n_0 near the border of ionizing zone increases then, starting from a moment governed by chance avalanches will overlap (Fig. 4B). It causes further diminishing of the field. By that reason the loss of electrons in the layer due to drift to the anode decreases. This stage of discharge is already observable in experiments and it is named as a burst pulse.

In the case of *X*-ray preionization triggering, electrons are created homogeneously near the point, and several parallel avalanches will develop towards anode and their concentration n_0 rises linearly in time. If the *X*-ray intensity is high, the stage *a* is absent and t_d varies with in narrow limits (Fig. 3). 10-fold decrease of intensity leads to the increase of jitter t_d, the density of n_0 is too low for owerlapping of avalanches and the conditions of ionization are similar to a single electron initiation. The last stage

(burst pulse stage) in plasma formation is presented in Fig. 4C. When a plasma density of ionized gas is achieved, the field distribution completely differs from the Laplacian field (Fig. 4D). The light emitted by burst pulse belongs to the 2^+system of nitrogen. The excitation of 2^+system by electron impact is possible only in the high field. Since the plasma concentration is $\approx 10^{10}$ cm^{-3}, the high field can exist only few tens of nanoseconds, later the excitation is not effective. This estimation corresponds well to the experiment (Fig. 1A). Plasma layer can exist near the anode for a long time. There are two loss mechanisms of electrons in plasma body: attachment and leakage to the anode. So the formation of negative ions is a result (not reason!) of existence of the low field strength near the point electrode. Burst pulse exists up to the moment when these losses are compensated by ionization in high field region on the cathode side of plasma layer. This explanation differs from Loeb's one [4] : he supposed that long duration of burst pulse current is connected with the ion component of current, and the duration of light pulse corresponds to the duration of time when electrons exist near the point. But as the mobility of ions is two orders less than that of electrons, there must be a peak at the beginning of current pulse which reflects electron movement. It was never observed in experiments.

At higher voltages ($U \geq (U_0 + 200)$V) there is an equilibrium between the loss and generation of electrons and steady state corona establishes.

Only the existence of plasma is not sufficient for streamer formation. A streamer can start from a site of plasma layer where the local ionization instability develops. There are the next experimental confirmation to this assumption:

(I) If $U > U_0$, both burst-pulses and streamer exist.

(II) Streamers can be suppressed by α-particles. An α-particle creates a big number of triggering electrons so the plasma layer is more homogeneous than it is in the case of single electron initiation, and the probability that instability may develope is lower.

(III) The initiation of streamer is possible at the voltage region of steady state corona if ionization instability is created artificially. It was done this way in our old unpublished paper [11] where to D.C. voltage U = 8 - 15 kV a short (100 ns) pulse voltage ($U > 500$ V) was added and a

streamer development was fixed.

(IV) In this paper burst-to-streamer transition occurs only for $\tau < 30$ ns (Fig. 2B), i.e. only when the field strength in plasma is high and so the probability that ionization instability may develope is high too.

References

1. Laan, M., Paris, P. Perelygin, V. Laser-assisted s+reamer development // Abstracts of invited talks and contr. papers-ESCAMPIG 90 - Orleans - 1990. - P. 371-372.

2. Levatter, J.S., Sandstrom, R.L., Morris, J.K. The corona-plasma cathode: a new long-life *e*-beams cathode for *X*-ray preionization // 4 JEEE Pulsed power Conf.(Albuquerque, N.M., 1983).- Dig. techn. Pap.- N.Y. - 1983. - P. 755-757.

3. Korge, H., Laan, M., Paris, P. On formation of negative corona pulse // J. Phys. D: Appl. Phys. - in print.

4. Loeb, L.B. Electrical coronas.- Berkeley; Los Angeles: Univ. of Calif. Press - 1965. - 694 p.

5. Raether, H. Electron avalanches and breakdown in gases - London. - 1964.

6. Omarov, O.A., Ruchadze, A.A., Schneerson, G.A. On plasma mechanism of high pressure gas breakdown in high electric field // Sov. J. Techn. Phys. - 1979. - V. 49.- P. 1997-2000 (in Russian).

7. Omarov, O.A., Ruchadze, A.A. Evidence of plasma stage of avalanche development in case of spark breakdown // Sov. J. Techn. Phys.- 1980. - V. 50. - P. 536-539 (in Russian).

8. Charrier, J., Boulloud, A. Positive Glow Corona Distribution of Light Emission in Point-to-Plane Gap // 8th. Int. Conf. Gas Discharges - Oxford, 1985.- P. 195-198.

9. Morrow, R., Lowke, J.J. Space-charge effects and drift dominated electron and plasma motion // J. Phys. D: Appl. Phys.- 1981.- V. 14.- P. 2027-2034.

10. Sigmond, R.S., Goldman, M. Corona discharge physics and application // Electrical breakdown and discharge in gases.- N.Y. and London: NATO, 1983. - P. 1-64.

11. Paris, P. Investigation of streamer characteristics on combined voltages (D.C. + pulse voltage) // Tartu Diploma Thesis.- 1976.- (in Estonian).

ИНИЦИИРОВАНИЕ СТРИМЕРА ИМПУЛЬСОМ РЕНТГЕНОВСКОГО ИЗЛУЧЕНИЯ

М. Лаан, П. Парис

Резюме

Целью работы являлось исследование формирования стримера в сильнонеоднородном разрядном промежутке острие - плоскость. Разряд инициировали при помощи импульсов рентгеновского излучения (средняя энергия кванта - 5 кэВ, длительность импульса - 140 нс). Рентгеновский импульс создавал в воздухе 10^7 $см^{-3}$ заряженных частиц. Измерено время формирования разряда в зависимости от интенсивности излучения при разных напряжениях. Найдено, что для формирования стримера необходимо существование плазменного слоя вблизи острия.

AIR-DISCHARGE PECULIARITIES AT VARIABLE HUMIDITY AND PRESSURE 1-20 TORR (SELF-ORGANISATION OF SUPERCOOLED HF-DISCHARGE PLASMA)

E.T. Protasevich

Introduction. During the recent years some research on the gas discharge in humid air ionized by laser or HF power has been carried out. It has been found that an injection of water vapour in the discharge first of all leads to cooling the plasma generated. At the relative humidity of air of 96-97 % this plasma is in non-equilibrium state and has the temperature close to the room temperature, at the same time the electron temperature is in a range of 1500-2000 K. That kind of plasma possesses the anomalous properties: drastically increases the decay time and in the distribution of radiating atoms of hydrogen on velocities the particles of high energy are absent.

The aim of this paper is twofold: first, to consider shortly and analyze the properties of the HF-discharge plasma in dependence on the air humidity, and secondly, to explain the formation of clusters in cool non-equilibrium plasma observed in the experiments.

Experiments. A scheme of the experiment is shown in Fig.1. The discharge was generated in the T-form quartz tube 1 with

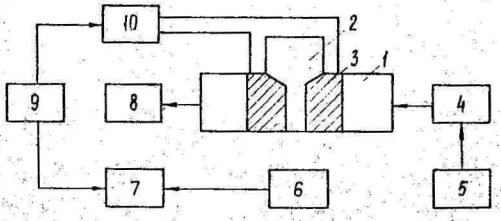

Fig.1. Scheme of an arrangement for generation of LPC : 1 - area of the discharge, 2 - vertical section, 3 - electrodes, 4 - buffer area, 5 - vapour source, 6 - photo-electron amplifier, 7 - oscillograph, 8 - pump, 9 - device for initiating, 10 - HF-generator.

inner diameter of 7,2 cm and length of 37,5 cm. The vertical section was of 15 cm length. (In some experiments no vertical section was used). The HF-generator for ionizing had following parameters: f = 37 MHz, P = 60 kW, τ_u = 10-60 ms, F = = 1 ÷ 5 Hz. The pressure in the tube was varied from 0.1 Torr up to atmospheric but did not exceed, as a rule, few tens of Torr to obtain the effective ionization of the air. The external circular electrodes 3 had the width of 5.5 cm and were 2 cm apart. The ionization of medium was realized in the capacitance of HF-discharge scheme.

The electron concentration was measured by Stark broadening of spectral line of H_β in combination with an interferometric method ($\lambda \approx 8$ mm). A duration of the post-discharge luminescence was estimated by means of photo-electron amplifier and fast movie-camera. A representative luminescence of the discharge at dry air is shown in Fig. 2.

To inject the water dosed in the discharge a gas mixture (air + H_2O) was preliminarily prepared in the retort 5. To create stable conditions the water vapour came in to the discharge area through a special buffer chamber 4. This allowed to control the water content and to eliminate a sudden change of a pressure difference between discharge chamber 1 and vapour source 5. An adjustment of flow and relative content of water was done by means of a special valve.

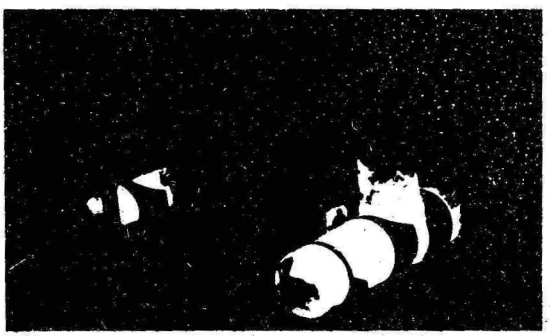

Fig. 2. Luminescence of the HF-discharge at dry air under the pressure in the range of 0.1 - 10.0 Torr.

Results. Since temperature determines the state of the substance it is not reasonable to determine the properties of the plasma considering the temperature of plasma ingredients depending on air humidity. Preliminary measurements of thermodynamic parameters of the plasma show that the water vapour cools both light and heavy particles, at the same time the plasma itself remains in the non-equilibrium (non-isothermal) state.

Dependences of translational temperature T [1] and electron temperature T_E [2] on the air humidity are shown in Fig. 3.

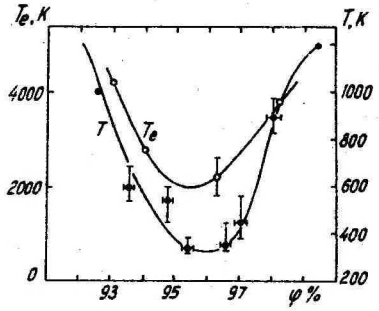

Fig. 3. Changes of translational temperature T and electron temperature T_E dependences on the relative humidity of air.

From this one can clearly see that the optimal contents of water vapour in the air, φ_{opt}, is when $T \dashrightarrow T_{min}$, $(T_E)_{min}$. In other words, the cool non-equilibrium plasma is generated at a relative humidity of air in the range of 95 - 98 %. Its density depends on temperature and in the vicinity of minimal temperature the plasma concentration is approximately two times higher as at the humidity less than optimal. It should be noted that the electron component of plasma is always retained [3].

As temperature of separate components of plasma decreases, the time of plasma decay τ increases. From Fig. 4 one can see that τ has the maximum when $\varphi = \varphi_{opt}$ and $T \approx T_{min}$. If the cool non-equilibrium plasma was generated dynamically, i.e. injecting the water vapour in a hot primary plasma (T = 3000 ÷ 4000 K, $T_E \approx (10 - 12) \cdot 10^3$ K), then a bright-orange plasmoid was formed. It had a quasispherical shape with the

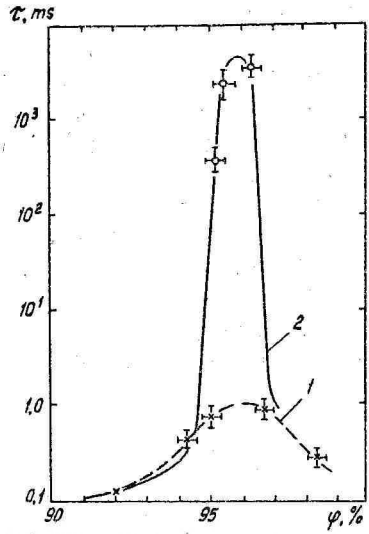

Fig. 4. Average time of decay of the cool non-equilibrium plasma *vs.* the relative humidity of air:
1 - preliminary measurements, $P \approx 15$ kW;
2 - correct measurements, $P \approx 40$ kW.

characteristic size of 2.0 - 2.5 cm and clean-cut contours and was localized in places of contact of the primary plasma with the flow of water vapour. The plasmoid is shown in Fig. 5. Its lifetime was diagnosed by luminescence photographed with a fast movie-camera and compared with the repetition period of the HF-power pulses. This time t=(0.4÷0.5) s appeared to be anomalously long. At the ionization generator

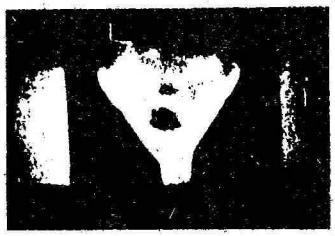

Fig.5. Photo of a cluster of the cool non-equilibrium plasma generated at pressures of 1 - 10 Torr in the HF-discharge (f = 37 MHz, P = 40 kW, τ = (10 ÷ 60)ms, F = (1 ÷ 5) Hz).

switched off the lifetime decreases twice. Note that at the ionization of dry air τ had the magnitude of (10 ÷ 20) ms (see also Fig. 4).

Subsequent investigations show that the plasmoid was easily carried away by the flow of air injected in the tube together with the disperse phase. The velocity of this drift to the centre of the discharge tube amounted to (0.5 ÷ 1.0) m/s. The plasmoid was easily reproduced in laboratory conditions and its appearance correlated with the most high degree of plasma cooling (see Fig. 3) when $T \approx (300 \div 350)$ K and $T_g \leq 2 \cdot 10^3$ K.

Measuring equidensitometrically the luminescence intensity of the humid air in HF-discharge it was found that the plasmoid contained a cool core surrounded by the hot layer. The equidensities of this HF-discharge at the presence of the long-living plasma clusters (plasmoid) are shown in Fig. 6.

Fig. 6. Black-white equidensities of the HF-discharge at dry air with LPC.

Following the structure of long-living plasma clusters (LPC) it is desirable to look at Fig. 6 and Fig. 5 together. These results are hardly explicable within the framework of traditional ideas. Note only that in nature a maximum rate of the ball-lightning occurence falls in the same range of relative humidity of air, that amounted 95-98 % [4]. This circumstance is not likely a chance phenomenon.

Discussion. As the translational temperature T caracterizes the temperature of hydrogen atoms we will qualitatively consider in the first place an occurence of the temperature mi-

nimum the dependence $T = f(\varphi)$ (see Fig. 3). A decrease of T is conditioned by the reaction going in the discharge:

$$H_2O \dashrightarrow H_2 + 1/2\ O_2 - 2.6\ \text{eV}\ , \qquad (1)$$

which has the rate $v \approx N^{3/2}$, where N is the concentration of H_2O molecules. If the rate of injection of the gas mixture (H_2O+ air) at the reaction area did not exceed several m/s then in the discharge an accumulation of water derivatives (H_2O^+, H_3O^+, e, H, H_2, H^-, O, O_2, OH, OH^- and other) takes place. In the long run this stimulates the reverse reaction :

$$OH + H_2 \dashrightarrow H_2O + H\ , \qquad (2)$$

which has the positive energy balance of 14.4 kcal (the right side of the curve $T = f(\varphi)$ is shown in Fig. 3).

The reaction (2) is of the interest because it describes a process of burning and as a result of it an active centre such as H atom is retained. By visual observations and by means of a movie-camera it was found that a spontaneous combustion of the water derivatives cause the LPC formation. Since in the combustion reaction its branches have such an energy threshold that the hydrogen atoms react then diminishing of them as a result of the reaction account for the absence of "hot" particles in the distribution on velocities $F(v)$ (see Fig. 7). A disappearance of these atoms in the distribution $F(v)$ has sufficiently correlated with a threshold of hydrogen combustion in oxygen.

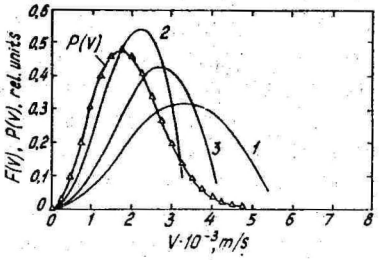

Fig. 7. Distributions of hydrogen atoms on velocity that were measured by Doppler broadening of H_β line:
1 - φ = 85 %, 2 - φ = 96 %, 3 - φ = 100 %;
$P(v)$ - Maxwell low of distribution.

The active substance of LPC resembles a fire-damp dissociated on ions with the specific power of (0.1-10) J/cm^3 [5]. Its burning pulsated that account for an occurrence of time periodical fluctuations observed on an oscillograph screen during the registration of the H_β line (see Fig. 8). In other words, processes working as a negative feedback are present in the cool non-equilibrium plasma. The effective coefficient of plasma recombination depends on temperature as $\alpha^* \approx T^{-k}$ ($k \approx 3/2 \div 5/2$).

Fig. 8. Typical line of H_β on an oscillograph screen [1]. The sweep time - 20 ms.

The period of the fluctuations, T (δI), was constant and did not depend on air humidity φ and plasma temperature. Almost always its value was ≈ 0.8 ms. The occurrence of time-periodical fluctuations can not be related to chance phenomena because they do not arise in discharges at dry air or pure hydrogen. Special investigations show that the fluctuations are related to a time-periodical process including plasmo-chemical reactions with participation of hydrogen. A physical meaning of such a process may be explained as follows. Vibrational excitation and dissociation of H_2O molecules lead to decrease in the plasma temperature and increase in the concentration of water derivatives (H, H_2, OH and other). At the same time cooling of the plasma causes its compression followed by a stimulation of reverse reactions. As a consequence, molecules of H_2O arise once again by burning of hydrogen in oxygen. And since the dissociation rate for water molecules is proportional to their concentration $\approx N^{3/2}$ the dissociation of water is repeated under the influence of the HF-field. This leads to the time-periodical

process in which the hydrogen acts as intermediate product and catalyst of direct and reverse reactions.

A "cutting of the high-energy tail" in the distribution $F(v)$ is equivalent to a decrease in entropy of hydrogen atoms radiating or, in other words, to the beginning of a plasma self-organization. One can say the same about the electron component. At φ_{opt} the excited vibrational levels of H_2O molecules have the energy of electrons up to ≈ 0.2 eV [6] therefore the electron subsystem is also characterized by a decrease in entropy. The formation of water molecules in the discharge indicates regularization of the cool non-equilibrium plasma and the occurrence of the LPC with the central core is other indication of this.

The cool non-equilibrium plasma is related to open structures. It is known that such a system is arranged by fluctuations increasing up to macroscopic magnitudes. In this connection we analyze here the character of fluctuation in such a plasma. One can more easily do it using the H_β line which is present in nearly all radiation spectra (see Fig. 8). At a humidity of $1 \div 10$ per cent the amplitude of fluctuations δI lies within the limits of 5 % of maximum intensity of the spectral line. In contrast, at the critical interval of φ it increases by $6 \div 7$ times and reaches a magnitude of 30 % as is shown in Fig. 9, a. Similarly an increase

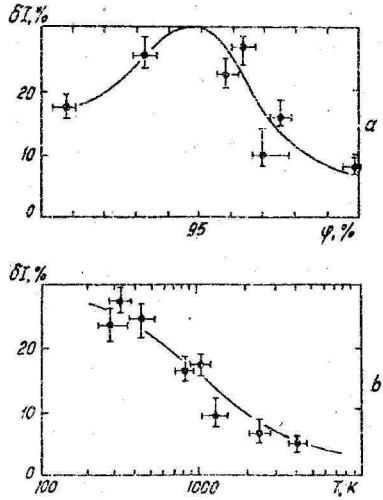

Fig. 9. Changes of amplitude fluctuations depending on air humidity (a) and translational temperature (b).

in δI when the temperature decreases (Fig. 8b).

A spatial localization of substance is probably a mechanism stabilizing the dissipative structure in respect of alterations of the chemical environment. In reference to the case of the plasma supercooled it is found that the presence of H_2O molecules lead to thermal diffusion and, what is more more important, the densities of hydrogen atoms radiating and of electrons increase. In other words the compression of the HF-discharge plasma by 1 ÷ 3 orders of magnitude was observed experimentally. Also the dissipative structure was stabilized by formation of supercooled plasma domains in the HF-discharge. The decay time regarded as a criterion of a structure stabiiization appear anomalously long.

Conclusions. The experimental results obtained in the subject of cooling the HF-discharge plasma by water vapour and accounting the ideas of non-equilibrium thermodynamics allow to assume that the cool non-equilibrium plasma is related to metastable formation with long lifetime. The plasma is easily generated in laboratory conditions at the relative humidity of air in the range of 95-98 %. Such a plasma can be considered as a basis to account for anomalous phenomena of atmospheric electricity [7]. As to a detailed description of the processes going in the cool non-equilibrium plasma this is of independent interest and will be published elsewhere.

The author thanks all whose aid and benevolence promoted the successful performance of this work.

References

1. Protasevich E.T., Kapichka B., Brablets A. Resonance cooling of an RF-discharge plasma by water vapour // Sov. Phys.- Tech. Phys. (USA).-1985.- V.30.- No. 4.- P. 440-1.

2. Protasevich E.T. Cool non-equilibrium plasma of gas discharge // Sov. J. Teplophys. Vyc. Temp.- 1989.- V.27.- No.6.- P. 1206-1218 (in Russian).

3. Protasevich E.T. Production of a dense supercooled plasma at reduced pressure // Sov. Tech. Phys. Lett.-1987. - V. 13.- No. 8.- P. 420.

4. Ohtsuki Y.H., Ofuruton H. Nature of ball lightning // Nuevo cim.- 1987.- V.10.- No. 5.- P. 517-580.

5. Kurilenkov Yu.K., Protasevich E.T. Long-living plasma formation // Sov. Tech. Phys. Lett. (USA).- 1989.- V. 15.- No. 7.- P. 539-41.

6. Olivero J.J., Stagat R.M., Green A.E.S. Electron deposition in water vapour with atmospheric application // J. Geophys. Research.- 1972.- V. 77.- No. 25.- P. 4797-4811.

7. Protasevich E.T. Physical nature of head lightning // Sov. J. Izvestiya AN SSSR. Ser.: Physics of atmosphere and ocean.- 1988.- V. 24.- No. 8.- P. 890-892 (in Russian).

ОСОБЕННОСТИ РАЗРЯДА В ВОЗДУХЕ ПРИ ПЕРЕМЕННОЙ ВЛАЖНОСТИ И ДАВЛЕНИЯХ 1 - 20 ТОРР

(самоорганизация переохлажденной плазмы высокочастотного разряда)

Е.Т. Протасевич

Р е з ю м е

Полученные экспериментальные результаты по охлаждению плазмы ВЧ-разряда парами воды и введение ряда представлений неравновесной термодинамики позволяют утверждать, что холодная неравновесная плазма принадлежит к числу метастабильных образований с большим временем жизни. Она легко создается в лабораторных условиях при относительной влажности воздуха, равной 95-98 %, и может быть полезна для объяснения природы таких аномальных явлений атмосферного электричества, как шаровая молния и четочная молния.

ELECTROSTATIC DISPERSION OF AIR IONS WITH A NORMAL MOBILITY DISTRIBUTION

J. Salm

The notion of air ion covers also electrically charged aerosol particles. If all the ions (charged particles) in a gas have one and the same mobility, then the process of electrostatic dispersion due to their mutual repulsion can be described strictly and simply [1-3]. Substantial mathematical difficulties connected with non-linearity of equations arise already at the handling of the dispersion of two ion groups of different mobilities [4]. In [5] it has been assumed that in electrostatic dispersion a lognormal mobility distribution is retained. Below we will prove that the lognormal distribution is not retained, whereas a normal mobility distribution is retained. The latter we will study more thoroughly.

Let us assume that at some initial moment (which is denoted by subscript 0) in a space there are homogeneously distributed unipolarily charged air ions, and that the mobilities of these ions are distributed accordingly to the normal curve

$$\rho_0(k) = \frac{\rho_0}{\sqrt{2\pi}\,\sigma_k} \exp\left[-\frac{(k-\bar{k}_0)^2}{2\sigma_k}\right], \qquad (1)$$

where $\rho_0(k)$ is the spectral function of charge density [6],
ρ_0 is the electric charge density, i.e. the integral of $\rho_0(k)$ over the whole domain of definition,
k is the mobility,
$\bar{k}_0$ is the mean of the mobility,
σ_k is the standard deviation of the mobility.

A supplementary assumption is that $\sigma_k < \bar{k}$ in order to disregard the part of the distribution function in the region $k < 0$. In practice a limitation $\sigma_k < 0.4\bar{k}$ can be used.

It is known that in the dispersion of a homogeneous air ion cloud there is the universal relation [3]

$$\frac{\rho(k)}{\rho_0(k)} = \left[\frac{\rho(k_1)}{\rho_0(k_1)}\right]^{\frac{k}{k_1}}, \qquad (2)$$

where k and k_1 are freely chosen mobilities and
$\rho(k)$ corresponds to another (later in comparison to the initial) moment of time.

An illustration of this argument is presented in Fig. 1.

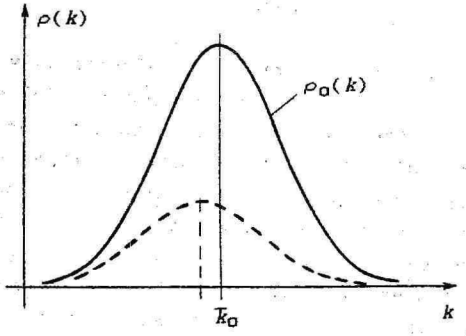

Fig. 1. The spectral function of charge density. The dashed line corresponds to a later moment of time.

For the sake of mathematical simplicity we will use undimensional variables

$$\left.\begin{aligned} k/\bar{k}_0 &= x \\ \sigma_k/\bar{k}_0 &= s \\ \bar{k}_0\rho(k)/\rho_0 &= y(x)\ . \end{aligned}\right\} \tag{3}$$

Equation (1) then acquires the shape

$$y_0(x) = \frac{1}{\sqrt{2\pi}\ s}\exp\left[-\frac{(x-1)^2}{2s^2}\right] \tag{4}$$

and equation (2) gets the shape

$$\frac{y(x)}{y_0(x)} = \left[\frac{y(1)}{y_0(1)}\right]^x\ . \tag{5}$$

Let us now express $y(x)$ from equation (5) in the assumption (4) and execute some transformations:

$$y(x) = \left[\frac{y(1)}{y_0(1)}\right]^x y_0(x) = A^x y_0(x) = \exp(x\ln A)y_0(x) =$$

$$= \exp(\alpha x)\frac{1}{\sqrt{2\pi}\ s}\exp\left[-\frac{(x-1)^2}{2s^2}\right] =$$

$$= \frac{1}{\sqrt{2\pi}\ s}\exp\left[-\frac{x^2-2x+1}{2s^2} + \alpha x\right] =$$

$$= \frac{1}{\sqrt{2\pi}\, s} \exp\left[- \frac{x^2 - 2x(1+s^2\alpha)+1}{2s^2} \right] =$$

$$= \frac{1}{\sqrt{2\pi}\, s} \exp\left\{ - \frac{[x-(1+s^2\alpha)]^2 - 2s^2\alpha - s^4\alpha^2}{2s^2} \right\} =$$

$$= \frac{1}{\sqrt{2\pi}\, s} \exp\left(\alpha + \frac{s^2\alpha^2}{2} \right) \exp\left\{ - \frac{[x-(1+s^2\alpha)]^2}{2s^2} \right\} , \quad (6)$$

where $A = y(1)/y_0(1)$

$\alpha = \ln A$.

Thus it was possible again to obtain a normal distribution for the later moment of time, the mean of which is

$$\bar{x} = 1 + s^2\alpha, \quad (7)$$

the ordinate of which are multiplied by the factor

$$z = \exp\left(\alpha + \frac{s^2\alpha^2}{2} \right) \quad (8)$$

and the standard deviation s of which is retained. Thus

$$y(x) = \frac{z}{\sqrt{2\pi}\, s} \exp\left[- \frac{(x-\bar{x})^2}{2s^2} \right] . \quad (9)$$

As the standard deviation of the distribution is retained, z characterizes also the decrease in the integral charge density

$$z = \rho/\rho_0 . \quad (10)$$

Equations (7) and (8) make it possible to find mutual relations of $\bar{x}$ and z :

$$\bar{x} = \sqrt{2s^2 \ln z + 1} \quad (11)$$

$$z = \exp\left(\frac{\bar{x}^2 - 1}{2s^2} \right) . \quad (12)$$

In the case of lognormal distribution of mobilities not the mobility, but the logarithm of the mobility has a normal distribution. In this case the exponent in equation (4) would be $\ln x$ instead of x . Carrying out transformations analogous to those for equation (6) it was not possible to obtain a lognormal distribution for the later moment of time.

In approximate estimations the use of lognormal distribution would be possible as far as it can be approximated to normal distribution (special cases involving small deviations).

Let us now consider the dependence of the dispersion on time. Here there are various possibilities to use different physical quantities but finally the results should be the same (differences might occur in the convenience of mathematical derivation).

In the general case, for a mobility k, the dispersion is described by the equation [3]

$$\frac{d\rho(k)}{dt} = -\frac{k}{\varepsilon}\rho(k) \quad , \tag{13}$$

where ε is the absolute permittivity of the environment (practically equal to the electric constant),
t is the time.

Integrating both sides of the equation (13) over k over the whole domain of definition we get

$$\frac{d\rho}{dt} = -\frac{\bar{k}}{\varepsilon}\rho^2. \tag{14}$$

Using undimensional variables (3) and (10) and adopting the undimensional time

$$\tau = \bar{k}_0\rho_0 t/\varepsilon, \tag{15}$$

we can write equation (14) as

$$\frac{dz}{d\tau} = -\bar{x}z^2. \tag{16}$$

Now we will replace z in equation (16) according to equation (12). After certain mathematical transformations we get a differential equation for $\bar{x}$, where the variables are separated

$$\exp\left(-\frac{\bar{x}^2}{2s^2}\right)dx = -s^2\exp\left(-\frac{1}{2s^2}\right)d\tau. \tag{17}$$

In integration the integrant of the left side of the equation is a function similar to normal distribution. The integral of the latter can be expressed through the error integral (the Laplace function) which is defined as

$$\mathrm{erf}(\eta) = \frac{2}{\sqrt{\pi}} \int_0^{\eta} \exp(-\xi^2) d\xi \ . \qquad (18)$$

Taking into account the initial conditions

$$\tau = 0; \qquad \bar{x} = 1 \qquad (19)$$

we can write the integral of equation (17) as

$$\mathrm{erf}\left(\frac{1}{2s}\right) - \mathrm{erf}\left(\frac{\bar{x}}{2s}\right) = \sqrt{\frac{2}{\pi}}\, s \exp\left(-\frac{1}{2s^2}\right) \tau \ . \qquad (20)$$

In applied problems the temporal variation of charge density is usually of primary interest. To find it $\bar{x}$ to equation (20) should be expressed through z with the help of equation (17). For small values of s (narrow distributions) the calculations may be simplified by the asymptotic equation [7]

$$1 - \mathrm{erf}(\eta) = \frac{\exp(-\eta^2)}{\sqrt{\pi}\,\eta}\left[1 + \sum_{k=1}^{m} (-1)^k \frac{(2k-1)!}{(2\eta^2)^k}\right] \ . \qquad (21)$$

As a specification to equation (21) it should be pointed out that the asymptotic series in the equation is semiconvergent and for concrete values of the argument there is an optimum number of the members of the series which guarantees a minimal approximation error.

Limiting ourselves to two first members of the series we can write the approximate equation

$$\frac{1}{z\sqrt{2s^2 \ln z + 1}}\left[1 - \frac{s^2}{2s^2 \ln z + 1} + \frac{3s^4}{(2s^2 \ln z + 1)^2}\right] - \left(1 - s^2 + 3s^4\right) = \tau. \qquad (22)$$

This equation may be recommended for the values of $s < 0.3$. With the decrease of the value of s first members with s^4 and then members with s^2 loose importance. Thus for very small values of s the equation for one discrete group of air ions remains valid.

The author thanks colleague A. Luts for a useful information.

References

1. Wolodkewitsch, N. Untersuchungen über die "elektrische Diffusion" der Ionen in Gasen unipolarer Beladung // Ann. Physik.- 1933.- Bd. 16.- S. 431-467.

2. Hidy, G.M., Brock, J.R. Dynamics of Aerocolloidal

Systems.- New York: Pergamon Press, 1970.

3. Сальм Я.Й. Об электростатическом рассеивании аэроионов // Уч. зап. Тарт. ун-та.- 1980.- Вып. 534.- С. 95-100.

4. Luts, A., Salm, J. Electrostatic scattering of two air ion groups of different mobilities // Acta et comm. Univ. Tartuensis.- 1990.- No. 880.- P. 105-110.

5. Берещагин И.П., Левитов В.И., Мирзабекян Г.З., Пашин М.М. Основы электродинамики дисперсных систем.- М., 1974.- 480 с.

6. Tammet, H. The aspiration method for the determination of atmospheric-ion spectra.- Jerusalem: Israel Program for Scientific Translations, 1970.- 200 p.

7. Janke, E., Emde, F., Lösch, F. Tafeln höherer Funktionen.- Stuttgart: B.G. Teubner Verlagsgesellschaft, 1960.

ЭЛЕКТРОСТАТИЧЕСКОЕ РАССЕИВАНИЕ АЭРОИОНОВ С НОРМАЛЬНЫМ РАСПРЕДЕЛЕНИЕМ ПОДВИЖНОСТЕЙ

Я.Й. Сальм

Р е з ю м е

Доказано, что нормальное распределение подвижностей аэроионов сохраняется в процессе электростатического рассеивания. При этом средняя подвижность и полная плотность заряда связаны функциональной зависимостью. Выведены приближенные формулы зависимости концентрации и средней подвижности от времени.

CHEMICAL KINETICS OF TROPOSPHERIC IONS AT HIGHER IONIZATION RATES

A. Luts

The paper deals with the modeling of the evolution (chemical kinetics) of tropospheric small ions for the case where the rate of ion generation is substantially above normal.

According to the current knowledge the evolution of small ions has the following stages.

1. Free electrons and positive primary (initial) ions arise due to the ionizing radiation of various origins. The electrons quickly combine with the neutral particles thus forming the negative initial ions.

2. The initial ions are at the start of an evolutionary process, meaning the transformation of one kind of ions into other kinds of ions through ion-molecular reactions; the final result is the emergence of the so-called final ions which do not decay in ion-molecular reaction but for other reasons.

3. The final ions generated in the evolution process decay in recombination or in combination with aerosol particles [1-4].

4. If the processes 1-3 are continual, they result in the emergence of certain concentrations of different kinds of ions. Such concentrations are called steady-state.

In the present paper the processes of stages 2 and 4 are simulated.

1. Description of the method of simulation

1.1. Methods of solution of the system of equations

On the assumption of taking into account only ion-molecular reactions, the chemical kinetics of tropospheric small ions is described by the system of differential equations

$$Y' = AY + BY \qquad (1)$$

where $Y(t) = y_k(t)$ is the vector of ion concentrations,

A - the matrix the elements of which express the rates of the concentration changes that take place through ion-molecular reactions,

B - the matrix describing ion generation and recombination, according to [2-5].

This system of differential equations is generally nonlinear as B contains concentrations $y_k(t)$. As in the case of normal rate of ion generation the concentration of tropospheric ions is considerably lower than the concentration of tropospheric neutral gases, it is customary in modeling to take the concentrations of the gases participating in ion-molecular reactions to be constant, thus we get A = const. This presumption is valid until the tropospheric ion concentration is not over some hundreds of ions/cm^3.

The situation is changed with the increase in the rate of ion generation. In this case the constancy of neutral gas concentrations is not self-evident, and for the problem (1) it means that in the case of increased ionization rate the time-dependence of the member A is added to the time-dependence of the member B.

In the general case the solution of the problem (1) is highly complicated, as this differential equation system is nonlinear, rather large (with the number of equations in the order of magnitude of 100), and quite stiff (the orders of magnitudes of the elements in the equations differ up to 10^{12} times). It has been shown in [5] that if A = const, the problem [1] can be solved in two stages, solving first the linear problem $Y' = AY$, and then, using the time variations of the concentrations, solving the problem that takes into account recombination and ion generation. It is important that as a result of the both solutions the curves of the ion evolution and the steady state of the ions are found, whereas it requires a relatively short time to solve the both subproblems.

1.2.Computation of concentration changes of neutral compounds

As it was said above, a method has been designed for the solution of the problem (1) if A = const. To apply this methodology in conditions where the concentrations of neutral compounds may vary, iteration is used in the present work. Namely, first the problem (1) is solved on the assumption A = const (for initial concentrations of neutral compounds) using the method described in [5]. Next, using the concentrations of the steady state of ions, the changes in the concentrations of neutral compounds are found as follows.

Let us have a reaction

$$A^+ + B + C \xrightarrow{k} D^+ + E + F ,$$

where A^+ and D^+ are ions,

B, C, E, F are neutral compounds, and

k is the rate constant of this reaction.

This formula does not mean the termolecular collision but only a reaction which can be described by termolecular equation. If there is a bimolecular reaction, the compounds C and F can be moved away.

If the concentration of the ions A^+ in the steady state is $[A^+]$, then, e.g. within 1s, the concentration of compound B changes by the value

$$[B]_{1s} = -k \cdot [A^+] \cdot [C]_0 [B]_0 ,$$

where $[C]_0$ and $[B]_0$ are the concentrations of neutral compounds B and C which were used for the determination of the matrix A of the problem (1). Adding up the changes $[B]_{1s}$ over all the ion-molecular reactions in the system, we obtain the total change of the concentration of compound B within 1s on the assumption that other concentrations are constant. Thus the changes of the concentrations of all the neutral compounds participating in ion molecular reactions are found, the changes are taken into account in the next determination of matrix A of the problem (1).

If the above iteration is executed several times, it is possible to estimate the influence of the concentration change of certain neutral compound on ion kinetics and on the concentration change of neutral compound itself. At the same time this estimate is a maximum that can be set as a purpose as far as only ion-molecular reactions are taken into account in the simulation of chemical kinetics. If we take into account also the reactions between neutral compounds, the system of equations (1) unavoidably becomes nonlinear which causes a substantial increase in computational difficulties.

1.3. Preliminary separation of more important reactions

If matrix A of the system of equations (1) is constant, then before solving problem (1), the more important reactions, ions, and neutral compounds can be separated. The list of separated parameters is naturally different for every concrete shape of matrix A. Such a preliminary procedure

described below makes it possible to decrease substantially the number of equations in system (1).

The procedure of choosing the more important reactions is generally as follows:

1) We make comparisons between the rates of ion molecular reactions proceeding from a concrete ion, i.e. between the rates of the reactions lowering the concentration of the ion. Thus we find the quickest irreversible reaction. The reactions proceeding from this ion, the rates of which are lower by at least a given number of times than the rate of the quickest reaction, are labeled as unimportant. This process is carried out for all the ions that occur in the system.

2) It is attempted to order the found important reactions into chains (a genetically connected ordering of reactions) starting from the given so-called initial ions. Reactions which cannot be joined into any chain are labeled. Also those reactions are labeled which can be ordered into a chain but which, on the assumption that the concentration of the reactant ion is 1, are slower than the given rate limit.

3) All labeled reactions and the compounds not participating in the important reactions are moved away.

The above procedure is illustrated by an example in Fig.1.

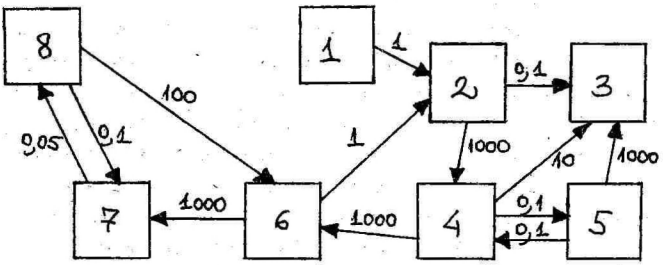

Fig. 1. Graph of reactions (example). The rectangles denote ions, the arrows denote reactions. The figure at an arrow can be considered to be the rate of the respective transformation.

1) Let us compare the rates of the reactions proceeding from the ion 2. The rate of the reaction 2 -> 4 is significantly higher than the rate of the reaction 2 -> 3, but the reaction 2 -> 4 cannot be taken to be the quickest

as it is reversible through the chain 2 -> 4 -> 6 -> 2. Thus the reaction 2 -> 3 is to be considered as the quickest reaction. As no slower reactions proceed from this ion, any unimportant reaction is not labeled here.

Now let us compare the rates of the reactions proceeding from ion 4. The reaction 4 -> 6 is reversible and the reaction 4 -> 3 is the quickest. As the reaction 4 -> 5 is slower, it can be labeled as unimportant.

Let us compare the rates of the reactions proceeding from ion 6. As both reactions are reversible, the rates are not compared and unimportant reactions not labeled.

2) All possible reaction chains between the important reactions found, starting from the initial ion (in this case ion 1) are searched. If the reaction 4 -> 5 has been labeled as unimportant, then ion 5 is not formed and the reactions 5 -> 4 and 5 -> 3 cannot be joined into chains. These reactions are labeled.

If the rate limit given for the reactions is, e.g. 0.1, then the reaction 7 -> 8 is slower than this limit. In this case the reaction 7 -> 8 is labeled. If so, then the reactions 8 -> 7 and 8 -> 6 cannot be joined into chains and they are to be labeled too.

3) The labeled reactions are moved off. As a result of this ions 5 and 8 are turned into into the not-usable-state and they are also to be separated. The number of equations in the system will be reduced from 8 to 6.

2. Data for the simulation of chemical kinetics

2.1. Ion-molecular reactions

The sets of ion-molecular reactions used in the present paper have been compiled on the basis of data presented in [2-4, 6, 7]. In the case of negative ions, the data of [2, 3, 7] have been added to the data presented in [6]. In the case of positive ions the data in [4, 7] have been added to the data presented in [6]. If the rate constants for the same reaction are not equal in different papers, then the data in papers [6] or [2,4] are preferred.

The models of ion chemical kinetics are highly sensitive to the values of rate constants of certain ion molecular reactions. The influence of this sensitivity on the possible

results of simulating deserves a separate study, the more so, as the rate constants of many very important ion-molecular reactions are known rather inexactly. Here we will confine ourselves to pointing out that we decreased 4 times the rate constants presented in [3] of the transformations $O_2^-(H_2O)_3$ -> -> $O_2^-(H_2O)_4$ and $O_2^-(H_2O)_4$ -> $O_2^-(H_2O)_5$. This was done to achieve a better agreement with certain experimental results.

The model describing the kinetics of positive ions contains 1044 reactions, 198 ions and 131 neutral compounds; the negative ion model has 474 reactions, 143 ions and 106 neutral compounds.

Table 1

Natural concentrations of neutral compounds

M CL	.12E11	M/2 O	.27E18	NO	.16E10
O/3	.81E12	CO	.61E13	CO/2	.87E16
M/2	.13E14	NO/2	.22E11	N /2 O	.10E14
HNO/2	.11E09*	HNO	.11E09*	N/2 O/5	.50E07
HNO/3	.10E11	NH/3	.10E12	SO/2	.30E12
SO/3	.31E09*	SO/4	.31E09*	M/2 SO/4	.40E09
M/2 S	.16E12	SF/6	.19E08	CS/2	.81E09
ME.	.14E15	CL	.44E10*	CL/2	.21E11*
CL O	.44E10*	MBR	.41E08	H	.11E03*
OH	.50E07	N	.13E05*	O	.20E05
HCO	.11E10*	CCL/3 F	.41E10	CCL/2 F	.33E10*
CH/3 BR	.39E09	CH/3 CL	.20E11	CH/3 F	.33E10*
CH/3NO/2	.11E10*	CCL/4	.15E11	CH CL/3	.36E09
CH/3 OH	.22E11*	C/2H/5OH	.22E11*	CH/3NH/2	.11E11*
C/2 H/2	.26E11	C/2 H/4	.69E11	C/2 H/6	.31E12
C/3 H/6	.19E12	C/3 H/8	.31E12	C/6 H/6	.32E12
C/7 H/8	.27E13	C/2 H/5	.22E10*	C/5 H/6	.35E10*
C/2 H/3	.22E10*	C/3 H/3	.22E10*	C/3 H/4	.22E10*
HCN	.41E09	CH/4	.39E14	2(CH/3) CO	.11E10*
2(CH/3) NH	.11E10*	C/2H/3 N	.54E10	2(CH/3) SO	.11E10*
C/2H/4 O	.22E10*	CCL/2F/2	.96E10	CH/3 SH	.11E10*
C/2 H/4 F	.44E10*	CH/2 CL/2	.21E10	2(CH/3) O	.11E10*
CH	.11E09*	C/2 O	.11E09*	BR NO/2	.11E10*
CH/2	.11E10*	NO/3	.11F10*	C/2 N	.11E09*
CL NO/2	.11E10*	HF	.11E10*	F NO/2	.11E09*
HO/2	.11E13	HS	.11E09*	CH/2 O	.50E11
NH/2	.11E10*	C/2H/5 NH/2	.11E10*	C CL/3	.11E11*
CH/3 O	.11E10*	CH/2 BR	.11E10*	CH/2 CL	.11E10*
CH/2 F	.11E10*	CH/3	.11E10*	C/2 H/2 O	.11E09*
C/3 H/5	.11E10*	C/3 H/7	.11E10*	2(CH/3) S	.11E10*
S	.11E09*	SO	.11E09*	C/6H/5CH/3	.71E12
H/2 O/2	.12E12	HN/2 O	.11E09*	C/3H/4 F	.11F10*
H/3 O	.11E09*	C/2H/5 NH	.11E09*	C/2H/5 O	.11E09*
C/4H/9	.11E09*	C/4H/8	.11E10*	C/4H/10	.11E10*
C/3H/5 O	.11E09*	KR	.30E14	COS	.13E11
C/2 N/2	.44E11*	CH/3 CHO	.10E12	CH/3 COOH	.18F11
CH/3COC/3H/7	.44E11*	C/2H/3 F	.33E10*	C/2H/3CL	.33E10*
C/2 F/4	.33E10*	C/2HF/3	.33E10*	CH/2 F/2	.33E10*
C/2H/5 CL	.11E09	C/2H/2F/2	.33E10*	HN	.11E10*
C F/4	.19E10	C/3H/7 OH	.11E10*	C/2 F/6	.11E09
C/3 F/8	.11E10*	3(C/2H/5) N	.11E10*	CCL F/3	.11E10*
CHCL/2 F	.38E09	SF/5	.11E10*	SF/4	.11E10*
SF/3	.11E10*	C	.11E10*	F	.11E10*
C/2H/2CL/2	.21E10	CH CL/2	.11E10*	C/6H/6F/2	.11E10*
CF/3	.11E10*	C/2F/5	.11E10*	CH/3 N	.11E10*
C/4H/6	.11E10*	C/4H/7	.11E10*	SI H/4	.11E10*
CIN	.11E10*	CH/2 S	.11E10*	CH/3 S	.11E10*
C CL/2	.11E10*	CH CL F/2	.11E10*	CH CL F	.11E10*
CH F/3	.11E10*	CH F/2	.11E10*	CS	.11F10*
CH/4 N	.11E10*				

2.2. Initial concentrations of ions

To solve sub-problem $Y' = AY$ of the problem (1) the initial concentrations of ions $y_{0,k} = 0$ are to be given. The latter have been taken to be proportional to the rate of formation of these ions in the tproposphere. As the solution of the linear problem $Y' = AY$ (the shapes of time - changes of the concentrations) is independent of the sum of initial concentrations $\Sigma y_{k,t=0}$, this sum can be taken to be 1 (one). In this case the initial concentrations in the case of positive ions would be

$[Ar^+] = 0.01$; $[N_2^+] = 0.64$; $[O_2^+] = 0.21$;

$[NO^+] = 0.05$; $[N^+] = 0.06$; $[O^+] = 0.03$ [4];

and in the case of negative ions

$[O_2^-] = 0.95$; $[O^-] = 0.05$ [3].

2.3. Concentrations of neutral compounds

The concentrations of several neutral compounds important for simulating the troposphere are not exactly known. We have estimated the concentrations of these compounds. The concentrations of all the neutral compounds used in the model are listed in Table 1; an asterisk by a concentration means that this concentration has been estimated.

2.4. Quantities characterizing ion formation and recombination

The balance of ion formation and recombination is described by the equation

$$Q = \alpha n_+^2 + \beta Z n_+$$

where Q - the rate of generation of initial ions
α - the coefficient of mutual recombination
n_+ - the total concentration of ions of one sign
β - the coefficient characterizing the rate of joining with aerosol particles
Z - the concentration of aerosol particles.

The quantities in this equation have in this paper the following values : $Q = 14\ cm^{-3} \cdot s^{-1}$ and $6 \cdot 10^6\ cm^{-3} \cdot s^{-1}$, $\alpha = 1.6 \cdot 10^{-6}\ cm^3 \cdot s^{-1}$, $\beta Z = 0.04\ s^{-1}$.

3. Ion kinetics in the conditions of increased rate of generation of ions

3.1. The changing of neutral gas composition

The computations showed that in the case of natural intensity of ion formation the concentrations of neutral gases in the troposphere change less than 10^{-3}% s^{-1}. Thus it would take several hours to change the concentration by 10% on the assumption that changes in the concentrations of neutral gases will not trigger any negative feedback. However, the computations make it possible to say that generally, negative feedback occurs already through ion-molecule reactions. Thus it can be supposed that in the case of natural intensity of ion formation we can really disregard the changes of the concentrations of neutral gases.

Next, we computed the change of the concentrations of negative gases for the case where the intensity of ion formation is $6.7 \cdot 10^{6}$ $cm^{-3} \cdot s^{-1}$. The concentrations of neutral gases considered to be natural (initial) are listed in Table 1. A sample of results is presented in Table 2.

Next we will give a survey of the processes presented in Table 2.

1) The concentration of NO usually increases, NO_2 decreases. Both changes are influenced by the negative feedback. If we increase the concentration of NO and lower the concentration of NO_2 about hundred times, the concentration of NO will lower also and the decrease in the concentration of NO_2 will be negligible. If the concentration of water accelerates the variations in the concentrations of NO and NO_2, the same can be observed if we increase the concentration of ozone or the concentration of SO_2. Besides, in the case of positive ions a decrease in the concentration of NH_3 speeds up the increase in the concentration of NO. In the case of negative ions an increase in the concentration of HNO_3 slows down the both variations in concentrations.

2) The concentration of NH_3 lowers, this is not compensated by feedback. If we diminish the concentration of NH_3 1000 times, the decrease in its concentration becomes retarded only 2 times. On one hand, only the concentration of CH_4 has a remarkable effect on the lowering of the concentration of NH_3, on the other hand, the lowering of the concentration of NH_3 will accelerate the changes of the

Table 2

Significant changes in neutral gas concentrations, in $s^{-1}cm^{-3}$

Gases / Conditions	NH_3	CH_4	N_2O	HNO_3	C_2H_2	C_2H_4	NO
Natural	$-4\cdot10^4$	$-1\cdot10^6$	$2\cdot10^6$	$-7\cdot10^5$	-	-	$2\cdot10^5$
[NO]=10x [NO_2]=0.1x	$-4\cdot10^4$	$-1\cdot10^6$	$2\cdot10^6$	$-1\cdot10^6$	-	-	$5\cdot10^4$
[NO]=0.1x [NO_2]=10x	$-4\cdot10^4$	$-1\cdot10^6$	$2\cdot10^6$	$-1\cdot10^6$	-	-	$2\cdot10^5$
[CH_4]=100x	$-2\cdot10^5$	$3\cdot10^4$	$3\cdot10^5$	$-1\cdot10^6$	$-2\cdot10^4$	$2\cdot10^4$	$1\cdot10^5$
[CH_4]=10^{-3}x	$-4\cdot10^4$	-170	$6\cdot10^5$	$-1\cdot10^6$	-	-	$1\cdot10^5$
[CH_4]=.001x [N_2O]=.001x	$-6\cdot10^4$	-2000	$6\cdot10^5$	$-1\cdot10^6$	-	-	$1\cdot10^5$
[CH_4]=.001x [N_2O]=1000x	$-6\cdot10^4$	$-9\cdot10^4$	$9\cdot10^6$	$-3\cdot10^5$	-	-	$1\cdot10^5$
[NH_3]=10x	$-8\cdot10^4$	$-4\cdot10^4$	$4\cdot10^5$	$-7\cdot10^5$	-	-	$1\cdot10^5$
[NH_3]=.001x	$-1\cdot10^4$	$-4\cdot10^8$	$5\cdot10^8$	$-1\cdot10^6$	$-7\cdot10^4$	$-2\cdot10^5$	$1\cdot10^7$
[CH_4]=.01x [NH_3]=$4\cdot10^{-5}$x	$-1\cdot10^4$	-2000	$1\cdot10^7$	$-1\cdot10^6$	370	-730	$1\cdot10^5$
[CH_4]=.01x [H_2]=0.1x [NH_3]=$4\cdot10^{-5}$x	-9800	-2900	$2\cdot10^6$	$-1\cdot10^6$	340	-700	$1\cdot10^5$
[H_2]=0.1x	$-2\cdot10^4$	$-7\cdot10^5$	$1\cdot10^6$	$-1\cdot10^6$	-	-400	$1\cdot10^5$
[H_2O]=0.5x	$-5\cdot10^4$	$-6\cdot10^4$	$4\cdot10^5$	$-4\cdot10^6$	-	-	$3\cdot10^5$
[C_2H_2]=.1x [C_2H_4]=100x	$-2\cdot10^4$	$-7\cdot10^5$	$1\cdot10^6$	$-1\cdot10^6$	$2\cdot10^4$	$-2\cdot10^4$	$1\cdot10^5$
[SO_2]=100x	$-4\cdot10^4$	$-1\cdot10^6$	$2\cdot10^6$	$-4\cdot10^5$	-	-	$8\cdot10^5$
[HNO_3]=.01x	$-4\cdot10^4$	$-1\cdot10^6$	$2\cdot10^6$	-200	-	-	$2\cdot10^5$
[HNO_3]=100x	$-4\cdot10^4$	$-1\cdot10^6$	$2\cdot10^6$	8000	-	-	$2\cdot10^5$
[O_3]=0.1x	$-4\cdot10^4$	$-1\cdot10^6$	$2\cdot10^6$	$-4\cdot10^5$	-	-	$2\cdot10^5$
[O_3]=10x	$-4\cdot10^4$	$-1\cdot10^6$	$2\cdot10^6$	$-3\cdot10^6$	-	-	$2\cdot10^5$
Stationary	$-4\cdot10^4$	-1000	$5\cdot10^5$	-600	-250	-1000	-1000

Table 2

Significant changes in neutral gas concentrations, in $s^{-1}cm^{-3}$

Gases / Conditions	NO_2	SO_3	H_2	H	HCO	CO	O_3
Natural	$-4\cdot10^5$	4500	$-2\cdot10^5$	$2\cdot10^5$	$2\cdot10^4$	$-4\cdot10^4$	$-2\cdot10^6$
$[NO]=10x$ $[NO_2]=0.1x$	$-5\cdot10^4$	100	$-2\cdot10^5$	$2\cdot10^5$	$3\cdot10^4$	$-4\cdot10^4$	$-2\cdot10^6$
$[NO]=0.1x$ $[NO_2]=10x$	$-3\cdot10$	$2\cdot10^4$	$-2\cdot10^5$	$2\cdot10^5$	$1\cdot10^4$	$-2\cdot10^4$	$-2\cdot10^6$
$[CH_4]=100x$	$-5\cdot10^5$	5000	-8100	$2\cdot10^4$	$3\cdot10^4$	$-4\cdot10^4$	$-2\cdot10^6$
$[CH_4]=10^{-3}x$	$-5\cdot10^5$	-5000	$-3\cdot10^5$	$3\cdot10^5$	$3\cdot10^4$	$-4\cdot10^4$	$-2\cdot10^6$
$[CH_4]=.001x$ $[N_2O]=.001x$	$-5\cdot10^5$	-5200	$-3\cdot10^5$	$3\cdot10^5$	$3\cdot10^4$	$-4\cdot10^4$	$-2\cdot10^6$
$[CH_4]=.001x$ $[N_2O]=1000x$	$-4\cdot10^5$	900	$-2\cdot10^7$	$1\cdot10^7$	5000	-7400	$-3\cdot10^4$
$[NH_3]=10x$	$-4\cdot10^5$	5200	-5300	5000	$3\cdot10^4$	$-4\cdot10^4$	$-2\cdot10^6$
$[NH_3]=.001x$	$-5\cdot10^5$	5200	$-7\cdot10^7$	$6\cdot10^7$	$3\cdot10^4$	$-4\cdot10^4$	$-2\cdot10^6$
$[CH_4]=.01x$ $[NH_3]=4\cdot10^{-5}x$	$-5\cdot10^5$	5000	$-1\cdot10^7$	$1\cdot10^7$	$3\cdot10^4$	$-4\cdot10^4$	$-2\cdot10^6$
$[CH_4]=.01x$ $[H_2]=0.1x$ $[NH_3]=4\cdot10^{-5}x$	$-5\cdot10^5$	5000	$-2\cdot10^6$	$1\cdot10^6$	$3\cdot10^4$	$-4\cdot10^4$	$-2\cdot10^6$
$[H_2]=0.1x$	$-5\cdot10^5$	5000	-9100	9500	$3\cdot10^4$	$-4\cdot10^4$	$-2\cdot10^6$
$[H_2O]=0.5x$	$-1\cdot10$	$3\cdot10^4$	-	8400	$1\cdot10^5$	$-2\cdot10^5$	$-4\cdot10^6$
$[C_2H_2]=.1x$ $[C_2H_4]=100x$	$-5\cdot10^5$	5000	$-1\cdot10^5$	$9\cdot10^4$	$3\cdot10^4$	$-4\cdot10^4$	$-2\cdot10^6$
$[SO_2]=100x$	$-1\cdot10$	$1\cdot10^5$	$-2\cdot10^5$	$2\cdot10^5$	6700	-7500	$-2\cdot10^6$
$[HNO_3]=.01x$	$-5\cdot10^5$	6000	$-2\cdot10^5$	$2\cdot10^5$	330	$-5\cdot10^4$	$-2\cdot10^6$
$[HNO_3]=100x$	$-2\cdot10^5$	200	$-2\cdot10^5$	$2\cdot10^5$	$9\cdot10^4$	1000	$-2\cdot10^6$
$[O_3]=0.1x$	$-4\cdot10^5$	1000	$-2\cdot10^5$	$2\cdot10^5$	7000	-7000	$-3\cdot10^5$
$[O_3]=10x$	$-7\cdot10$	$1\cdot10^4$	$-2\cdot10^5$	$2\cdot10^5$	$5\cdot10^4$	$-8\cdot10^4$	$-5\cdot10^6$
Stationary	-6900	-	$4\cdot10^4$	860	470	$-7\cdot10^4$	$-2\cdot10^6$

concentrations of many gases.

3) The change of the concentration of CH_4 in normal conditions is negative. At the same time, there is the negative feedback that stops the decrease in the concentration of CH_4 and the positive feedback supporting the growth of the concentration. The alteration of the concentration of CH_4 is influenced by the concentration of NH_3, at the same time the growth of the concentration of CH_4 has an effect on the concentrations of NH_3, C_2H_2, C_2H_4, H_2 and H. As there is the feedback supporting the growth of the concentration of CH_4 it could increase and not decrease but the increase is hindered by the feedback with NH_3.

4) The concentration of N_2O is increasing. Besides, in the case of positive ions there is a positive feedback that speeds the increase up. The negative feedback , existing in the case of negative ions is too weak to prevent the increase in the concentration of N_2O. The increase in the concentration of N_2O is accelerated by the decrease in the concentration of NH_3. The influence of NH_3 can be partially reduced by the decrease in the concentration of H_2.

5) The concentration of HNO_3 usually decreases. The decrease will be negligible either by the increase of this concentration (positive feedback) or by the decrease of that (negative feedback). The rate of change in the concentration of HNO_3 depends on the concentrations of O_3, water and SO_2.

6) The total change in the concentrations of SO_3 and H_2SO_4 is generally weakly positive (some thousands $cm^{-3} \cdot s^{-1}$). The growth in the concentrations of SO_3 and H_2SO_4 is limited by strong negative feedback. For instance, if we increase the concentrations of both compounds 10000 times, the total change of the concentrations of SO_3 and H_2SO_4 is negative $4 \cdot 10^5$ $cm^{-3} \cdot s^{-1}$.

The generation of SO_3 and H_2SO_4 would be substantially increased, if the concentration of NO decreased and the concentration of NO_2 increased. In this case the total change of concentration is $2 \cdot 10^4$ $cm^{-3} \cdot s^{-1}$. At the same time if the concentration of NO grows and the concentration of NO_2 decreases (which is more likely), the total change of the total concentrations of SO_3 and H_2SO_4 is nearing to zero. The generation of SO_3 will increase if we increase the concentration of SO_2.

7) In the case of positive ions it appears, that the concentration of H_2 should be decreasing. There is a negative feedback but it is too weak to prevent the decrease in the concentration of H_2. It must be said that the decrease in the concentration of H_2 would be quite incredible as the concentration of H_2 should be one of the most stabile concentrations.

The decrease in the concentration of H_2, if existing, will reduce the influence of decrease in the concentration of NH_3. The increasing in the concentration of CH_4 hinders the decrease in the concentration of H_2, and can also cause the increase in that concentration.

8) The changes in the concentrations of C_2H_2 and C_2H_4 are usually small, the concentration of C_2H_2 is slighly decreasing and the concentration of C_2H_4 is increasing. There is a negative feedback for the both concentrations of C_2H_2 and C_2H_4. The changes in these concentrations are influenced by the decrease in the concentration of NH_3, that causes a substaintial variation of both concentrations.

9) The concentration of CO decreases. The rate of that process is influenced by the concentrations of ozone and HNO_3. The increase in the concentration of HNO_3 will cause the concentration of CO to start increase.

In addition to Table 2, the following changes in the concentrations of neutral compounds are to be pointed out.

1) Nearly independently of the concentration of neutral compounds in one second $6 \cdot 10^6$ cm^{-3} OH; $5 \cdot 10^5$ cm^{-3} HNO_2; $2.2 \cdot 10^5$ cm^{-3} O; $3.7 \cdot 10^5$ cm^{-3} N; $3 \cdot 10^5$ cm^{-3} HO_2; $2 \cdot 10^5$ cm^{-3} H are generated. In same time about $5 \cdot 10^4$ cm^{-3} SO_2 disappears.

2) The concentration of ozone decreases with a speed which usually is about $2 \cdot 10^6$ $cm^{-3} \cdot s^{-1}$. At the same time there is a negative feedback, namely if we give $[O_3] = 0.1 \cdot [O_3]_0$, the decrease in the concentration of ozone is about 10 times slower. The increase in the concentration of N_2O will also slow down the decrease in that concentration. The actual decrease in the concentration of ozone cannot be large because at the same time ozone is constantly formed of generated mono-oxygen. It is possible that actually a growth in ozone concentration occurs.

For exact modeling of concentration changes the reactions occurring between neutrals should be taken into account in addition to ion-molecular reactions. If this is not done, the

results are definitely estimational. AS A CONCLUSION, taking into account only the feedback processes through ion-molecular reactions, the probable changes in the concentrations of neutral compounds are as follows.

The extent of the change in the concentrations of OH, N, O, H, HO_2 and HNO_2 cannot be estimated, as the feedback processes through ion-molecular reactions are practically absent. Taking into account the extent of their generation, the concentrations of the above compounds grow substantially, this is likely to be followed by the changes in the reactions between neutrals occurring with these compounds.

The concentrations of NO and CH_4 grow; the concentrations of NH_3, HNO_3, NO_2, C_2H_2 and C_2H_4 lower. The possible extent of the change in the concentration of the latter compounds can be estimated. We achieved a situation where the changeability of all these compounds is significantly decreased (see Table 2, row "stationary"). The respective concentrations would be the following (the unit of measurement is cm^{-3}):

$[NO] = 3.2 \cdot 10^{10}$; $[NO_2] = 2.0 \cdot 10^{8}$; $[C_2H_2] = 2.6 \cdot 10^{7}$

$[N_2O] = 2 \cdot 10^{13}$; $[HNO_3] = 1 \cdot 10^{8}$; $[C_2H_4] = 7.0 \cdot 10^{9}$

$[NH_3] = 1 \cdot 10^{9}$; $[CH_4] = 1 \cdot 10^{14}$;

We have to point out that all the above concentrations are rather unusual. In natural troposphere $[NO] < [NO_2] \approx [HNO_3]$, but here $[NO_2]$, $[HNO_3]$ and $[NH_3]$ are unusually small.

3.2. Chemical kinetics of positive ions

We have dealt with the kinetics of positive ions at natural ion generation intensity in [8]. The present paper additionally presents a modeling of kinetics at the ion generation intensity $Q = 6.7 \cdot 10^{6}$ $cm^{-3} \cdot s^{-1}$. The results are presented in Table 3 and in Fig. 2.

The evolution of positive ions proceeds according to the graph presented in [7]. As we can see in Fig. 2, the main part of the primary ions (mainly N_2^+ and O_2^+) has already at an age of 10^{-8} s undergone the transformation to the ions $H_3O^+(H_2O)_k$. Starting from this age to an age of about 1 s the amount of the ions $H_3O^+(H_2O)_k$ exceeds that of other ions by several orders of magnitude. At an age of about 1 s starts the formation of the final ions. If the concentrations of neutral gases of are more or less natural, then, on the basis of computations, the part of the final ions should be not

Table 3

Steady state concentrations of positive ions

Conditions \ Ions	$NH_4^+ \cdot X \cdot Y$	$H_3O^+(H_2O)_k$	NH_4^+
Natural	25%	74%	0.5%
Gas composition according to Table 1, $Q=6.7\cdot10^6$ $cm^{-3}s^{-1}$	-	99%	0.5%
Changed gas composition, $Q=6.7\cdot10^6$ $cm^{-3}s^{-1}$	-	99%	0.5%

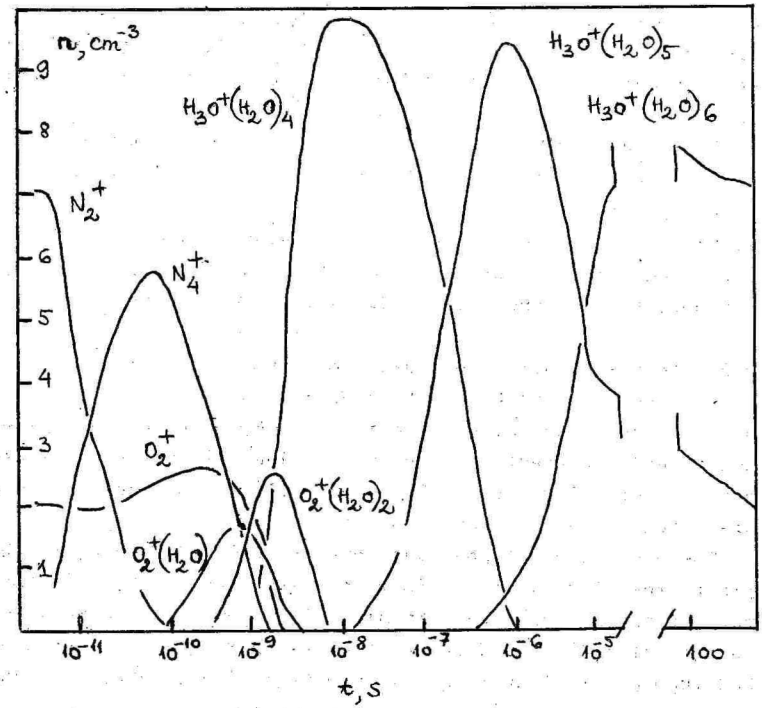

Fig. 2. The curves of the evolution of positive ions in the conditions of changed gas composition.

very ladge. This so-called natural situation is given in the first row of Table 3.

It should be pointed out that in comparison with measurement results [9-10], the generation of the ions $NH_4^+ \cdot X \cdot Y$ is too slow, and the part of the ions $H_3O^+(H_2O)_k$ is too ladge. The situation where the number of the ions $NH_4^+ \cdot X \cdot Y$ would be larger could in principle be achieved by certain small changes in rate constants. We have not carried out such a correction, as many ions important in the measurements (e.g. with masses 60, 80, 94, supposedly pyridine, and others) cannot be modeled because of the lack of data. If this is so, then let the superfluous part of the ions $H_3O^+(H_2O)_k$ be a sign that the model is as yet incomplete.

In the steady state at a increased rate of ion generation, younger ions are more important than in the case of normal ion formation intensity. As among younger ions the ions $H_3O^+(H_2O)_k$ are dominant, they are also dominant in the steady state as can be seen in the second row of Table 3.

The last row of Table 3 presents the results of the case where, in addition to the increased rate of ion generation, the neutral gas composition is also changed. The changed concentrations are listed in the end of section 1. The kinetics in this case is different from that at the natural conditions mainly due to the fact that because of a significant decrease in the concentration of NH_3 the formation of the final ions does not start at an age about 1s but starts later.

For the easiest way to check preliminarily up the presented modeling results it is necessary to measure the mobility spectra in the conditions of a increased rate of ion generation. While in the natural case (Table 3, first row) the ions $NH_4^+ \cdot X \cdot Y$ are important in the troposphere, then in the conditions of heightened intensity and consequent changes in the gas composition other types of ions are important. As the ions $H_3O^+(H_2O)_k$ are generally heavier than the ions $NH_4^+ \cdot X \cdot Y$, the mobility spectrum of positive ions should be shifted towards smaller mobilities in comparison with the normal mobility spectrum [12].

3.3. Chemical kinetics of negative ions

We have dealt with the kinetics of negative ions at normal ionization rate in [11]. In the present paper, the set of

ion-molecular reactions has been supplemented. The additions, however, do not have significant influence on ion kinetics up to an age of 0.1s. The kinetics has been modeled for natural and hightened ion formation intensity, the results are presented in Table 4 and Fig. 3.

Fig. 3 illustrates rather well the variation of the evolution of negative ions. The ions $O_2^-(H_2O)_k$ are mainly formed from the initial ions and achieve their equilibrium concentrations in same microseconds. At an age of about 0.1s the formation of final ions from these ions in started, whereas partially the process occurs directly and partially through the ions $CO_3^-(H_2O)_k$, considerable amounts of which may be formed under certain conditions for a certain time. For the normal gas composition the final ions are mostly clusters with the core NO_3^- (see table 4, first row). These modeling results generally agree with the experimental results. Indeed, the clusters with the core NO_3^- are the most important in the troposphere with a small addition of clustern with the core HSO_4^- [9, 10].

The concentrations of the stationary state at greatest intensity of ion formation but normal gas composition are presented in the second row of Table 4.

If the gas composition is changed in the manner mentioned in the end of section 1, the effects conditioned by the change of gas composition are added. First, as the concentration of NO_2 is lower than normal, the direct formation of final ions through the channel $O_2^-(H_2O)_k \rightarrow NO_2^-\cdot X\cdot Y \rightarrow \rightarrow NO_3^-\cdot X\cdot Y$ is slowed down, and in comparison with normal a larger amount of final ions is formed through the ions $CO_3^-(H_2O)_k$. Second, as the concentration of HNO_3 is lower the clusters with the nucleus NO_3^- are lighter than in the normal case. Lighter clusters, however, are more easily capable of transformations into the ions of the next stage, in the present case $NO_3^-(HCl)$ and HSO_4^-.

As we can see in Table 4, the steady states of changed gas compositions are significantly different from the natural state. If ion formation intensity is higher, and the gas composition changed, the other kinds of ions are important in the stationary state.

In the terms of mobility spectrometry this means that the two spectral lines of the natural state should be replaced by two new lines, whereas one of these (the ions $O_2^-(H_2O)_k$)

Table 4

Steady state concentrations of negative ions

Conditions \ Ions	$NO_3^-(HNO_3)_k \cdot (H_2O)_n$		$O_2^-(H_2O)_k$	$CO_3^-(H_2O)_k$
	$NO_2^- \cdot X \cdot Y$			
Natural	86%	10%	2,5%	1%
Gas composition according to Table 1 $Q=6.7 \cdot 10^6$ $cm^{-3}s^{-1}$	13%	3%	66%	17%
Changed gas composition $Q=6.7 \cdot 10^6$ $cm^{-3}s^{-1}$	2%	-	64%	31%

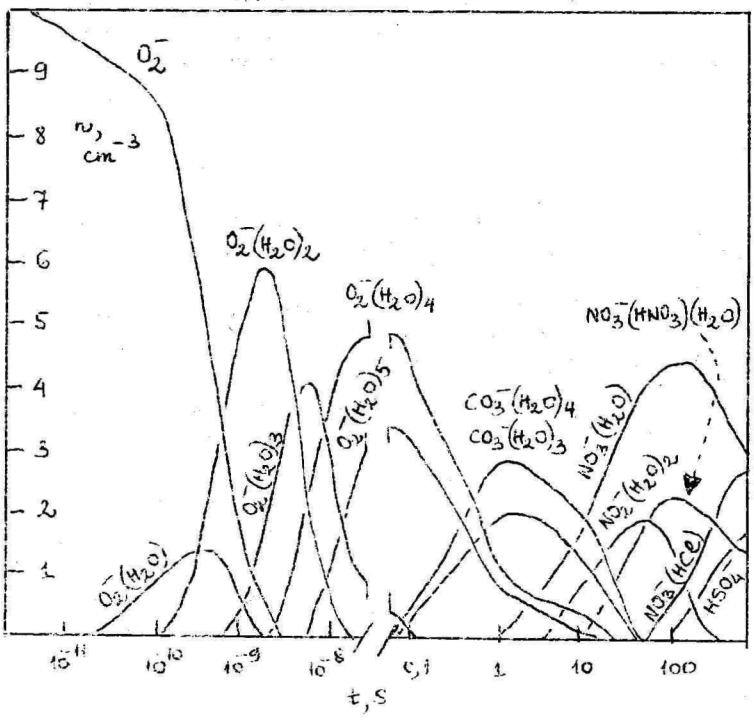

Fig. 3. The curves of the evolution of negative ions in the conditions of changed gas composition.

should have a smaller mobility than the previous line and another (the ions $CO_3^-(H_2O)_k$) a larger mobility.

4. Conclusions

The results of the investigation can be shortly summarised as follows :

If the ion formation intensity is $Q = 6.7 \cdot 10^6$ $cm^{-3} \cdot s^{-1}$, the concentration of neutral gases are changed. Some of the steady state concentrations of the neutral gases are (all in cm^{-3}) : $[NO] = 3.2 \cdot 10^{10}$; $[NO_2] = 2.0 \cdot 10^8$; $[N_2O] = 2 \cdot 10^{13}$; $[HNO_3] = 1 \cdot 10^8$; $[NH_3] = 1 \cdot 10^9$; $[CH_4] = 1 \cdot 10^{14}$; $[C_2H_2] = 2.6 \cdot 10^7$; $[C_2H_4] = 7.0 \cdot 10^9$. The chemical kinetics of ions at such of gas composition is significantly different from the kinetics at normal gas concentrations. In the steady state of positive ions $H_3O^+(H_2O)_k$ become dominant, in the steady state of negative ions the ions $O_2^-(H_2O)_k$ become dominant, whereas the ions $CO_3^-(H_2O)_k$ hold the second place.

References

1. Mohnen, V.A. Formation, nature and mobility of ions of atmospheric importance // In: Electrical processes in atmospheres.- Darmstadt.- 1977.- P. 1-17.

2. Kawamoto, H. and Ogawa, T. First model of negative ion composition in the troposphere // Planet. Space Sci.- 1986.- V. 34.- No. 12.- P. 1229-1239.

3. Huertas, M.L., Fontan, J. and Gonzalez, J. Evolution times of tropospheric negative ions // Atm. Env.- 1978.- V. 12.- P. 2351-2362.

4. Huertas, M.L. and Fontań, J. Evolution times of tropospheric positive ions // Atm. Env.- 1975.- V. 9. - P. 1018-1026.

5. Сальм Я.Й., Лутс А.М. Метод вычисления стационарных концентраций одного класса задач химической кинетики // Уч. зап. Тарт. ун-та.-1988.- Вып. 824.- С. 52-59.

6. Albritton, D.L. Ion-neutral reaction rate constants measured on flow reactors through 1977 // At. Data Nucl. Data Tables.- 1978.- Vol. 22.- No. 1.- P. 1-101.

7. Вирин Л.Н., Джагацпанян Р.В., Карачевцев Г.В., Потапов В.К., Тальрозе В.Л. Ионно-молекулярные реакции в газах.- М., 1979.- 548 с.

8. Лутс А.М., Сальм Я.Й. Кинетика образования положительных легких аэроионов в тропосфере // Уч. зап. Тарт. ун-та.- 1988.- Вып. 824.- С. 60-68.

9. Heitmann, H. and Arnold, F. Composition measurements of tropospheric ions // Nature.- 1983.- V. 306.- P. 747-751.

10. Eisele, F.L. and McDaniel, E.W. Mass spectrometric study of tropospheric ions in the southwestern and northeastern United States // J. Geophys. Res.- 1986.- V. 91.- P. 5183-5188.

11. Сальм Я.Й., Лутс А.М. Кинетика образования отрицательных легких аэроионов в тропосфере // Уч. зап. Тарт. ун-та.- 1988.- Вып. 809.- С. 64-70.

12. Таммет Х.Ф., Ихер Х.Р., Сальм Я.Й. Спектр атмосферных ионов в диапазоне подвижности 0.32-3.2 $см^2/(В.с)$ // Уч. зап. Тарт. ун-та.- 1987.- Вып. 755.- С. 29-44.

КИНЕТИКА ТРОПОСФЕРНЫХ ЛЕГКИХ ИОНОВ ПРИ ПОВЫШЕННОЙ ИНТЕНСИВНОСТИ ИОНООБРАЗОВАНИЯ

А.М. Лутс

Р е з ю м е

В настоящей работе с помощью математического моделирования исследована химическая кинетика тропосферных легких ионов. В математической модели химической кинетики используются линейные уравнения. Влияние химической кинетики ионов на концентрацию нейтральных газов оценивается с помощью итерации.

Согласно результатам работы повышенная интенсивность ионообразования должна оказывать влияние как на химическую кинетику ионов так и на концентрацию нейтральных газов. При интенсивности ионообразования $Q = 6{,}7 \cdot 10^{6}$ см$^{-3} \cdot$с$^{-1}$ вероятными являются следующие концентрации нейтральных газов (в см$^{-3}$):

$[NO] = 3{,}2 \cdot 10^{10}$; $[NO_2] = 2 \cdot 10^{8}$; $[N_2O] = 2 \cdot 10^{13}$;
$[HNO_3] = 1 \cdot 10^{8}$; $[NH_3] = 1 \cdot 10^{9}$; $[CH_4] = 1 \cdot 10^{15}$;
$[C_2H_2] = 2{,}6 \cdot 10^{7}$; $[C_2H_4] = 7 \cdot 10^{9}$.

При таких же условиях преобладающими положительными ионами должны быть ионы $H_3O^+(H_2O)_k$, главными отрицательными ионами должны быть ионы $O_2^-(H_2O)_k$ и ионы $CO_3^-(H_2O)_k$.

THE EFFECT OF SOME ALKYLAMINES ON MOBILITY SPECTRA OF SMALL AIR IONS

T. Parts

Organic nitrogen containing compounds (ONC) occur in the atmosphere as trace gases [1-3]. Some of these could be responsible for the positive air ions present in the troposphere [3]. Amines are one of the groups of ONC that appear more in rural stations than in urban air [2,4,5] and therefore may influence the chemical composition of ions in the rural air.

The major sources of airborne amines are volatilization of animal wastes from feedlots, ammonia based fertilizers, fossil fuel combustion and farm land after application to soils. The amines are organic derivates of ammonia, most of them are liquids with unpleasant "fishlike" odors, quite soluble in water. The detection of amines in the air is connected with some difficulties. The sensitivity of known analytical methods is low and the determination is time consuming [6]. In Air Electricity Laboratory of Tartu University a special air-ion spectrometer for the detection of some air impurities was designed and constructed [7]. This spectrometer measures the mobilities of small air ions produced by corona discharge and precipitated by electric field on the measurement capacitor. The mobility spectra is sensitive to the composition of the air. Previously the influence of some ONC on the mobility of small ions of one second age has been studied by means of this equipment [8,9]. The mobility of negative ions had no changes in comparison to the background spectra. Only spectra of positive ions had evident alternations even if concentrations were too small, in the range of 1 ppt (10^{-9}).

The ONC studied in this paper include alkylamines such as methylamine (MA), dimethylamine (DMA), diethylamine (DEA), *tert*-butylamine (*t*-BA), dibutylamine (DBA), and NNN′N′-tetramethylethylenediamine (NNN′N′-TMEDA) (Table 1).

The non-bonded or lone pair of electrons on N-atom gives amines their basic and nucleophilic character.

$$\underset{(R_2NH,\ R_3N)}{RNH_2} + H_2O \longrightarrow \underset{(R_2NH_2^+,\ R_3NH^+)}{RNH_3^+} + OH^-$$

Table 1

Some properties of ammonia and alkylamines [10]

Compound	Structure	Molecular weight, amu	Boiling point, °C	Basicity constant
1. Ammonia	NH_3	17	-33,5*	$1.8 \cdot 10^{-5}$
Primary amines				
2. MA	CH_3NH_2	31	6*	$4.4 \cdot 10^{-4}$
3. *t*-BA	$(CH_3)_3CNH_2$	73	45	$2.8 \cdot 10^{-4}$
Secondary amines				
4. DMA	$(CH_3)_2NH$	45	7*	$5.2 \cdot 10^{-4}$
5. DEA	$(C_2H_5)_2NH$	73	56	$9.6 \cdot 10^{-4}$
6. DBA	$(C_4H_9)_2NH$	129		
Diamine				
7. NNN'N'-TMEDA	$[(CH_3)_2NCH_2-]_2$	116		

* Water solutions have been used in experiments.

Experimental equipment and conditions are the same as described in [8,9]. Air ion spectrometer for one second age ions was used. The spectra were measured in mobility regions from 0.7 to 2.2 $cm^2/(V \cdot s)$. The masses of such ions are 50-1000 amu, the size - some nanometers. 0.5-1 ml of amines have been put on the plate before the spectrometer. The vaporization at room temperature was determined the concentration. Mobility spectra of air ions with and without adding amines were compared. All experiments were carried out at normal pressure $\sim 10^5$ Pa and room temperature ~ 295 K in a relatively clean laboratory room. Relative humidity was 33 - 40 %. The concentrations of added amines are 0.1 ppm - 1 ppt.

Average mobilities of the observed air ions are presented in Table 2. Opposite to heterocyclic amines [8] the mobility of both negative and positive ions changes.

Negative ions. All negative ions become heavier, the mobilities have been decreased (Table 2, Figs. 1-3b). The average mobility is the lowest for DBA. As it can be seen in Fig.2b, there are some ions with mobilities < 0,75 $cm^2/(V \cdot s)$. This fact allows us to persume that DBA may act as a nucleation center for larger particles, for aerosol.

Table 2

Experimental data about average mobilities ($cm^2/(V \cdot s)$)

Spectra of	Positive ions	Negative ions
1. Background	1.15	1.67
2. NH_3	1.22	1.57
3. CH_3NH_2	1.12	1.60
4. $(CH_3)_3CNH_2$	1.00	1.54
5. $(CH_3)_2NH$	1.15	1.33
6. $(C_2H_5)_2NH$	1.15	1.33
7. $(C_4H_8)_2NH$	0.94	1.30
8. $(CH_3)_2N(CH_2)_2N(CH_3)_2$	1.34	1.37

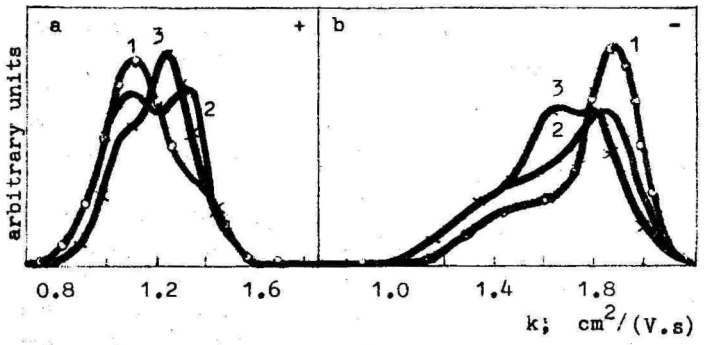

Fig. 1. Mobility spectra of small ions of one second age: 1 - background spectra; 2 - NH_3; 3 - CH_3NH_2.

Secondary amines have more obvious effect on the mobility spectra of negative ions. For DMA there are two clearly seen peaks 1.5 and 0.9 $cm^2/(V \cdot s)$ in addition to background more expressed 1.9 $cm^2/(V \cdot s)$. DEA causes 3 additional peaks ~1.45, ~1.20, and ~0.90 $cm^2/(V \cdot s)$; but DBA at least 3 new peaks ~1.28, ~1.00, and < 0.75 $cm^2/(V \cdot s)$.

The masses ~120, ~150, and ~200 amu [11] may be responsible for the first main peaks (Fig. 2b). It has been suggested that attachment reactions of secondary amines to stable air ions occur. If the most stable negative ions of one second age in air are $NO_3^-(H_2O)$ and $OH^-(H_2O)_3$ [3,12] ,

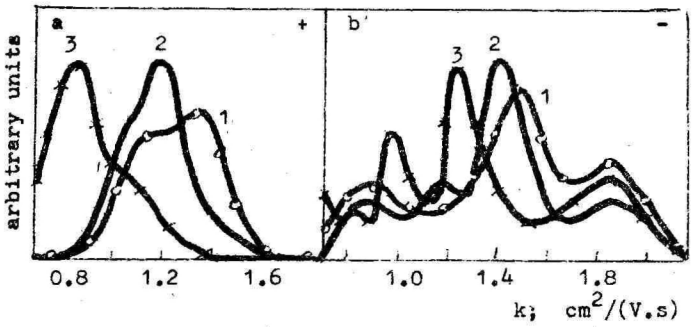

Fig. 2. The influence of secondary amines on the mobility spectra: 1 - $(CH_3)_2NH$, 2 - $(C_2H_5)_2NH$, 3 - $(C_4H_9)_2NH$.

alkylamines can agglomerate with these clusters to produce larger negative ions.

DMA: $NO_3^-(H_2O) + (CH_3)_2NH \rightarrow NO_3^-((CH_3)_2NH)(H_2O)$; m =123 amu
$OH^-(H_2O)_3 + (CH_3)_2NH \rightarrow OH^-((CH_3)_2(H_2O)_3$; m =114 amu

DEA: $NO_3^-(H_2O) + (C_2H_5)_2NH \rightarrow NO_3^-((C_2H_5)_2NH)(H_2O)$; m =153 amu
$OH^-(H_2O)_3 + (C_2H_5)_2NH \rightarrow OH^-((C_2H_5)_2NH)(H_2O)_3$; m =144 amu

DBA: $NO_3^-(H_2O) + (C_4H_9)_2NH \rightarrow NO_3^-((C_4H_9)_2NH)(H_2O)$; m =209 amu
$OH^-(H_2O)_3 + (C_4H_9)_2NH \rightarrow OH^-((C_4H_9)_2NH)(H_2O)_3$; m =200 amu

And so we can conclude that the formation of such larger negative ions is connected with the changing of mobilities to ~1.50, ~1.45, and ~1.28 $cm^2/(V \cdot s)$ for DMA, DEA, and DBA respectively.

The second peaks 1.20 (DEA) and 1.00 $cm^2/(V \cdot s)$ (DBA) are connected with masses ~ 230 and ~ 350 amu [11]. Ions $NO_3^-((C_2H_5)_2NH)(H_2O)$, $OH^-((C_2H_5)_2NH)_2(H_2O)_3$, and $NO_3^-((C_4H_9)_2NH)_2(H_2O)$, $OH^-((C_4H_9)_2NH)_2(H_2O)_3$ have such masses. Agglomeration of 2 amine molecules occurs. These results are in agreement with [13] , clusters with amines have greater stability than with other organic molecules. In addition, our experiment shows that only alkylamines take part in formation of stable negative clusters. Heterocyclic amines

don't produce stable clusters, they have no effect on mobility spectra of negative ions [8].

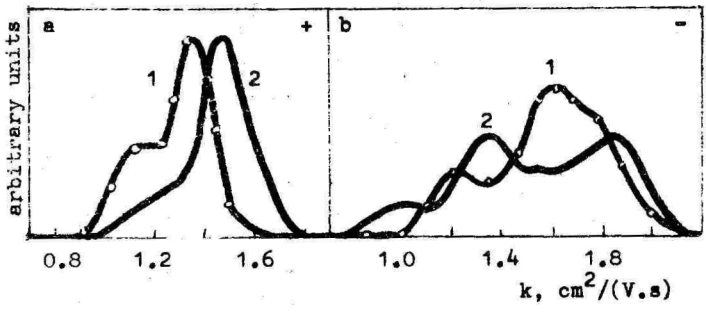

Fig. 3. The influence of *t*-BA and NNN'N'-TMEDA on the mobilities. 1 - $(CH_3)_3CNH_2$; 2 - $(CH_3)_2NCH_2CH_2N(CH_3)_2$.

Positive ions. The shape of mobility spectra of studied positive ions is less complicated than of negative ions, only 2 peaks have been shown (Figs. 1-3a). The average mobility of positive ions compared to background spectra changes more for DBA - decreases and for NNN'N'-TMEDA - increases (Table 2). The higher mobility of diamine is in agreement with results obtained by Karpas [14], internal hydrogen bonding takes place. If ions of family $NH_4^+(H_2O)_n$ and $H_3O^+(H_2O)_n$ are the most distributed ones in relatively unpolluted air [3, 9], alkylamines as stronger bases than H_2O and NH_3 may give proton transfer reactions:

$$NH_4^+(H_2O)_n + xRNH_2 \longrightarrow (RNH_2)_xH^+(H_2O)_m + NH_3 + (n-m)H_2O$$

$$H_3O^+(H2O)_n + yR_2NH \longrightarrow (R_2NH)_yH^+(H_2O)_m + (n+1-m)H_2O,$$

where R = CH_3-, C_2H_5-, C_4H_9-, etc.

In surroundings of positive ion core there may occur changes in a number of water and/or neutral amine molecules. At present it is difficult to explain the structure of positive ions in air polluted with amines. Mass-spectrometric and gas-chromatographic experiments should be carried out but we do not have the necessary equipment for them. Nevertheless it has been suggested that protonated amines surrounded with

molecules of water and/or amines may be responsible for mobility spectra of positive ions. In case of DBA the peak ~0.88 $cm^2/(V \cdot s)$ is connected with mass ~500 amu, which may be DBA in surroundings of 20 molecules of H_2O : $((C_4H_9)_2NH)H^+(H_2O)_{20}$ - all hydrogen bounds of protonated DBA are realized:

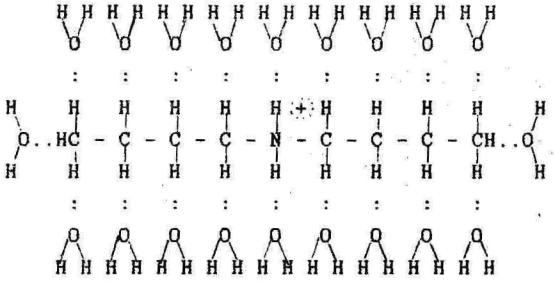

Conclusions. Alkylamines influence both positive and negative small air ion mobility spectra. The chemical composition as well as mass of air ions changes. Therefore the differences in mobilities of ions in rural and urban air [15] may be connected with the higher concentration of amines in the rural air.

The mobility spectrometry at atmospheric pressure is an easy way to identify alkylamines in the air.

References

1. Environmental Chemistry, ed. by J.O'M. Bockris, New York: Plenum Press, 1977.- 662 p.

2. Söderlund, R., Rosswall, T. The Nitrogen Cycles // The Handbook of Environmental Chemistry, ed. by O. Hutzinger.- V. 1, Part B.- Berlin: Springer Verlag, 1982.- P. 61-81.

3. Eisele, F.L. Identification of tropospheric ions // J. Geophys. Res.- 1986.- V. 91, No. D7.- P. 7897-7906.

4. Cadle, S., Countess, R., Kelly, N. Nitric acid and ammonia in urban and rural locations // Atmos. Envir.- 1982.- V. 16, No. 10.- P. 2501-2506.

5. Хорват Л. Кислотный дождь.- М.: Стройиздат, 1990.- 192 p.

6. Leithe, W. Die Analyse der Luft und ihrer Verunreinigungen in der freien Atmosphare und am Arbeitsplats. - Stuttgart: Wissensch. Verlagsg. mbH, 1974. - 340 S.

7. Таммет Х.Ф., Хилпус А.О. и др. Спектрометр аэроионов для обнаружения некоторых примесей воздуха // Уч. зап. Тарт. ун-та. - 1977. - Вып. 409. - С. 84-88.

8. Партс Т.М., Сальм Я.Й. Воздействие пиридина и некоторых его гомологов на спектр подвижности положительных легких аэроионов // Уч. зап. Тарт. ун-та.- 1988.- Вып. 809.- С. 71-78.

9. Партс Т.М. О природе положительных легких аэроионов односекундного возраста // Уч. зап. Тарт. ун-та.- 1988.- Вып. 824.- С. 69-77.

10. Atkins, R.C., Carey, F.A. Organic Chemistry.- N.-Y.: McGraw-Hill Publ. Company, 1990.- 1002 p.

11. Kilpatrick, W.D. An experimental mass-mobility relation for ions in air at atmosheric pressure // Proc. 19th Conf. Mass Spectrometry.- 1971.- Atlanta.- P. 320-325.

12. Parts, T. On the nature of negative small air ions of an ageing time of one second // Acta et comm. Univ. Tartuensis.- 1990.- V.880.- P. 52-60.

13. Huertas, M.L., Fontan, J. Formation of stable positive and negative small ions of troposheric interest // Atmos. Envir.- 1982.- V. 16.- No. 10.- P. 2521-2527.

14. Karpas,Z. Evidence of proton induced cyclization of α,ω diamines from ion mobility measurements // Int. J. Mass. Spectrom. Ion Process.- 1989.- V.93.- P. 237-242.

15. Таммет Х.Ф., Ихер Х.Р., Миллер Ф.Г. Спектр подвижностей односекундных легких аэроионов в природном воздухе //Уч. зап. Тарт. ун-та.- 1985. - Вып. 707. - С. 26-36.

ВЛИЯНИЕ НЕКОТОРЫХ АЛКИЛАМИНОВ НА СПЕКТРЫ ПОДВИЖНОСТИ ЛЕГКИХ АЭРОИОНОВ

Т.М.Партс

Р е з ю м е

Измерены спектры подвижности легких аэроионов односекундного возраста в лабораторных условиях. Алкиламины влияют на спектры обоих полярностей. Подвижность отрицательных ионов всегда уменьшалась. Подвижность положительных ионов под влиянием алкиламинов или уменьшалась или увеличивалась. Наибольшее влияние на спектры имели диамины.

ЗАВИСИМОСТЬ ПОДВИЖНОСТИ ИОНА ОТ ЕГО МАССЫ

Я.И. Салъм

Спектрометрия подвижности является самым простым, недорогим и распространенным методом экспериментального исследования аэроионов в естественных условиях атмосферы. Результатов измерения спектров подвижности этим методом накоплено относительно много как в естественных условиях [1, 2, 3], так и в условиях искусственной ионизации [4, 5, 6]. Однако подвижность не является фундаментальной величиной, она характеризует не только ионы, но также и среду. В целях решения фундаментальных проблем, например, о составе и структуре ионов, целесообразно было бы перейти от подвижностей к массам или размерам ионов. С одной строны, для этого можно использовать теорию подвижности ионов, с другой - экспериментальные данные о совместном измерении подвижностей и масс ионов.

Первую достаточно строгую теорию подвижности ионов, основанную на методе передачи импульса, опубликовал Ланжевен [7]. Теория относилась к случаю слабых полей и наряду с силами отталкивания непроницаемых сфер учитывала также силы притяжения между ионами и молекулами, обратно пропорциональные пятой степени расстояния.

Спустя около десятка лет, Чепмен и (независимо) Энског разработали строгую кинетическую теорию неоднородных газов, состоящих из сферически симметричных частиц. Они применили свои результаты к задачам переноса для неионизованных газов, чо полученное ими выражение для коэффициента взаимной диффузии можно с помощью соотношения Эйнштейна использовать для определения подвижностей [8, 9]. Первое приближение теории Чепмена-Энскога можно считать наиболее адекватной теорией подвижности ионов в слабых полях. Подвижность иона по теории выражается формулой

$$K = \frac{3\,\pi\,q}{8N\sqrt{2kT\mu}\;\Omega^{(1,1)}}, \qquad (1)$$

где q - заряд иона,

N - концентрация молекул газа,

k - постоянная Больцмана,

T - температура,

$\mu = (m^{-1} + M^{-1})^{-1}$ - приведенная масса,

m - масса молекулы газа, M - масса иона,

$\Omega^{(1,1)}$ - интеграл столкновений первого порядка, который представляет собой взвешенное среднее транспортное сечение рассеяния.

$$\Omega^{(1,1)} = \frac{1}{2}(kT)^{-3}\int_0^\infty \exp[-E/(kT)]E^2\sigma^{(1)}(E)\mathrm{d}E \,, \qquad (2)$$

где E - исходная кинетическая энергия относительного движения сталкивающихся частиц.

Транспортное сечение

$$\sigma^{(1)}(E) = 2\pi\int_0^\pi (1 - \cos\vartheta)\sigma(\vartheta,E)\sin\vartheta\,\mathrm{d}\vartheta \,, \qquad (3)$$

где ϑ - угол рассеяния,

$\sigma(\vartheta,E)$ - дифференциальное сечение рассеяния.

Нормировочные постоянные в приведенных формулах выбраны так, чтобы интеграл столкновений и транспортное сечение равнялись πd^2 в случае столкновений классических твердых сфер диаметром d .

В общем случае угол рассеяния и дифференциальное сечение рассеяния зависят от вида потенциала взаимодействия иона с нейтральной молекулой. Одним из наиболее простых потенциалов взаимодействия, представляющих практический интерес, является потенциал поляризационного взаимодействия

$$U_P(r) = -\frac{\alpha q^2}{2r^4} \,, \qquad (4)$$

где α - поляризуемость нейтральной частицы (молекулы),

r - расстояние между частицами.

В таком предельном случае, когда размеры частиц пренебрежимо малы, а действует только потенциал $U_P(r)$, приведенную к нормальным условиям подвижность иона можно выразить в виде

$$K_P = \frac{35,9}{\sqrt{\alpha\mu}} \,, \qquad (5)$$

где α выражена в атомных единицах (куб боровского радиуса),

μ - в а.е.м., а K_P измеряется в $см^2/(В\cdot с)$.

По мере увеличения размеров частиц роль дальнодействующих сил уменьшается, а в пределе может оказаться адекватной модель твердых шаров

$$K_S = \frac{3q}{8N\sqrt{2\pi kT\mu}\,d^2} \,, \qquad (6)$$

где $d = (d_I + d_M)/2$,

d_I и d_M - эффективные диаметры иона и молекулы.

Ланжевен рассматривал потенциал вида

$$U(r) = \begin{cases} \infty \text{ при } r < d \\ U_P(r) \text{ при } r > d \end{cases} \quad (7)$$

По теории Ланжевена получены предельные формулы (5) и (6), а в промежуточном случае решение опирается на специальную функцию, найденную численным расчетом [6,9]. На самом деле потенциалы взаимодействия иона с нейтральной частицей сложнее, чем по формуле (7), и расчеты сложнее. Соответствующий обзор содержится в монографии [10].

Экспериментальные данные о подвижностях идентифицированных ионов получены в основном в чистых однокомпонентных газах, измерений в обычном воздухе мало. Наиболее близкими данными к воздушной среде можно считать те, которые получены в азоте. На рис. 1 приведены результаты ряда исследований идентифицированных ионов в сухом воздухе [11, 12] и в азоте [13-21].

Основная масса данных лежит в промежутке подвижности от 1 до 3 $см^2/(В \cdot с)$. Наибольший интервал перекрыт данными из работы [20]. По данным последней работы, как видно из рис. 1, нетрудно провести четкую функциональную кривую. Тамметом составлена аппроксимирующая формула для этих данных, которая согласована с формулой Стокса-Кенингема-Милликена, а также с формулой Ланжевена-Эпштейна, вытекающей из модели твердых шаров [22]. С уточнениями от автора этой формулы (в СИ):

$$K = \frac{\gamma q}{6\pi\eta r_T}\left(1 + \frac{l}{r_T}\{A + B\exp(-C\frac{r_T}{l}) + (\frac{9}{4} - A - B)\exp[-(\frac{r_I}{r_C})^h]\}\right), \quad (8)$$

где $\gamma = \sqrt{1 + \frac{m}{M}} \Big/ \left(1 + \frac{0{,}201q^2\alpha}{8\pi\varepsilon_0 kTr^4}\right)$, $l = \frac{\eta}{N}\sqrt{\frac{\pi}{2kTm}}$, $r_T = r_0 + r_I$,

ε_0 - электрическая постоянная, η - динамическая вязкость газа, l - средняя длина свободного пробега молекул газа, r_T - эффективный транспортный радиус иона, $r_I = d_I/2$. В случае больших ионов $2r_T$ совпадает с размером d, фигурирующим в формуле (6). $A = 1{,}4$; $B = 0{,}35$; $C = 0{,}45$ - эмпирические постоянные.

Эффективный радиус иона r_I принят равным $\sqrt[3]{3M/(4\pi\rho)}$, где ρ - плотность иона. Размер r_C перехода от режима упругих столкновений к режиму термической аккомодации и крутизна этого перехода h определены по критерию наилучшей аппроксимации, также как r_0 и ρ . Исходя из экспериментальных данных работы

[20], найдены значения r_0 = 0,36 нм, ρ = 1,8 г/см^3, r_c = 0,66 нм, и h = 6. Значение r_c близко к физической границе между кластерами и малыми частицами [23].

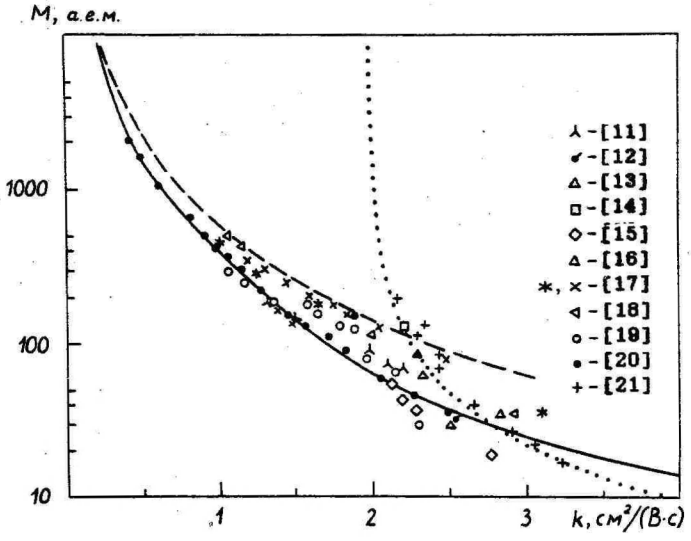

Рис. 1. Зависимость подвижности ионов от их массы: пунктирная линия - расчет по формуле (5); точечная - (6); сплошная - (8).

Видно, что значительное число экспериментальных точек отклоняется от сплошной кривой на рис. 1, а строгая функциональная зависимость не соблюдается. Более тесную корреляцию можно ожидать, если ограничить класс рассматриваемых ионов. По выводам работы [17], если рассмотрены всевозможные различные сорта ионов, то среднеквадратическая погрешность определения массы по подвижности составляет ±20%. В случае же ограничения класса ионов структурно родственными соединениями (например, ионами полициклических углеводородов) погрешность не превышает ±2%. На рис. 1 данные из [17] для ионов полициклических углеводородов обозначены крестиками, а для остальных ионов - звездочками. Более подробные данные о зависимостях масса-подвижность разных классов ионов приведены в [24].

Кроме экспериментальных точек и вышеупомянутой аппроксимирующей функции, на рис. 1 приведены также графики функций по формулам (5) и (6). В последнем случае использованы одина-

ковая плотность ионов 1,2 г/см^3 и радиус молекулы азота 0,205 нм, рассчитанный по плотности жидкого азота. На самом деле можно ожидать уменьшение плотности ионов с уменьшением их радиуса, что привело бы к улучшению совпадения кривой с экспериментальными данными.

Разброс экспериментальных точек вокруг функциональной кривой по всей вероятности обусловлен природой дрейфа ионов. Однако, некоторые данные наводят на мысль о возможных методических ошибках. Так, например, для иона хлора в азоте опубликованы различающиеся значения приведенной подвижности 2,49; 2,83; 2,87; 2,92 и 3,13 см^2/(В·с) соответственно в работах [20, 13, 25, 18, 17]. Для иона йода опубликованы значения 1,52; 2,45; 2,51 и 2,69 в работах [20, 19, 18, 17]. По-видимому, нужен более глубокий анализ этих данных.

Литература

1. Misaki, M. Studies on the atmospheric ion spectra (II) // Pap. on Meteorol. and Geophys. - 1961.- V. 12, Nos. 3-4.- P. 261-276.

2. Eichmeier, J. Vergleich der Beweglichkeitsspektren von "natürlichen" Luftionen und der verwendeten Messverfahren // Z. Geophys.- 1972.- Bd. 38.- S. 915-923.

3. Таммет Х.Ф., Ихер Х.Р., Сальм Я.Й. Спектр атмосферных ионов в диапазоне подвижности 0,32-3,2 см^2/(В·с) // Уч. зап. Тарт. ун-та.- 1987.- Вып. 755.- С. 29-44.

4. Ихер Х.Р., Сальм Я.Й. Зависимость спектра подвижности легких аэроионов от химических примесей в воздухе // Уч.зап. Тарт. ун-та.- 1982.- Вып. 631.- С. 27-34.

5. Таммет Х.Ф., Ихер Х.Р., Миллер Ф.Г. Спектр подвижностей односекундных легких аэроионов в природном воздухе // Уч. зап. Тарт. ун-та.- 1985.- Вып. 707.- С. 26-36.

6. Партс Т.М., Сальм Я.Й. Воздействие пиридина и некоторых его гомологов на спектр подвижности положительных легких аэроионов // Уч. зап. Тарт. ун-та.- 1988.- Вып. 809.- С. 71-78.

7. Langevin, P. Une formule fondamentale de théorie cinétique // Ann. chim. phys.- 1905.- T. 5.- P. 245-288.

8. Смирнов Б.М. Физика слабоионизованного газа.- М.: Наука, 1967.

9. Мак-Даниель И. Процессы столкновений в ионизованных газах.- М.: Мир, 1967.

10. Мак-Даниель И., Мэзон Э. Подвижность и диффузия ионов в газах.- М.: Мир, 1976.

11. Huertas, M.L., Marty, A.M., Fontan, J. On the nature of positive ions of tropospheric interest and on the effect of polluting organic vapors // J. Geophys. Res.- 1974.- V. 79, No. 12.- P. 1737-1743.

12. Sinnott, G., Golden, D.E., Varney, R.N. Positive--ion mobilities in dry air // Phys. Rev.- 1968.- V. 170, No. 1.- P. 272-275.

13. Viehland, L.A., Fahey, D.W. The mobilities of NO_3^-, NO_2^-, NO^+, and Cl^- in N_2: A measure of inelastic energy loss // J. Chem. Phys.- 1983.- V. 78, No. 1.- P. 435-441.

14. Thackston, M.G., Eisele, F.L., Ellis, H.H.W., McDaniel, E.W. Mobilities of Cs^+ ions in molecular gases N_2, O_2, CO, and CO_2 // J. Chem. Phys.- 1977. - V. 67, No.3.- P. 1276-1277.

15. Dotan, I., Albritton, D.L., Lindinger, W., Pahl, M. Mobilities of CO_2^+, N_2H^+, H_3O^+, $H_3O^+H_2O$, and $H_3O^+(H_2O)$ ions in N_2 // J. Chem. Phys. - 1976.- V. 65, No. 11.- P. 5028-5030.

16. Thackston, M.G., Ellis, H.W., Pai, R.Y., McDaniel,E.W. Mobilities of Rb^+ ions in He, Ne, Ar, H_2, N_2, and CO_2 // J. Chem. Phys.- 1976.- V. 65, No. 5.- P. 2037-2038.

17. Griffin, G.W., Dzidic, I., Carroll, D.I. et al. Ion mass assignments based on mobility measurements. Validity of plasma chromatographic mass mobility correlations // Anal. Chem.- 1983.- V. 45, No. 7.- P. 1204-1209.

18. Karasek, F.W., Tatone, O.S., Kane, D.M. Study of electron capture behaviour of substituted aromatics by plasma chromatograph // Anal. Chem. - 1973. - V. 45 No. 7.- P. 1210-1214.

19. Carroll, D.I., Mason, E.A. The theoretical relationship between ion mobility and mass // Proc. Annu. Conf. Mass Spectrosc. 19th.- 1971.- P. 315-319.

20. Kilpatrick, W.D. An experimental mass-mobility relation for ions in air at atmospheric pressure // Proc. Annu. Conf. Mass Spectrosc. 19th.- 1971.- P. 320-325.

21. Mitchell, J.H., Ridler, K.E.W. The speed of positive ions in nitrogen // Proc. Roy. Soc. A. - 1934. - V. 146.- P. 911-921.

22. Tammet, H. Fair-weather electricity on ground level // Proc. 8th Int. Conf. on Atmospheric Electricity.- Uppsala,

1988.- P. 21-30.

23. Петров Ю.И. Кластеры и малые частицы.- М.: Наука, 1986.

24. Plasma Chromatography / Ed. by T.W. Carr.- N.Y. and Lond.: Plenum Press, 1984.

25. Byers, M.S., Thackston, M.G., Chelf, R.D. et al. Mobilities of Tl^+ ions in Kr and Xe, Li^+ in Kr and Xe, and Cl^- in N_2 // J. Chem. Phys. - 1983. - V. 78, No.5.- P. 2796-2797.

THE DEPENDENCE OF ION MOBILITY ON THE MASS

J. Salm

S u m m a r y

There is a significant amount of data about mobilities of ions measured in various conditions. However, for solving more fundamental problems concerning the chemical composition and structure of ions, the dependence of ion mobility on the mass is to be determined. An analytical survey of the above dependence is presented in this paper.

The first fairly strict theory for ion mobilities was developed by Langevin [7]. At present, the first approximation of the theory by Chapman and Enskog may be regarded as the most adequate theory for ion mobilities in weak fields (equations 1-3).

On the other hand, there are experimental data of simultaneous measurements of ion mobilities and masses, a number of which is presented in Fig. 1. The data by Kilpatrick [20] cover a wide range of masses, have a fairly functional shape, and a semiempirical equation has been published by Tammet on this basis [22]. However, the whole amount of data in Fig. 1 demonstrates a considerable scattering and obviously the problem needs further study.

THE IDENTIFICATION OF PARTICLE SOURCES BY AEROSOL SPECTRA MEASUREMENTS

Ü. Kikas

In aerosol measurements, especially in the polluted areas the identification of particle sources is an important problem.

An attempt has been made on the basis of measured aerosol spectra to ascertain aerosol flux from different directions and to connect them with real sources.

Measurement conditions. Measurements have been carried out on the coast of the *Baltic Sea* on *Kura* peninsula (*Lithuania*) at field station *Preila*. The measurements were carried out on an open beach at ~ 300 m from water on the roof of a pavilion at about 4 m above ground. The probable aerosol sources are situated sparsely in different directions as it can be seen in the map of surroundings (Fig. 1). The most important sources of contamination, the city and harbour of *Klaipeda* are situated at about 40 km to *North East* (direction 1, Fig.2), the main long-distance source *Kaliningrad* ~ 200 km to *South* (direction 5). The village *Preila* and the road along

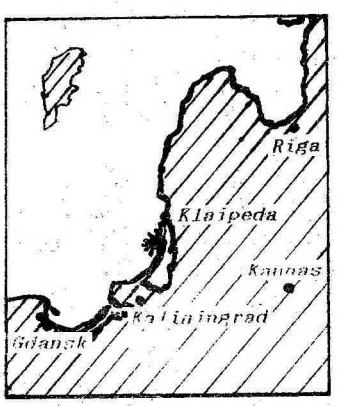

Fig.1. The map of surroundings of measurement location.

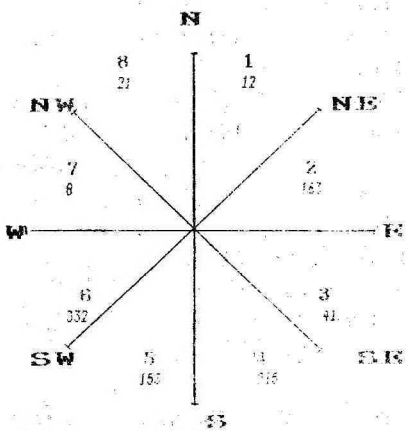

Fig.2. Diagram of codes and of occurence frequencies of wind direction.

the peninsula can be considered the main local sources within a radius of 4 km. The particles from the natural sources, the sea and the forest, come from well distinguishable directions.

The aerosol spectra, the wind velocity and the wind direction have been measured in every 15 minutes during 12 days. The electric aerosol spectrometer (EAS) designed in Tartu University [1] was used for aerosol spectra measurements in the size range of 0.01 to 10 μm.

Data analysis. The effect of wind direction on the aerosol concentration was analyzed by means of "*STATIGRAPHICS*" data processing system. The wind directions have been divided into 8 groups according to the Fig. 2 (the *North* direction is included into group 1, the *NE* direction into group 2 etc.).

The measured aerosol spectra are presented as a set of 12 fractional number concentrations n_k (k = 1 ... 12). (Table 1). For each n_k the mean concentrations from each wind direction j (n_{k1}, n_{k2} ... n_{k8}) have been calculated, statistically tested in terms of difference and arranged in order.

Before statistical processing the normal distribution hypothesis was checked for n_k . It appeared, that the values of n_1 - n_4 and n_8 - n_{12} fitted in with lognormal distribution, those of n_5 - n_7 rather with normal distribution. Thereby, for the following analysis the logarithms of concentrations log n_1 - log n_4, log n_8 - log n_{12} and the concentrations n_5 - n_7 have been used.

Also, the frequency diagram of wind directions was calculated. As it can be seen in the diagram (Fig. 2) the winds from directions 1, 7 and 8 occurred seldom, thereby their statistical weights were low. Later on the directions 7 and 8 will be considered together because they have similar source characteristics.

Results and discussion. We found, that the mean aerosol concentrations from different directions n_{k1}, n_{k2} ...n_{k8} are significantly different for all fractions. After arranging n_j in order and filling in Table 1 we found that the highest amounts of fine, submicron and coarse particles were connected with different directions.

In Table 1 the coarse particle group (above 1.8 μm dia) and the small particle group (below 1.8 μm dia) are clearly distinguishable : the highest concentrations of coarse particles are coming from direction 6 (5 and 4), the highest number of smaller particles from directions 1 and 2. In addition, there are differences inside the small particle group; the third preferable direction for fine particles (below 0.1 μm dia) is 6 while that of for submicron ones (0.1 to 1 μm dia) is 5; the highest amounts of very fine particles (below 0.018 μm dia) are coming from directions 2 and 3. Evidently, the aerosol flux is distributed according to the wind directions and the main sources of different size particles are not the same.

Table 1

The effect of wind direction
on the aerosol fractional concentrations

Size limits d, μm	Wind direction	*N-NE*	*NE-E*	*E-SE*	*SE-S*	*S-SW*	*SW-W*	*W-N*
	Code	1	2	3	4	5	6	8
	Fract.No.	Position in order of concentrations						
0.010 - 0.018	1	5	1	2	4	6	3	7
0.018 - 0.032	2	2	1	4	5	6	3	7
0.032 - 0.056	3	1	2	6	4	5	3	7
0.056 - 0.10	4	1	2	6	3	5	4	7
0.10 - 0.18	5	1	2	4	5	3	7	8
0.18 - 0.32	6	1	2	4	5	3	7	8
0.32 - 0.56	7	1	2	4	5	3	6	7
0.56 - 1.0	8	1	3	4	5	2	6	7
1.0 - 1.8	9	1	3	4	5	2	6	7
1.8 - 3.2	10	8	4	5	3	2	1	7
3.2 - 5.6	11	8	4	5	2	3	1	7
5.6 - 10.0	12	8	4	5	3	2	1	7

For the identification of aerosol sources we have to evaluate the distance the particles have covered. The particles can originate from as faraway distance as they can cover during their life time. Theoretical estimations of life time (decay constant) of coarse particles give the values from 180 to 20 hours [2, 3]. The mean wind velocities from directions 5 and 6 are about 8 m/s. Accordingly, the coarse particles may theoretically be driven even from the distances from 600 to 5000 km and originate from land sources in *Europe*. Most likely the main part of them originates from sea which stretches in hundreds of kilometers in direction 6. This idea is supported also by the results of an experimental estimation of the residence times of atmospheric aerosol (Table 2). We obtained the fractional residence times τ from measurement data as the time constants of fractional autocorrelation functions [4]. These experimental residence times are the result of combined effect of residence of a single particle and of the spatial inhomogenity of particles. The short experimental residence times of coarse aerosol (much

Table 2

Residence times of aerosol fractions in Preila

Size limits, μm	Frac. No.	τ, min
0.010 - 0.018	1	< 15
0.018 - 0.032	2	< 15
0.032 - 0.056	3	15
0.056 - 0.10	4	45
0.10 - 0.18	5	75
0.18 - 0.32	6	270
0.32 - 0.56	7	320
0.56 - 1.0	8	260
1.0 - 1.8	9	90
1.8 - 3.2	10	25
3.2 - 5.6	11	20
5.6 - 10.0	12	25

shorter than theoretical ones) refer to the high inhomogenity of particles. The rate of inhomogenity depends on the distance from the particle generators: the smaller the distance the smaller the smoothing rate of inhomogenity caused by uneven acting of generators. Thus, the coarse particles have likely been born over the sea surface due to the dispersion of sea water.

The highest flux of smaller particles (below 2 μm dia) from directions 1 and 2 (Table 1) is an expected result. Particles coming from these directions can originate from *Klaipeda*, from inland of *Lithuania* or from local sources.

The submicron particles (5-9 fraction) are of highest residence, their life times have been estimated to be about 200 hours [2,3]. Thereby, they are likely to be originated from long distance sources. As it can be seen in Table 1, the three preferable directions of submicron particles are 1, 2 and 5. The directions 1 and 2 have been analysed before, the particles from direction 5 can be originated from *Kaliningrad* and from farther *East-European* sources.

The finest particles (below 0.032 μm dia) differ from others in this group and their first preferable direction is 2. The theoretical life times of those particles in background conditions are below 1 hour [2]. Also the experimental residence times of them (Table 2) are very short. By average winds of 6 m/s these particles can reach measurement place from distance not longer than 20 km. Thereby, the finest particles are mostly generated over the peninsula by emissions from the local sources (village, road, forest) and over the gulf. While also the "pure" sea direction 6 is inside the preferable directions, the importance of sea surface as a generator of very fine particles is to be appointed here. Presumably they are dry residues of sea particles. The finest particles born in polluted air over Klaipeda hardly reach the measurement place in their original size (life times about 1 hour; the average winds from direction 1 9 m/s). During motion they grow larger and transfers into the submicron part of spectra.

In addition, the wind velocities and daily frequencies of wind direction were studied. The results do not contradict the above interpretations.

Conclusions. From the analysis of the effect of wind direction on the aerosol spectra the result was obtained that the distribution of particle concentrations by wind is not the same for particles of different size. It was confirmed that the main sources of very fine, submicron and coarse aerosol particles reaching measurement place are not the same.

The distribution of particle flux was in agreement with location of probable aerosol sources. The distances from the sources were estimated taking into account the life times of particles.

Acknowledgement

The author thanks Institute of Physics of the Republic of Lithuania, Dr. Girgzdysh and Dr. Ulevicius for organizing the measurements.

References

1. Mirme, A. et al. A multichannel electric aerosol spectrometer // 11th Int. Conf. Atmospheric Aerosols, Condensation and Ice Nuclei.- Budapest, 1984.- Pre-print Vol. 2.- P. 155-159.

2. Розенберг Г.В., Любовцева Ю.С., Горчаков Г.И. Фоновый аэрозоль Абастумани // Изв. АН СССР ФАО 1982.- Т. 18.- No.8.- P. 822-839.

3. Jaenicke, R. Our knowledge about the atmospheric aerosol // Eleventh Int. Conf. Atmosph. Aerosols, Condensation and Ice Nuclei. - Budapest, 1984.- Pre-print Vol. 1.- P. 99 - 107.

4. Мирме А.А., Кикас Ю.Э., Тамм Э.И. Динамика спектра атмосферного аэрозоля приземного слоя // Acta et comm. Univ. Tartuensis.- 1988.- V. 824.- P. 109-122.

О ВОЗМОЖНОСТИ ОПРЕДЕЛЕНИЯ ИСТОЧНИКОВ ЧАСТИЦ ПО ИЗМЕРЕНИЯМ СПЕКТРА АЭРОЗОЛЯ

Ю.Э. Кикас

Р е з ю м е

На берегу Балтийского моря проведены измерения атмосферного аэрозоля. Изучена зависимость спектра аэрозолей от направления ветра. Получено, что аэрозольные потоки из разных направлений статистически отличаются. При этом распределение потоков частиц по направлениям отличалось для мелких ($d < 1.8$ m), и больших ($d > 1.8$ m) частиц. Сделан вывод, что частицы различного размера связаны с различными источниками.

Показано, что по измеренным спектрам аэрозоля, учитывая времена жизни частиц, можно идентифицировать удаленные источники аэрозоля.

THE NEUTRALIZATION OF AEROSOL

E. Tamm, L. Langus

During formation aerosol particles often get unipolar charges (electrostatic spraying, electrical separation), or large bipolar charges (balloelectric effect in spraying of liquids, triboelectricity in atomization of powders). In practical applications these charges are sometimes inadmissible as they can cause additional loss of particles. Therefore the aerosol should be neutralized. It is not possible to ensure complete neutralization. Let us assume that the neutralization is the formation of a stationary charge distribution of particles when the percentage of particles with i elementary charges remains constant at any time. An existence of bipolar ionic atmosphere in the aerosol is necessary during a rather long period to achieve such charge distribution.

The aim of this paper is to study the conditions of the formation of the stationary charge distribution in one concrete case. For instance, it is of interest in the graduation of aerosol spectrometers, using test aerosols obtained in electrical separation.

Many papers have been written about the functions describing the stationary charge distribution. The most wide-spread distribution is the Boltzmann distribution. Different researches have got different regions of applicability for the Boltzmann distribution. According to literature the most suitable region is $r \geq 0.2$ μm [1,2] or $r \geq 0.1$ μm [3,4] for the Boltzmann equation (1) describing the charge distribution in the unsymmetrical bipolar environment [5]:

$$N_i = N_0 \left(\frac{u_+}{u_-}\right)^i \exp\left(-\frac{i^2 e^2}{2kTr}\right), \qquad (1)$$

where i - the number of elementary charges of a particle,
k - the Boltzmann constant,
u_+, u_- - the conductivities of the environment due to the positive and negative ions respectively,
T - the absolute temperature,
e - the elementary charge,
N - the concentration of particles.

The limit of applicability for the Boltzmann equation have been shifted to the smaller particles ($r \geq 5$ nm) by the improvement term for radius that was first used by Kojima [2] in 1978

$$r' = r\,[1 + \exp\,(-\frac{r^2}{\varrho})], \qquad (2)$$

where $\varrho = 1.4 \cdot 10^{-12}$ cm^2.

W. Haaf [6] offers $\varrho = 0.27 \cdot 10^{-12}$ cm^2.

C.S. Liu and J.W. Gentry [7] estimated the applicability of the Boltzmann equation for the aerosol particles with radii $r = 2...8$ nm. In comparison with experiment they got the following errors:

without improvement $\approx$ 27%,
with Kojima's improvement ($\varrho = 1.4 \cdot 10^{-12}$ cm^2) $\approx$ 1%,
with Haaf's improvement ($\varrho = 0.27 \cdot 10^{-12}$ cm^2) $\approx$ 5%.

Haaf [6], working with the radioactive ^{241}Am source in the case of quick neutralization, in addition to the improvement of radius used another improvement of i^2

$$i'^2 = (i - \xi \frac{r' kT}{e^2})^2 , \qquad (3)$$

where $\xi = -0.1$.

Every particle has to undergo a large number of inelastic collisions with ions of different signs before the state of stationary charge distribution is realized. This is guaranteed by a rather large value of the parameter

$$\beta = \int_0^t n\,dt , \qquad (4)$$

where n – the equal concentration of the ions of both signs in the case of symmetrical bipolar ionization,
t – the period of particle residence in the environment of bipolar ions.

Assuming that ion concentration is constant we can obtain simply $\beta = nt$. The value $\beta = \beta_0$ needed for obtaining the stationary charge distribution can be found in Takahashi's paper [8] (Table 1).

The dependence of β_0 on r is negligible, thus we can leave out the sizes of particles in approximated calculations and take $\beta_0 \approx 10^6$ s/cm^3.

Let us deal with the neutralization of an aerosol flowing

Table 1

Dependence of β_0 necessary for realizing the stationary charge distribution on the radius of monodisperse particles

r (μm)	β_0 ($\cdot 10^6$ s/cm^3)
0.1	6.8
0.3	8.3
1	11.4
3	7.6

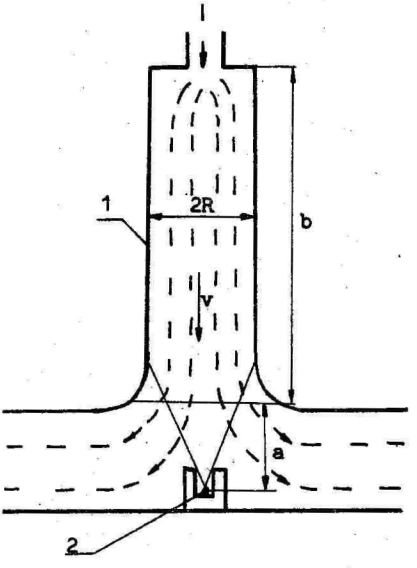

Figure 1. Equipment for neutralization.

in the cylindrical tube 1 using the radioactive point source 2 radiating into a limited solid angle (Figure 1). The flow of aerosol branches symmetrically with respect to the axis of the above angle. Let us denote with a the distance of the branch-point from the radioactive source along the axis. The problem is to find the interdependence between

the activity of the radioactive source A, the length of the tube b and the mean velocity of the flow v in order to achieve the equilibrium charge distribution. Let us assume that the profile of the velocities of the aerosol flow is flat in the tube and $z > R$ so we can take surfaces isodistant from the point source as flat surfaces in the tube.

For solving this problem we have to calculate the value of the integral (4) for the flow of the aerosol going through the tube and to find the conditions when $\beta = \beta_0$. For that we have to find the dependence of the ion-concentration n on the distance from the source 2 (on the co-ordinate z). This dependence is described by the differential equation

$$\frac{dn}{dt} = -\alpha n^2 + q \,, \tag{5}$$

where $\alpha = 1.6 \cdot 10^{-6}$ cm^3/s is the factor of the mutual recombination of small ions,

q is the power of the ion source per a unit of volume, it is the number of pairs of ions coming into being in a unit of volume during a unit time. It was checked experimentally that at short distances (up to 2 m) from our point source the dependence of the quantity q on this distance z is well approximated by function $q \approx z^{-2}$. Thus

$$q = \frac{q_0}{z^2} = \frac{q_0}{v^2(z_0/v - t)^2} \,, \tag{6}$$

where q_0 is a constant numerically equal to the power of the ion-source per a unit of volume at a unit of distance from the emission source,

$z_0 = a + b$ is the co-ordinate of the spot of the entrance of the aerosol flow into the tube,

t is the time interval during which the particles that have reached distance z have been in the tube. The particular solution of this equation that is corresponding to the conditions of this problem can be expressed as

$$\begin{cases} n = C/z \\ C = \dfrac{v(1 + \sqrt{1 + 4\alpha q_0/v^2})}{2\alpha} \end{cases} \,. \tag{7}$$

Now we can calculate the integral (4) easily. By a change

of variables $t = v^{-1}(z_0 - z)$ we obtain

$$\beta = \int_0^t n\,dt = -\frac{c}{v}\int_{a+b}^{a}\frac{dz}{z} = \frac{c}{v}\ln\frac{a+b}{a}. \qquad (8)$$

The condition $\beta = \beta_0$ for the establishment of the stationary distribution of charge is expressed as follows

$$\left(1 + \sqrt{1 + \frac{4aq_0}{v^2}}\right)\ln\frac{a+b}{a} = 2a\beta_0 . \qquad (9)$$

Thus the desired connection between v, b and A is expressed by equation (9), as the activity A of the radioactive point source is uniquely connected with constant q_0 as follows

$$A = 4\pi q_0/N_0, \qquad (10)$$

where N_0 is the number of pairs of ions generated by a radioactive particle on a unit way in the air at standard conditions.

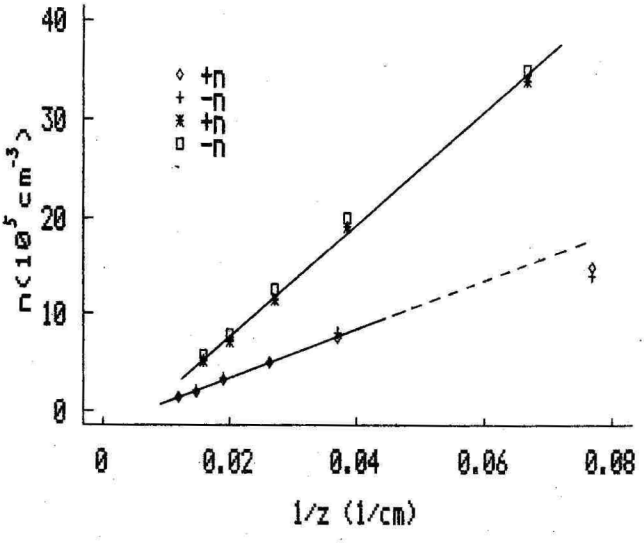

Figure 2. The dependence of ion concentration on the distance z from the radioactive source.

For experimental checking of equation (7) equipment similar to the one depicted in Figure 1 was used, only the direction of the air flow was reversed and the emission source was shifted along the axis of the tube, at the same time the z-axis was connected with this point emission source. The whole equipment was returned and the outlet of the tube 1 was located immediately on the inlet orifice of the measuring capacitor of the air ion counter UT-8401 [10]. The measurement was carried out in the mode of small air ions (limiting mobility k_0 = 2.0 cm^2/(V·s)).Two β-active ^{90}Sr preparations were used as sources of emission, one had the nominal activity 10mCu (received in 1969), the activity of the other was unknown.

The results are shown in Figure 2. Deviation from the inversely proportional dependence at little values of z in the case of the second source is probably explicable with the large surface of this source and in consequence of that the model of the point-source is inexact. On the ground of experimental results, having determined the slope of the straight by the least-squares method and taken N_0 = 65 cm^{-1}

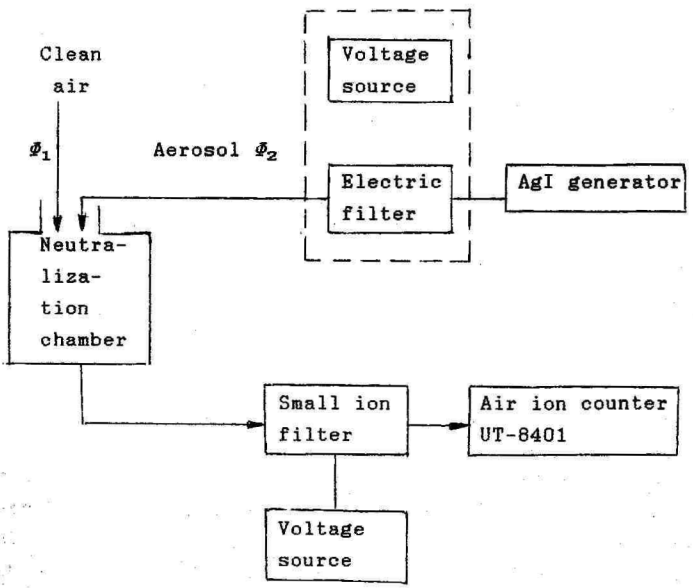

Fig. 3. The equipment for checking the formation of the state of stationary charge distribution.

[9] for the β particle of ^{90}Sr, we can calculate the activity of the emission source from equations (7) and (10). Thus for our preparations we get A_I = 3.6 mCu and A_{II} = 0.3 mCu.

Taking into account the half-life of the ^{90}Sr (27.7 years) the result obtained for A_I coincides satisfactorily with the above nomined value.

The equipment for experimental checking of equation (9) has been depicted in Figure 3.

The equipment consists of

- AgI aerosol generator giving approximately monodisperse particles with mean diameter D = 65 nm,
- passive electrofilter that makes it possible to get uncharged aerosol,
- neutralization chamber: a steel tube with height 34 cm and diameter 10 cm,
- small ion filter,
- counter of air ions UT-8401.

The summary flow rate of aerosol and clean air in the neutralization chamber was Φ = 1400...4000 l/h. For neutralizing we used two different ^{90}Sr radioactive preparations with the activities A_1 = 3.8 mCu and A_2 = 0.05 mCu, respectively. We measured the polar charge densities of the aerosol at the limiting mobility $k_0 = 3.2 \cdot 10^{-4}$ cm^2/(V·s). Small ions were removed before the counter by means of the electrofilter. We were hoping that increasing of the residence of the aerosol in the neutralization chamber forces polar charge densities to approach a constant value, that is the character of the stationary charge distribution. But the method of measuring appeared to be of low sensibility, variability of results was too large to decide when the stationary charge distribution had come into being. For that reason we used an indirect method - we conducted unipolarly charged aerosol into the neutralization chamber and decided about the formation out of the stationary charge distribution by an equal charge density of particles of both signs.

For getting charged aerosol we replaced the electrofilter (Fig. 3) with an electrical separator [11], and thus obtained charged particles with a positive elementary charge. In that case we fixed the reaching of the stationary charge distribution at Φ = 1400 l/h for the weaker preparation. Then the velocity of aerosol in the tube is v = 5 cm/s and the particle stays in the tube for 6.8 s.

Using equation (8) we got for A_2 = 0.05 mCu $\beta_0 = 3 \cdot 10^8 s \cdot m^{-3}$ which is ≈ 3 times higher than the respective theoretic value (Table 1). The difference can be explained by the fact that the initial conditions of the experiment did not correspond to those assumed in the derivation of formula (8) (we use charged aerosol in place of neutral) (Fig. 2).

References

1. Пейль И.А., Тамм Э.И., Зубченко П.К., Холм И.К., Мяги Э.К. Генерирование узкого биполярного распределения заряда на частицах аэрозоля // Уч. зап. Тарт. ун-та.- 1987.- Вып. 755.- С. 89-97.

2. Kojima H. Measurements of equilibrium charge distribution on aerosols in bipolar ionic atmosphere // Atmospheric Environment.- 1978.- V. 12.- P. 2363-2368.

3. Adachi M., Kousaka Y., Okuyama K. Unipolar and bipolar diffusion charging of ultrafine aerosol particles // J. Aerosol Sci.- 1985.- V. 16.- No. 2.- P. 109-123.

4. Pui D.Y.H., Liu B.Y.H. Electrical aerosol analyzer : calibration and performance // Particle Technology Laboratory Publication.- 1976.- No. 304.- 13 p.

5. Сальм Я.И. О стационарной зарядке аэрозолей в несимметрично-биполярной ионной атмосфере // Изв. АН СССР. Физ. атм. и океана.- 1971.- No. 4.- С. 468-469.

6. Haaf W. Accurate measurements of aerosol size distribution.- I. Theory of a plate condenser for bipolar mobility analysis // J. Aerosol Sci.- 1980.- V. 11.- P. 189-200.

7. Liu C.S., Gentry J.W. Charge distribution of ultrafine aerosols undergoing bipolar charging // J. Aerosol Sci.- 1982.- V. 13.- No. 2.- P. 127-138.

8. Takahashi K. Numerical verification of Boltzmann's distribution for electrical charge of aerosol particles // J. of Colloid and Interface Sci.- 1971.- V. 35.- No. 3.- P. 508-510.

9. Таблицы физических величин. Справочник // М.- 1976.- С. 929-939.

10. Таммет Х.Ф. Аспирационный метод измерения спектра аэроионов // Уч. зап. Тарт. ун-та.- 1967.- Вып. 195.- 232 с.

11. Кикас Ю.Э., Мирме А.А., Пейль И.А., Тамм Э.И. Об электростатической сепарации аэрозольных частиц // Методы и приборы контроля параметров биосферы.- Л. 1984.- С. 36-42.

НЕЙТРАЛИЗАЦИЯ АЭРОЗОЛЕЙ

Э. Тамм, Л. Лангус

Р е з ю м е

Теоретически исследованы условия для получения стационарного распределения зарядов в аэрозоле с использованием точечного источника β-излучения в канале течения аэрозоля. Экспериментальная проверка полученных результатов показала удовлетворительное согласие. Описанный метод нейтрализации аэрозоля полезен, в частности, при градуировке электрических аэрозольных спектрометров.

ИЗМЕРЕНИЯ РАСПРЕДЕЛЕНИЯ ВЫСОКОДИСПЕРСНЫХ АЭРОЗОЛЬНЫХ ЧАСТИЦ ПО РАЗМЕРАМ

Я.Й. Сальм, И.Я. Сергеев

В последнее время существенно возрос интерес к фотохимическому и радиохимическому образованию атмосферного аэрозоля из примесных газов, например SO_2, NO_x, C_nH_{2n}, O_3. Атмосферный аэрозоль, охватывающий протяженный диапазон размеров частиц от единиц нанометров (молекулярные кластеры) до десятков микрометров, оказывает значительное влияние на оптические свойства атмосферы, на ее электрическое состояние и химический состав. Основной физической характеристикой аэрозоля является распределение частиц по размерам, иначе - спектр размеров частиц. До начала семидесятых годов одна из важных составляющих атмосферного аэрозоля - высокодисперсная фракция - с радиусами частиц 0,01-0,1 мкм и, в частности, распределение ее частиц по размерам могло изучаться, в основном, методами электронной микроскопии и диффузионных батарей, которые трудоемки и малопригодны для автоматизации. С развитием спектрометрии электрических подвижностей заряженных частиц аэрозоля стал возможным автоматический мониторинг спектра размеров и частиц высокодисперсного атмосферного аэрозоля.

Аппаратура.

Создание аппаратуры для измерения высокодисперсной фракции аэрозоля исходит из разработки многоканального автоматического спектрометра аэроионов типа *UT-7205* [1]. Вскоре этот спектрометр был использован для измерения распределения частиц по размерам, т.е. по соответствующей терминологии, в качестве спектрометра (гранулометра) аэрозоля [2]. Затем, для улучшения характеристик спектрометра аэрозоля прибор был снабжен зарядовой камерой для зарядки исследуемого аэрозоля в зоне униполярного коронного разряда [3].

В самых общих чертах, упомянутый спектрометр имеет много общего с электрическим анализатором аэрозоля Уитби и др., выпускаемым фирмой *Термосистемс* [4]. Однако, имеются и существенные отличия от прибора Уитби и др., из которых в первую очередь отметим принцип одновременного (параллельного) измерения всех фракций аэрозоля, что осуществляется благодаря разделению внешней обкладки измерительного конденсатора на изолированные секции [1]. Принцип параллельного получения

информации весьма целесообразен для изучения поведения спектра размеров атмосферного аэрозоля. В то же время в условиях естественных вариаций распределения аэрозоля по размерам приборы последовательного типа (например, *TSI-3030*) существенно усиливают погрешность концентрации.

В дальнейшем на основе модернизированного спектрометра *UT-7205* и мини-ЭВМ "*Электроника-60*" был создан измерительный комплекс "*Ион-1*". Для этого был разработан и изготовлен интерфейс, обеспечивающий программный доступ в память мини-ЭВМ сигналов измерений. После накопления 8 массивов данных мини-ЭВМ начинает обработку и выводит информацию на печать, не прерывая процесс накопления данных. На печать выводятся значения фракционных концентраций аэрозольных частиц в диапазонах радиусов: 0,010-0,018 мкм, 0,018-0,032 мкм, 0,032-0,056 мкм, 0,056-0,10 мкм, 0,10-0,18 мкм, 0,18-0,32 мкм, 0,32-0,56 мкм, 0,56-∞ мкм и погрешности их определения.

Программа обработки на мини-ЭВМ основывается на алгоритме, предложенном Х.Ф.Тамметом для обработки данных многоканального спектрометра *UT-7205*. Алгоритм обработки представляет собой процедуру вычисления распределений по размерам частиц атмосферного аэрозоля по методу наименьших квадратов. Вычисления производятся с использованием аппаратной матрицы прибора после предварительной корректуры сбоев отдельных каналов с учетом веса канала. Математической основой такой процедуры служит конечномерная модель расчета распределения по размерам частиц атмосферного аэрозоля [5]. Для расчета спектра размеров частиц нужно знать число элементарных зарядов на частицах и подвижность частиц в зависимости от размера (радиуса) частиц. Зависимость среднего заряда частицы от радиуса частицы определена экспериментально [3]. Минимальным возможным зарядом частицы является один элементарный заряд. У высокодисперсной фракции аэрозоля учитывается поправка на долю незаряженных частиц, также как у прибора Уитби и др. Зависимость подвижности частиц от их радиуса рассчитывается по известной формуле Стокса-Кэнингема-Милликена.

В Тартуском университете разработан также усовершенствованный электрический спектрометр аэрозоля *ЭСА-ТГУ* [6], который по общему принципу аналогичен вышеописанному комплексу.

Метрологические характеристики аппаратуры.

Многолетний опыт работы с установкой позволил оценить в реальных условиях шумовые параметры. Шумы прибора слагаются

из шумов измерительного тракта и шумов утечки изоляторов, последние прямо зависят от степени загрязненности изоляторов проводящей пленкой из аэрозольного вещества и составляют от 10^{-15} А до 10^{-14} А. При верхнем значении шумов изоляторы нуждаются в чистке, после чего восстановление их характеристик происходит в течение нескольких дней. Интересно отметить следующую особенность в долговременной работе прибора. После длительного периода измерений (около 1000 часов работы) шумы измерительного тракта, возникающие по причине наброса заряда при работе коммутирующих реле (опрашивающее устройство) уменьшились существенно и составляют 10^{-16} А.

Весной 1986 г. в ходе комплексного эксперимента по сверке аэрозольных приборов на Звенигородской научной станции Института физики атмосферы АН СССР было проведено сравнение "*Ион-1*", *TSI-3030* и *ЭСА-ТГУ* [7]. Приборы были расположены не далее 30 м друг от друга в приземном слое воздуха. Среднечасовые распределения, полученные с помощью "*Ион-1*", сравнивались с аналогичными спектрами *ЭСА-ТГУ* и единичными спектрами *TSI-3030*. По сравнению с *TSI-3030* для частиц высокодисперсного аэрозоля "*Ион-1*" завышал размеры частиц в 1,13 раза и занижал концентрацию в 1,15 раза. Согласие данных "*Ион-1*" и *ЭСА-ТГУ* было еще лучшим. Не исключено, что систематическое отклонение вызвано только различиями в границах измеряемых диапазонов и недостатками способа пересчета концентраций в соответствующих границах фракций ввиду незнания точного поведения распределения внутри фракции. Для размеров частиц $r > 0{,}1$ мкм значения концентрации рассогласуются ("*Ион-1*" сильно занижает концентрацию) с увеличением погрешности измерений. Погрешности определения фракционных концентраций в диапазонах радиусов 0,01-0,1 мкм составляют 10-20%, резко увеличиваясь при $r > 0{,}1$ мкм, что связано с многозарядностью таких частиц, и, как следствие, ослаблением зависимости подвижности от размера частиц. Пределы измеряемых концентраций высокодисперсного аэрозоля составляют $0{,}1\text{-}10^3$ мм$^{-3}$.

Результаты измерений.

Приборным комплексом "*Ион-1*" были проведены многочисленные измерения распределения по размерам частиц атмосферного аэрозоля в приземном слое в относительно чистых условиях района г. Звенигорода (средние весенних сезонов 1980-1983 гг.) и в более загрязненном воздухе г. Москвы (Останкино, апрель 1982 г.). Усредненные распределения частиц аэрозоля (счетные и по-

верхностные) в линейно-логарифмическом виде представлены на рис. 1 и 2.

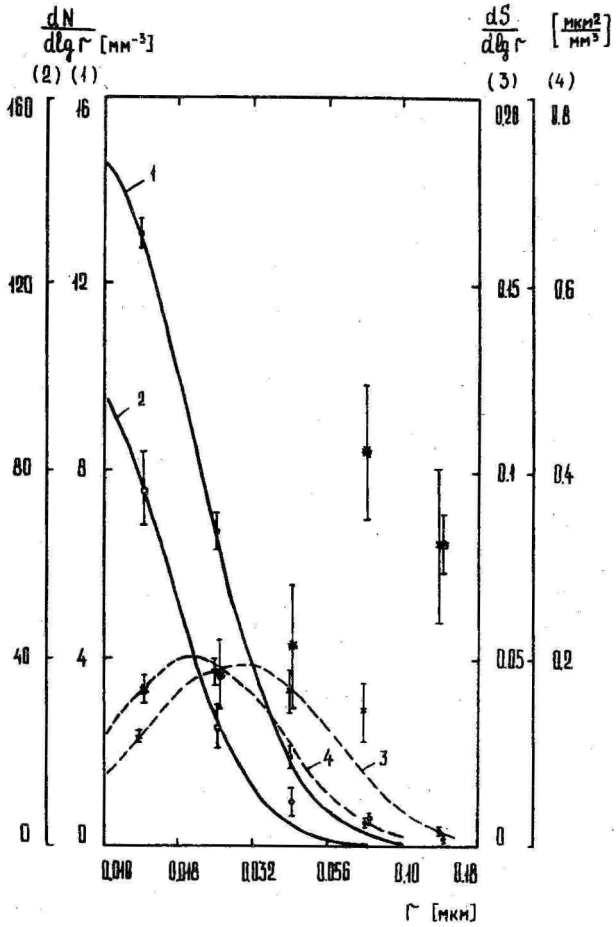

Рис. 1. Средние счетные и поверхностные распределения частиц аэрозоля воздуха Звенигорода (1) (3) и Москвы (2) (4) в приземном слое в дневное время, аппроксимируемые логнормальными распределениями, для счетных концентраций - сплошные линии, для поверхностных - прерывистые. Вертикальные отрезки прямых - оценки промежутка средних концентраций, проведенные по 8-10 значениям.

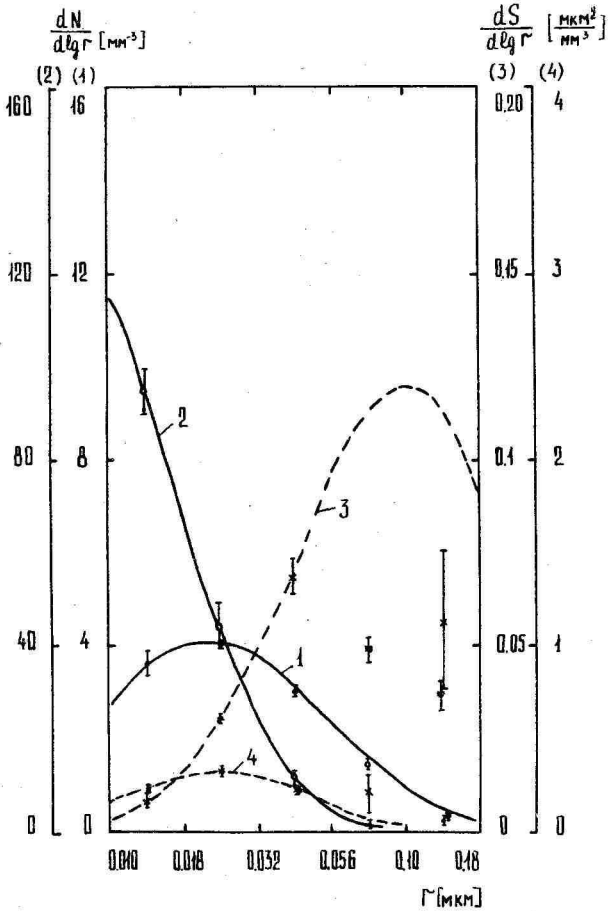

Рис. 2. То же, что на рис. 1, для ночного времени.

Для сопоставления с данными Уитби [8], гистограммы фракционных концентраций аппроксимировались логнормальным распределением:

$$\frac{dN}{d\ \lg r} = \frac{N_T}{\sqrt{2\pi}\ \lg\sigma_g} \exp\left[-\frac{(\lg r - \lg r_g)^2}{2\ \lg^2\sigma_g}\right],$$

где N_T - интегральная концентрация аэрозольных частиц, определяемая из логнормального распределения, r_g - среднегеометрический радиус, σ_g - стандартное геометрическое отклонение. Поверхностное распределение $dS/d(\lg r) = 4\pi r^2 dN/d(\lg r)$ и со-

ответственно $S_т$ - интегральная концентрация площади поверхности частиц.

В таблице приведены характерные значения параметров высокодисперсного аэрозоля, полученные нами в указанных условиях, и данные Уитби [8] для "ядерной моды".

Таблица

Характерные значения параметров высокодисперсного аэрозоля

Условия	r_g мкм	σ_g	$N_т$ $мм^{-3}$	$S_т$ $мкм^2 \cdot мм^{-3}$
Звенигород				
весна, день	0,009	2,1	12	0,04
ночь	0,022	2,4	4	0,03
Москва				
весна, день	0,008	2,0	70	0,2
ночь	0,008	2,1	100	0,5
Данные Уитби				
средние континентальные условия	0,008	1,7	6,4	0,015
городские условия	0,007	1,8	106	0,25

Параметры неплохо согласуются, некоторое превышение σ_g обусловлено тем, что данные Уитби приведены для одного ("ядерная мода") из трех распределений. Кроме того из рис. 1 и 2 видно, что рассогласование экспериментальных точек и аппроксимирующих кривых для поверхностных распределений в диапазоне $r > 0{,}056$ мкм обусловлено не только погрешностями, но и необходимостью учета "аккумулятивной" моды. Аппроксимация наших данных двумя распределениями улучшила бы согласование σ_g и $S_т$, однако данные не позволяют этого сделать из-за отмеченного увеличения погрешности для частиц с $r > 0{,}1$ мкм.

Характер распределений по размерам высокодисперсного аэрозоля в условиях Москвы и Звенигорода в ночное время существенно различается. Этот факт, а также значительное превышение концентрации высокодисперсных частиц в Москве по сравнению со Звенигородом являются, вероятно, следствием преимущественно антропогенного образования таких частиц в воздухе Москвы. Это подтверждается также увеличением отношения $N_{т\ моск.}/N_{т\ звен.}$ в ночное время. Отношение масс высокодисперсной фракции аэрозоля воздуха Москвы и Звенигорода составляло 6-20 раз.

Выводы

1. Приборным комплексом "*Ион-1*", работающим на основе измерения электрических подвижностей частиц (параллельным анализатором, в реальном времени) концентрации высокодисперсных частиц атмосферного аэрозоля надежно измеряются выше выше 0,1 мм$^{-3}$. Погрешности измерения в диапазоне радиусов ниже 0,1 мкм в типичных условиях не превышают 10-20 %.

2. Распределения высокодисперсных частиц в приземном слое в условиях Москвы и Звенигорода существенно различаются. Это, вероятно, обусловлено преимущественно антропогенным образованием высокодисперсного аэрозоля в воздухе Москвы.

3. Сравнение наблюдаемых параметров r_g , σ_g , N_T , S_T , в воздухе Москвы и Звенигорода с соответствующими данными, полученными Уитби [8], указывает на неплохое согласие представленных величин.

В заключение авторы выражают благодарность за помощь коллективу Аэроэлектрической лаборатории Тартуского университета, а также сотрудникам Лаборатории спектроскопии дисперсных сред Института физики атмосферы АН СССР.

Литература

1. Таммет Х.Ф., Якобсон А.Ф., Сальм Я.Й. Многоканальный автоматический спектрометр аэроионов // Уч. зап. Тарт.ун-та.- 1973.- Вып. 320.- С. 48-75.

2. Якобсон А.Ф., Сальм Я.Й., Таммет Х.Ф. Некоторые результаты испытания автоматического спектрометра аэроионов // Уч. зап. Тарт. ун-та.- 1975.- Вып. 348.- С. 16-23.

3. Мирме А.А., Сальм Я.Й., Тамм Э.И., Таммет Х.Ф. Гранулометр субмикронного аэрозоля // Методы и приборы контроля параметров окружающей среды. Межвузовский сборник.- Л., 1979.- Вып. 1 (136). - С. 64-67.

4. Whitby, K.T., Clark, W.E. Electric aerosol particle counting and size distribution measuring system for the 0.015 to 1 micron size range // Tellus. - 1966. - V. 18, No 2.- P. 573-586.

5. Таммет Х.Ф. Введение в линейную конечномерную теорию спектрометрии.- Таллин: Валгус, 1975.- 100 с.

6. Мирме А.А., Тамм Э.И., Таммет Х.Ф. Электрогранулометр аэрозольных частиц с широким пределом измерения // Уч. зап.

Тарт. ун-та.- 1981.- Вып. 588.- С. 84-92.

7. Кикас Ю.Э. и др. Комплексное измерение характеристик аэрозоля и аэроионов в приземном слое атмосферы // Тр. ин-та эксперим. метеорологии.- 1990.- Вып. 51(142).- С. 109-117.

8. Whitby, K.T. The physical characteristics of sulfur aerosols // Atmos. Envir.- 1978.- V. 12.- P. 135-159.

MEASUREMENT OF SIZE SPECTRA OF FINE AEROSOL PARTICLES

J. Salm and I.Ya. Sergeev

S u m m a r y

A computer-controlled electrical aerosol spectrometer "*Ion-1*" is described in the paper. The basic part of the apparatus is the multichannel spectrometer of air ions *UT-7205* built in 1972 [1]. A couple of years later the spectrometer was applied for the measurements of the size spectra of aerosol particles [2]. Fractional concentrations of aerosol particles are simultaneosly measured in the subranges of the radii: 0.01-0.018; 0.018-0.032; 0.032-0.056; 0.56-0.1; 0.1-0.18; 0.18-0.32; 0.32-0.56 and 0.56-∞ μm.

An essential feature of the apparatus is the principle of parallel measurement of particles with different mobilities.

The principal metrological parameters of the apparatus are given. Results of the measurements carried out in Moscow and near Zvenigorod (Moscow Region) are presented.

PRACTICAL OPERATIONAL PROBLEMS OF VIBRATING ORIFICE AEROSOL GENERATOR

V. Tamme

In the Air Electricity Laboratory of Tartu University the vibrating orifice standard aerosol generator has been used since 1986 both for aerosol studies and for the calibration of a wide-range aerosol analyzer in the particle diameter range 0.5 - 10 μm.

Technical problems largely coincide with those described by Boyd [1]. Below the difficulties which have arisen and solutions be described in detail.

Breakdown of syringes and leaks in the liquid system is usually an increase of pressure in the liquid system caused by a clogup of the nozzle or preliminary filters. Usually the operational pressure in the syringe pump (for 10 μm orifice diametre) is 3 - 5.5 at (depending on the preliminary filters that are used). The whole liquid system should be tested for a pressure of 10 at (i.e. at this pressure no visible leaks should appear). It is not advisable to choose preliminary filters with very low pore diametres. E.g. a 0.05 μm pore filter clogs up quicker than a 10 μm nozzle and the result is a heightened pressure in the liquid system.

Our experience suggests that it is best to choose a 1/10 pore/nozzle ratio. From 2 at operational pressure we use special pressure proof glass-metal syringes which do not break.

Clogging of the air nozzle is an infrequent breakdown occurring mostly with saturated *NaCl* solutions. The cause is a small deviation of the jet from the axis of symmetry. It is possible to eliminate the difficulty using a rectangular air nozzle oriented towards the deviation of the liquid jet. The degree of monodispersity of the aerosol does not diminish with the use of rectangular air nozzle.

Clogging of the liquid nozzle is one of the most frequent breakdowns specially in the dispersion of water solutions. There are two kinds of cloggings : sharp and cumulative cloggings. In the first case the jet occurs during some se-

conds after mountin g a new nozzle and is then disrupted. In the second case a partial and increasing clogging appears after a couple of hours of operation; this kind of clogging is manifest in slowly growing pressure in the liquid system, the jet length decreases, the angle of deviation from the axis of symmetry increases and the turbulence inside the jet is growing.

The sharp clogging is likely to be caused by incorrect mounting of the nozzle, whereas the cumulative clogging can be caused by a hydrosol contained in the liquid which has not been eliminated by preliminary filtering.

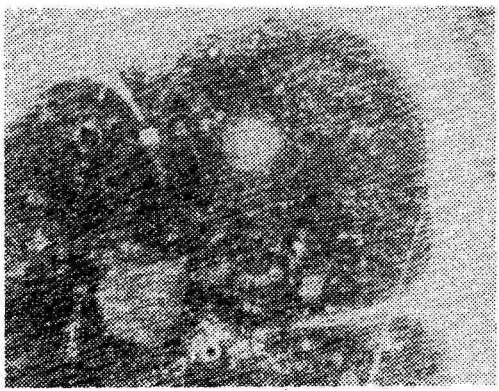

Fig. 1. 20 μ dia. aperture after 24 hours atomization of distilled water.

The photo in Fig. 1 depicts the inner side of a 20 μm dia. liquid nozzle after 24 hours dispersion of distilled water. Fig. 1 clearly shows places covered with the solid particles contained in distilled water which have passed the preliminary filters and precipitated on the nozzle. The particles do not clog a 20 μm orifice but are the main reason for cumulative clogging of 5 μm and 10 μm dia. orifices. Generally, if special measures are not taken to clean the liquid and the liquid system from solid particles, cumulative clogging should be considered an inevitable difficulty in operating vibrating orifice aerosol generators.

The study of orifice clogging over a long period made it possible to find an average operative age of orifices in de-

pendence of their diameter, mounting technology and the design of the liquid system.

Trying 30 orifices using distilled water we found that by average operative age these orifices can be classified into three groups: a) large orifices with diameters over 20 μm, b) medium orifices - 10...13 μm, c) small orifices 3...5 μm. The respective average operative ages (for the liquid system mounting technology we found best) were: for large orifices over 24 h, for medium orifices 3-4 h, and for small orifices up to 1 h. These average operative times can be used in planning aerosol experiments. At the expense of increasing operational costs the operational time of aerosol generators can be extended by ultra-filtering of liquid, standardization and measurement of hydrosol numerical concentration, cleaning of the inner surface of the syringe pump and liquid tract, etc.

After clogging an orifice disc should be dismounted. If after cleaning no corrosion damage is evident, the orifice can be mounted again, otherwise a new orifice is to be used. As a rule, this causes a change in aerosol diameter as it is not possible to manufacture identical orifices.

In short (some hours) uninterrupted operation with especially aggressive water solutions (*NaCl*) we have found orifice corrosion. This is also true of stainless steel, copper and nickel orifices.

Clean mounting of orifices is carried out in a plexiglass box (1 x 1 x 0.5 m). The box is provided with a *HEPA*-filter. The required aerosol concentration in the box is not over 1000 m^{-3} (for aerosol particles d ≥ 1 μm dia), the speed of laminar air flow is ca 1 m/sec.

Losses of aerosol concentration. In the calibration of aerosol devices it is necessary, in addition to the average diameter of monodisperse aerosol, to know the numerical concentration of aerosol particles. The theoretical numerical concentration N in a vibrating orifice aerosol generator can be determined quite simply : $N = \nu/\Phi$; where ν is the frequency of ultrasound and Φ is the flow rate of dilution and atomization air. The actual numerical concentration is always smaller than theoretical. The concentration of the aerosol is diminished by: a) losses of droplets in dispersion and neutralization of electric charges - ca 10 %, b) losses in

multiplet formation ca 7 %, c) losses on the vertical walls of the drying chamber - ca 3 %, d) losses due to gravitational precipitation of aerosol particles - ca 1-14 % in the particle size range 0.5 - 10 μm dia. Thus the total decrease of aerosol article concentration may amount to 34 % in comparison to the theoretical concentration.

Reference

1. Boyd J.V. The commissioning of a commercially available vibrating orifice aerosol generator // J. Aerosol. Sci.- 1982.- V. 13.- P. 221.

К ПРОБЛЕМЕ ЭКСПЛУАТАЦИИ ГЕНЕРАТОРА АЭРОЗОЛЕЙ С ВИБРИРУЮЩИМ ОТВЕРСТИЕМ

В. Б. Тамме

Резюме

В статье приведен перечень возможных причин отказов генератора: засорение микроотверстия, засорение воздушного сопла, утечки в жидкостном тракте и т.п. Приведены наиболее вероятные времена безотказной работы генератора в зависимости от диаметра используемого микроотверстия. Проанализирована проблема потерь аэрозольных частиц в данном типе генератора и дана поправка к расчетной концентрации калибровочного аэрозоля.

Усовершенствована конструкция генератора калибровочных аэрозолей с вибрирующим отверстием и повышена надежность работы последнего.

DEPOSITION OF ELECTRICALLY CHARGED AND UNCHARGED AEROSOLS IN CHAMBER

M. Kaasik, L. Visnapuu and R. Priiman

On the comparative study of the diffusion and precipitation of electrically charged and uncharged aerosols has been devoted relatively few works, e.g. [1,2].

In the present paper the distribution of mass and charge of liquid precipitated on different sections of the interior surface of the chamber, have been studied at different charging regimes.

The measurements were carried out in the closed chamber of (4.6 x 2.2 x 2.6) m^3, Fig. 1.

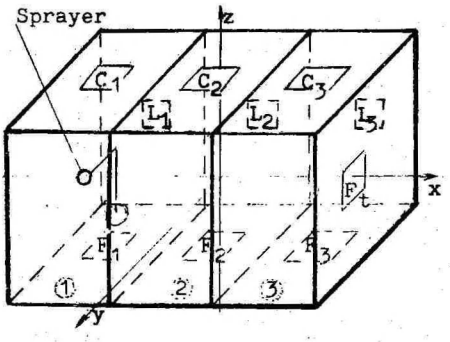

Fig. 1. Aerosol chamber. Quadrangleplates (F - floor, L - lateral well, C - ceiling, Ft - front wall), circles-positions of air ions counter. Origin of coordinates - geometrical centre of the chamber.

The floor and the frontal wall of the chamber were covered with metal, the ceiling, the lateral and rear walls relative to sprayer are made of glass and timber.

The liquid was sprayed and electrically charged by a pneumatic sprayer with inducing electrode [3], placed at the distance of 0.5 m from the rear wall, on the axis of the chamber. The working regime of the sprayer: pressure and expenditure of the compressed air, 0.15 MPa and 6 g/s, expenditure of the liquid 1 g/s, in the charging regime the voltage

of the inducing electrode 0 or 1 kV, the current of convection 0 or 3 μA. The liquid was sprayed within 5 min and then exposed 10 min.

For the measurement of densities of the accumulated mass and the electric charge of the liquid in different sections of the chamber, insulated metallic plates with the area of 0.25 m^2 were used. By the measurement of electric current in a certain plate, the other plates were earthed. In the same way the floor and the frontal wall of the chamber were earthed. The model liquids were water solutions of methylen blue (0.05 %), potassium hypermanganate (0,3 %) and pine conifer extracts (0-5 %). The accumulated methylene blue mass on the plate was colorimetrically determined using red colour filter, and the solution of potassium hypermanganate was titrimetrically determined by the acidified solution of Mohr's salt. On the basis of the results the surface density of precipitated liquid was calculated. The electric charge density and the conductivity of the air in the chamber were measured with the counter of air ions *UT-8401* at the limiting mobilities 10^{-3}, 10^{-2}, 10^{-1} and 2 $cm^2/(V \cdot s)$ during the whole period in the three positions of the counter (Fig.1). Also the relative humidity of the air in the chamber was measured.

Of principal importance in the estimation of the densities of the accumulated mass and electric charge of the liquid is the precondition of the distribution of the precipitation on a fixed surface in dependence on electrical properties of the surface. For this purpose experiments with metallic and glass (dielectrical) plates were carried out.

The data obtained in this way were presented in Table 1.

As seen from the numerical data, the density of the precipitated liquid mass in different sections of the chamber with the electrically charged liquid is tens of times greater than that without the charge (the total precipitation of the sprayed liquid is correspondingly 44.6 % with the charge and 2.3 % without the charge). Analogical results were obtained with solutions of potassium hypermanganate.

The difference in the precipitation can be explained by electrostatic scattering: the charged drops scatter quickly under the influence of electrostatic forces and precipitate on the surfaces. The uncharged drops precipitate considerably slower under the influence of gravitation and diffusion forces. Earthed metallic plates, placed on the dielectric

Table 1

The relative density of the charge (a) and the mass (b) of the sprayed methylene blue solution, accumulated on the unit area of metallic plates in the different sections of the chamber (per cent from total charge (a) or mass (b) sprayed, accumulated on the m^2 of surface).

Potential on the electrode, kV		The relative density of the accumulation, %/m^2			
		on the ceiling (9,5 m^2)	on the lateral wall (23,6 m^2)	on the front wall (5,9 m^2)	on the floor (9,5 m^2)
-1	a)	1.29	0.60	4.05	5.09
	b)	0.27	0.71	1.88	1.48
0	a)	0	0	0	0
	b)	0.01	0.03	0.03	0.14

surfaces (lateral walls, ceiling) of the chamber, distort electrical field: power lines of the electric field would concentrate to the plates. In order to get more objective results, measuring the accumulation of the mass, the metal plates on lateral walls and ceiling were replaced with dielectric (glass) plates. Charge depositions, achieved from measurements on metal plates, were extrapoled over all surface for the conductive surfaces (floor, front wall, uniform precipitation supposed) and devided by area of the surface (precipitation only on the plates supposed). The value of the convective current, calculated from these data was 3-6 μA. According to the theoretical accounts, carried out in [3], we get for the given regime of spraying the average diameter of the drops 8 μm. By microscopic measurements the average diameters of the drops fluctuate within the limits of 4-16 μm (Table 2), with the standard deviation (2-11). The stationary velocity of the gravitational precipitation of a drop [4, p. 73].

$$v = d^2 \gamma_m g / 18\mu, \qquad (1)$$

where g is the acceleration of free fall, γ_m density and d the diameter of the drops and μ viscosity of the air. In

Table 2

The arithmetical averages of the diameters of the drops, precipitated on the surfaces at spraying of phytoextract solution (microscopically measured)

electrod kV	C,%	floor	lateral* walls	ceiling*	frontal* wall
0	0	9.6+6.5	-	-	16.4+11.0
0	2.0	8.4+5.1	-	-	10.8+6.3
-1	0	10.3+6.5	8.8+5.8	-	8.8+5.7
-1	0.5	7.9+4.5	-	-	7.1+4.5
-1	1.0	6.2+3.5	7.3+4.7	10.6+8.9	5.2+3.0
-1	2.0	6.9+4.4	9.0+6.5	8.0+4.5	-
-1	5.0	4.3+2.8	4.1+2.8	3.7+2.7	3.9+2.3

* The drawn lines are denoting cases where the amount of precipitated drops was small for statistically reliable data.

normal conditions for the water drops with the diameter d = 8 μm we get $v = 2 \cdot 10^{-3}$ m/s. It is considerably less than the velocity of the air current, created by sprayer (some m/s). Consequently, gravitational precipitation becomes apparent only after turning out the sprayer. A certain amount of the uncharged liquid precipitated on the walls and ceiling is conditioned by diffusional precipitation. With electric charge the precipitation of the drops takes place more uniformly.

Owing to the complicated processes of evaporation, condensation and coagulation in the chamber, distribution of the size of initial drops, created by the sprayer changes. Nevertheless by the data obtained from microscopic investigation of the precipitated drops we can notice the conservation of the order of magnitude of the average diameter of drops.

Sharp difference in the densities of the precipitated mass of the drops with and without electric charge was observed in the sections of the chamber, distanced away from the sprayer, Fig. 2. It is conditioned by the transport of the aerosol with the air current from the sprayer and electrostatic scattering. Simultaneously with the distance from the sprayer the charged drops precipitate, and the greater part of them reach the surface at the distance of about 2 m.

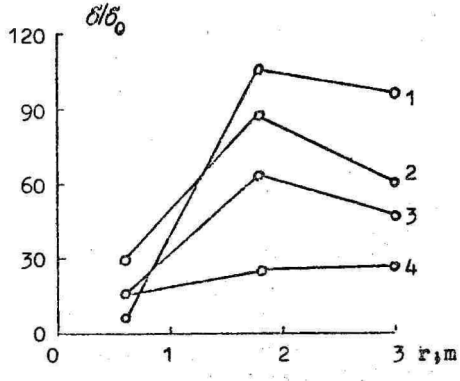

Fig. 2.
Depending δ/δ_0 on the distance from the rear wall r, δ -density of the substance with and δ_0 - without electric charge;
1 - ceiling,
2 - lateral wall,
3 - average,
4 - floor.

The measurement of the electric charge density of air ions shows that it practically does not depend on the position of the air ion counter and in the lower part of the chamber it might be considered uniform.

From the relation between the electroconductivity λ, the charge density ϱ and average mobility of air ions k :

$$\lambda = k\varrho \qquad (2)$$

the average mobility of the air ions can be estimated.

At the beginning, by (2) was estimated the contribution of the intermediate $k = 10^{-2}...10^{-1}$ cm^2/(V·s) and large $10^{-3}...10^{-2}$ cm^2/(V·s) air ions in the general electroconductivity of the air. In all cases it was negligible (less than 3%).

Next, by average data of several experiments, the effective mobility of the small air ions was calculated. The results were carried in Fig. 3, at 1-2 % phytosolution (conifer extract) minimum mobility of small air ions was observed.

The data of experiments shows that the distribution of air ions by the mobility depends on the concentration of phytosolution (Fig. 4). The total density of electric charge decreases with the increase in concentration.

The charge density of large air ions decreases especially sharply. According to theoretical estimations [3] for water the average charge of the drops of average size $q = 8\cdot10^{-18}$ C $= 5\cdot10^3$ e.

From Stokes' Formula [4, p. 40] and definitions of mobility and electrostatic field strength we get

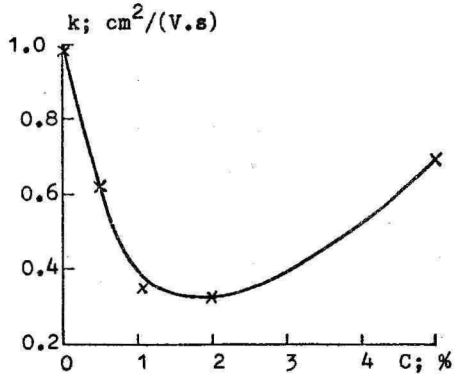

Fig. 3.
Dependence of the average mobility k of small air ions on the concentration of sprayed phytosolution.

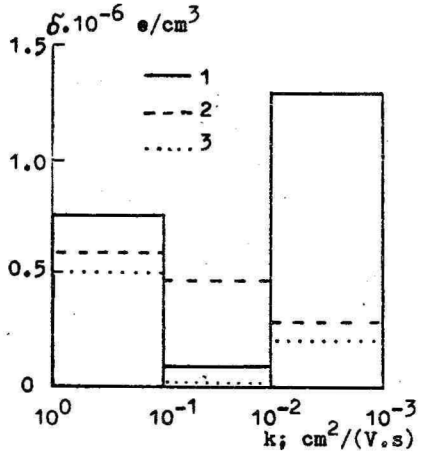

Fig. 4.
Distribution of the electric charge density according to mobility at different concentrations of phytosolution;
1 - 0%; 2 - 2%; 3 - 5%.

$$k = q/3\pi\mu d \quad , \qquad (3)$$

where μ is the dynamic viscosity of the medium (air).

From (3) we get in standard conditions for average drops $k = 5.8 \cdot 10^{-3}$ cm²/(V·s). Consequently the original drops belong to large air ions.

It follows that the reasons of decrease of charge density of large air ions with increase in concentration of phytosolution are directly related to the process of spraying. Shifts incharge density of small and intermediate air ions are probably connected with the secondary effects, as evaporation of large ones etc. [5].

In order to get proofs for the directed precipitation of the charged drops on the earthed surfaces, approximate mea-

surements of the electric potential of insulated plates in certain point in central, horizontal plane of the chamber with unearthed and earthed plates in relation to Earth by spraying of the tap water, were carried out. For approximate measuring of potential an electrostatical voltmeter was used. As detector was used an end of metal wire in shape of cylinder of diameter 5 mm and height 30 mm. Remaining part of the wire was insulated.

The data of four successive measurements were averaged. Likewise the reliability of the earthing of the plates, the floor and the rear walls was controlled. The potentials of the remaining points were presented in Table 3.

Noticeably essential is the difference between the electric potentials in the presence of earthed plates and without them. In the case of earthed plates the electric potential, as a whole, decreases due to the flowing down of the electric charge in the plates and the maximum potential is replaced

Table 3

Potentials measured in chamber during the spraying of tap water

Point of measurement*		Potential relative to Earth, V/m	
		without plates	with earthed plates
Lateral wall	L1	500+240	0
	L2	1380+260	0
	L3	-	0
Ceiling	C1	1550+10	0
	C2	1230+50	0
	C3	2200+500	0
On the x-axis at 120 cm from the sprayer		1280+100	1740+380
On the x-axis at the front wall		550+260	450+100

* On the floor and front wall the potential in all cases was equal to 0.

closer to the lateral plates (the plates were only in one wall). The most considerable difference however, becomes evident close by the plates: near the earthed plates (layer of 20 cm) the normal component of the electric field strength (normal derivative of the potential with opposite sign, i.e. slope of the curve in Fig. 5) is about +3800 V/m, without earthing considerably less (within the limits of standard deviation might be both positive and negative, the maximal value +750 V/m). Applying the Formula (3), it is evident that the velocity of precipitation of electrically charged particles near the earthed surface of the conductor being minimum 5 times greater than near the dielectric walls. This also proves the intensified precipitation of charged drops on the earthed conducting surfaces.

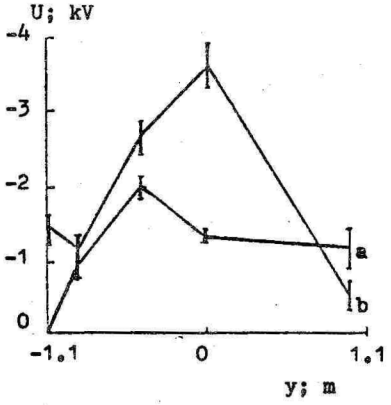

Fig.5.
Distribution of the potential on the y-axis (Fig. 1) with (a) and without (b) the earthed plates in the lateral wall.

From our experiments will succeed:

1. Electrically charged aerosols precipitate on the surface of rooms under the influence of electrostatic force tens of times quicker than those uncharged. At the same time the precipitation on the surfaces is more uniform.

2. Spraying the electrically charged aerosols the distortion of electric field causes the precipitation of aerosols preferably on the earthed conducting surfaces.

3. The admixture to water 1-2% conifer extract diminishes the mobility of charged drops.

The aforesaid is useful to be taken into account when treating rooms with aerosols (disinfection, painting), but also when studying the nature of aerosols.

Some results of present paper are theoretically discussed in [5].

References

1. Дунский Б.Ф., Китаев А.В. Осаждение униполярно заряженного аэрозоля // Коллойдн. ж.- 1960.- *22*.- С. 159-167.

2. Дунский В.Ф., Сидоров А.И. Физико-технические основы аэрозольной и газовой обработки закрытых помещений // Аэрозоли в сельском хозяйстве.- М.: Колос.- 1973.- С. 202-229.

3. Виснапуу Л.Ю. Пневматический распылитель с индуцирующим электродом // Уч. зап. Тарт. ун-та.- 1973.- Вып. 320.- С. 209-216.

4. Reist P.C. Introduction to Aerosol Science.- Macmillan Publishing Company. New York, London.- 1984.

5. Kaasik, M. Electrostatic dispersion of air ions at continuous ionization of the air // See this volume.

РАССЕЯНИЕ ЭЛЕКТРИЧЕСКИ ЗАРЯЖЕННОГО И НЕЗАРЯЖЕННОГО АЭРОЗОЛЯ В КАМЕРЕ

М.А.-Х. Каазик, Л.Ю. Виснапуу, Р.Э. Прийман

Резюме

В настоящей работе исследовано распределение заряда и массы аэрозоля распыленной жидкости (водопроводная вода, растворы хвойных экстрактов) на разные участки внутренней поверхности камеры (4,6 x 2,2 x 2,6 $м^3$). Аэрозоль создавали пневматическим распылителем с индуцирующим электродом [3].

Электрически заряженный аэрозоль осаждался более равномерно и в десятки раз быстрее, чем незаряженный. Осаждение аэрозоля происходит предпочтительно на заземленных проводящих поверхностях.

ELECTROSTATIC DISPERSION OF AIR IONS GENERATED BY A PNEUMATIC SPRAYER IN A CHAMBER

M. Kaasik

The air ionization in a chamber, using experimental data from [1], will be theoretically studied in this paper. In the paper [1] the deposition of unipolar negative charged particles generated by a pneumatic sprayer with inducing electrode, was experimentally studied. The solution of the pine extract (phytosolution) was sprayed. The space charge densities of large and small air ions and charge and mass of liquid, precipitated on the surfaces of aerosol chamber (4.6 x 2.2 x x 2.6 m^3) were measured.

For ions of identical mobility the dependence of the charge density on time t has been derived in various papers:

$$\varrho = \varrho_0/(\varrho_0 kt/\varepsilon + 1), \qquad (1)$$

where ϱ_0 is the initial charge density at the moment $t = 0$ and ε is the absolute permittivity of the air.

In the case of two considerably different mobilities $k_S >> k_L$, the dependence of ϱ_S for small air ions has been derived in [2]

$$\varrho_S = \varrho_{S0}/((1 + \varrho_{S0}/\varrho_{L0}) \exp(\varrho_{L0} k_S t/\varepsilon) - \varrho_{S0}/\varrho_{L0}), \qquad (2)$$

where ϱ_{S0} and ϱ_{L0} correspond to the initial charge densities of small and large air ions. As the dispersion of small air ions takes place quickly, the charge density of large air ions during the same time might be regarded as constant: $\varrho_L = \varrho_{L0}$. Large air ions disperse accordingly to the formula (1) during a longer time.

In the present work we deal with the electrostatic dispersion of aerosols during the continuous process of ionization.

Proceeding from the law of conservation of charge in the presence of spatially homogenous air ion source of intensity Q :

$$\partial \varrho/\partial t + \varrho \operatorname{div} \vec{v} = Q, \qquad (3)$$

where $\vec{v}$ is the velocity of air ions. Through transformations analogous with those derived in [2], the equation for one mobility k is :

$$d\varrho/dt + (k/\varepsilon)\varrho^2 = Q. \qquad (4)$$

This equation is formally analogous with the equation for recombination of air ions [4, p. 636].

Integrating with regard to the initial condition $\varrho = 0$ at $t = 0$ and expressing ,

$$\varrho = \varrho_\infty [\exp(t/\tau - 1)]/[1 + \exp(t/\tau)], \qquad (5)$$

where

$$\varrho_\infty = \sqrt{\varepsilon Q/k} \qquad (6)$$

and

$$\tau = 0.5\sqrt{\varepsilon/kQ}. \qquad (7)$$

The Eq. (5) gives for ϱ an ascending curve at small t and following saturation. Developing the exponent in the Eq. (5) into power series at $t \ll \tau$, we get $\varrho \sim t/\tau$. In this way τ turns out to be the time constant determining the slope of the curve at regimes far from saturation. On the other hand, if $t \to \infty$, $\varrho \to \varrho_\infty$, consequently ϱ_∞ is stationary charge density. The constants ϱ_∞ and τ depend only on the mobility of air ions and intensity of the source.

At discrete distribution of mobilities and independent sources [2,3]

$$d\varrho_j/dt + k_j\varrho_j/ = Q_j, \qquad (8)$$

where ϱ is the total charge density, ϱ_j charge densities of air ions with mobilities k_j and Q_j are the corresponding intensities of the sources.

Analytical solution of the system (8) is difficult from the mathematical point of view and requires approximation.

In steady state $d\varrho_j/dt = 0$ system (8) will turn into a system of algebraic equations:

$$k_j\varrho\varrho_j/\varepsilon = Q_j, \qquad (8)$$

which easily can be solved.

The experiment was carried out, using methods and techniques described in [1]. The electric charge density of the air ions at the limiting mobilities 10^{-3}, 10^{-2} and 10^{-1} $cm^2/(V \cdot s)$ was measured. The dependence of the charge density on time using Eqs. (5-7) (the sprayer switched on), and (1) (after switching off the sprayer) was calculated. The initial data

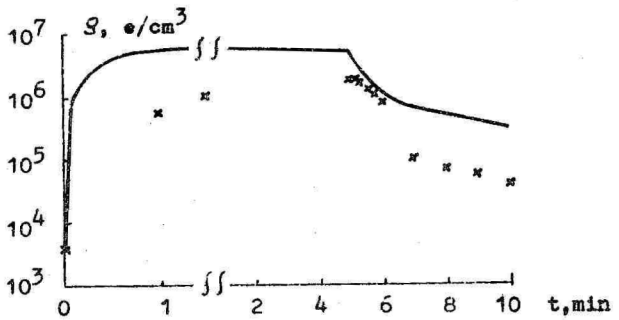

Fig. 1. Experimental (crosses) and calculated (solid line)* dependences of total charge density ($k > 10^{-3}$ cm^2/(V·s)) on time (tap water sprayed). The time of abscissas is changed at 2 min.

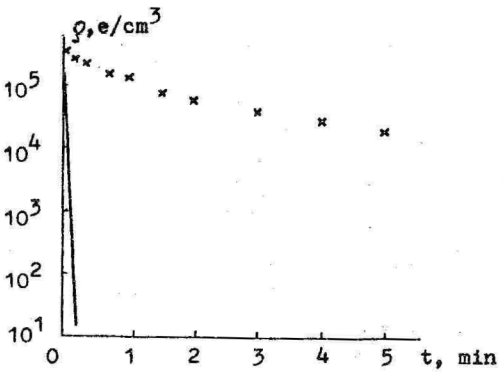

Fig. 2. Experimental (crosses) and calculated (solid line)* dependences of charge density of small air ions ($k > 10^{-1}$ cm^2/(V·s)) on time after switching off sprayer (tap water sprayed).

* Initial charge densities and average air ion mobilities from the experiment are used [1].

from [1] are the following: $Q = 0.11$ μA/m^3 (the current of of convection from the sprayer divided by the volume of the chamber), $k = 5.6 \cdot 10^{-3}$ cm^2/(V·s) (average mobility of original drops from sprayer). The calculated dependence of charge density on the time corresponds qualitatively well to the theory, but the calculated steady charge density is several times higher than the experimental (Fig. 1). This is apparently caused by the fact that the greater part of the generated charge is created by the small air ions which disperse quickly, and, as can be seen from the Eq. (2), create rather a small density of the charge.

It should be noted that there is a strong effect of the added phytoextract on the formation of the small air ions. The nature of this phenomenon is not known yet. The results, given out here and in [1], show that the average mobility of small air ions, when 1-2 % phytosolution is sprayed, is 2-3 times smaller than in the case when tap water is sprayed, and so corresponds well to the shift of the spectra of small negative air ions to smaller mobilities under the influence of some phytoorganic substance [5]. The superlarge air ions ($k < 10^{-3}$ cm^2/(V·s)), which did not undergo to measurement, could have a definite influence on the results obtained here.

One more problem concerning the dependence of the sources of large and small air ions on time should be considered. Dependence of the charge density of small air ions on time, after switching off the sprayer, calculated by Eq. (2), was compared with the experimental data (Fig. 2). According to the experimental data the slope is much smaller than the calculated one and is similar to the data of total charge density (Fig. 1). Consequently, the small air ions preserve their role in the total charge density in spite of the quick dispersion. We may come to the conclusion that the source of small air ions depends on charge density of large air ions, which is the main component of total charge density, as seen from experiment [1]. The formation of small air ions by the way of evaporation of the large ones may be the possible mechanism explaning the dependence [6].

Conclusions: Equations for electrostatic dispersion of air ions at permanently acting sources have been derived and a comparison with certain experimental data has been carried out.

The dependence of the source of small air ions on the charge density of large air ions have been suggested.

References

1. Kaasik, M., Visnapuu L., Priiman, R. Deposition of electrically charged and uncharged aerosols in chamber. (See this volume P. 101-109).

2. Сальм Я.Й. Об электростатическом рассеивании аэроионов // Уч. зап. Тарт. ун-та.- 1980.- Вып. 534.- С. 95-100.

3. Luts, A., Salm, J. Electrostatic scattering of two air ion groups of different mobilities // Acta et comm. Univ. Tartuensis.- 1990.- V. 880.- P. 105-110.

4. McDaniel, E.W. Collision Phenomena in Ionized Gases.- New York - London - Sydney, 1964.

5. Прийман Р.Э., Виснапуу Л.Ю., Партс Т.М. Влияние некоторых антропогенных загрязнителей и их очистителей на спектры подвижности легких аэроионов // Уч. зап. Тарт. ун-та.- 1988.- Вып. 824.- С. 138-145.

6. Tamme, V. Charge generation and separation in the evaporation of water aerosol droplets // Acta et comm. Univ. Tartuensis.- 1990.- V. 880.- P. 94-98.

ЭЛЕКТРОСТАТИЧЕСКОЕ РАССЕЯНИЕ АЭРОИОНОВ ПРИ ПОСТОЯННОЙ ИОНИЗАЦИИ ВОЗДУХА

М.А.-Х. Каазик

Резюме

Получены формулы для электростатического рассеяния аэроионов при постоянно действующем генераторе. Сопоставлены расчетные и экспериментальные данные [1].

Установлена зависимость между интенсивностями образования легких и тяжелых аэроионов, которая может быть обусловлена образованием легких аэроионов при испарении тяжелых.

Под влиянием фитоорганических веществ экстракта сосновой хвои уменьшается подвижность и интенсивность образования легких аэроионов.

AIR ION METER OF SMALL AIR IONS UT-8007

R. Matisen, F. Miller

The measurement of the concentration of air ions is sometimes to be conducted under conditions where the operator cannot operate the device directly. The reasons here might be poor accessibility of the measurement location, harmful influence of the environment or the necessity to avoid the operator's influence on the environment near the measurement place. In such cases remote switching of the operational regimes and data reading are to be ensured.

This paper describes an air ion meter meant for the measurement of the concentrations of small ions with the limiting mobility k_0 = 0.5 $cm^2/(V \cdot s)$. The remote control unit makes it possible to carry out measurements when the sensor is located at a distance of up to 8 m from the operator.

The aspiration measurement method is used in the air ion meter. A measurement capacitor with a grounded outer and collecting inner electrode is used. The inner electrode is switched to the voltage source through an electrometer located in the inner electrode. The amber insulator of the inner collector plate is simultaneously the input insulator of the electrometer. This set-up ensures a significant decrease in the amount of parasitic currents [1]. To achieve high reliability of the device in humid environments the insulator is heated and its temperature maintained at +40 °C. A diagram of the air ion meter clarifying the connections between all the functional units is presented in Fig. 1.

Generally the electrometer of the air ion meter is structurally identical to the construction described in [2]. A field transistor *КП*305 (specially chosen for the low level of parasitic gate current) and an operational amplifier *КР*140*УД*7 were used. The electrometer is connected with the switch of measurement limits; the switch is a high-resistivity resistor which by means of a relay can be switched in parallel to the measuring resistor of the electrometer.

The protection circuit ensures the switching off of the measurement mode (shorts the electrometer input) when the voltage on the electrometer output achieves 10 V and in the case of unpermitted switching of regimes. The output device based on the operational amplifier *КР*140*УД*8 transforms the

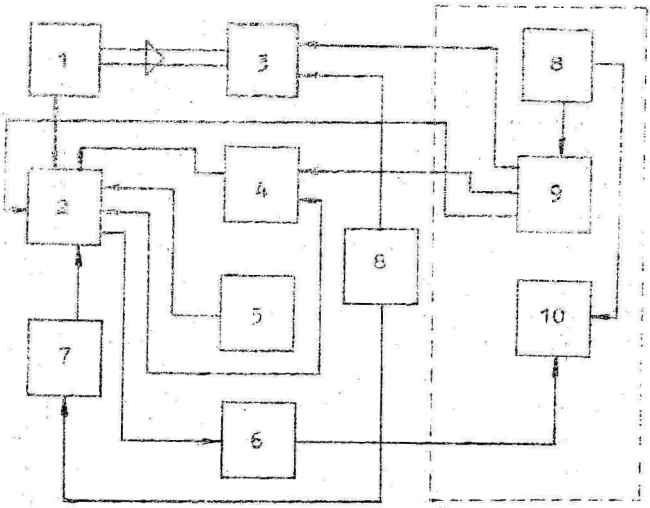

Fig. 1. Structural diagram of the air ion meter.
1 - measuring capacitor; 2 - electrometer with adjustable measurement limits; 3 - fan; 4 - stabilizer of the voltage on the measuring capacitor; 5 - protective circuit; 6 - output device; 7 - thermostat; 8 - power source with voltage stabilizer; 9 - control circuit; 10 - indication circuit.

signal coming from the electrometer to values needed for the operation of arrow and numerical indicators. The voltage source operates on the mains AC 220 ± 22 V and ensures on its output stabilized DC voltage ± 15 V for the electrometer, ± 15 V for the output device and the protection circuit, from +8 to +14 V for the thermostat, ± 14 V for the measuring capacitor, + 27 V or ~ 220 V for the motor of the fan (depending on the motor used).

The control and indication blocks are located in separate unit connected to the sensor block by a multichannel cable. The block consists of three plates; the first plate accommodates the liquid crystal display and the processor. the second are the control circuit of the sensor block, and the third plate accommodates the stabilizer of the voltage for the control block ± 15 V.

The control circuit ensures the switching of the measuring range, polarities, zero corrections of the indicator and

the electrometer, making [illegible] taking the indications [illegible] of the measurement mode.

Technical data of the device

- range of the measurement of air ion concentration $10 - 2 \cdot 10^5$ e/cm^3;
- limiting mobility 0.5 cm^2/(V·s);
- power consumption not over 25 W;
- size of the sensor block 185 x 135 x 310 mm;
- size of the control block 215 x 90 x 185 mm;
- total weight (with the connecting cable) not over 10 kg.

References

1. Миллер Ф.Г., Эевель Я.Е. Новая конструкция измерительного конденсатора в измерителе электропроводности воздуха // Уч. зап. Тарт. ун-та.- 1984.- Вып. 669.- С. 67-71.

2. Миллер Ф.Г. К разработке электрометров прямого усиления для многоканальных спектрометров аэроионов // Уч. зап. Тарт. ун-та.- 1981.- Вып. 588.- С. 124-131.

АЭРОИОНОМЕТР ЛЕГКИХ АЭРОИОНОВ Т-8007

Р.Л. Матизен, Ф.Г. Миллер

Р е з ю м е

Описывается конструкция аэроионометра для измерения концентраций легких аэроионов с предельной подвижностью K_0 = 0,5 см^2/В·с и пределом измерения концентрации аэроионов от 10^2 до $2 \cdot 10^5$ эл.з/см^3. Блок дистанционного управления позволяет производить измерения на расстоянии до 8 м от датчика.

БЫСТРОДЕЙСТВУЮЩИЙ ИЗМЕРИТЕЛЬ МАЛОГО ТОКА УТ-9003

М.Э. Роос, О.В. Сакс

Измерение быстроменяющихся (переменных и/или импульсных) токов в диапазоне 10^{-8} А и меньше с помощью электрометрического усилителя связано со специфическими проблемами: при подключении ко входу измерительного устройства с заданной полосой пропускания любого источника тока, обладающего электрической емкостью, 1) возрастает уровень шумов на выходе усилителя [1]; 2) увеличивается динамическая погрешность усилителя [2].

При разработке прибора УТ-9003 целью являлось уменьшение уровня шумов и ослабление зависимости быстродействия усилителя от емкости источника сигнала в диапазоне 10^{-13} - 10^{-8} А.

Обычно электрометрический усилитель состоит из входного устройства (Э) с большим входным сопротивлением и последующего усилителя, состоящего из одного или нескольких операционных усилителей (ОУ). Входное устройство быстродействующего электрометра нередко представляет собой повторитель напряжения на полевом транзисторе или совокупность полевого транзистора с другими активными элементами, в том числе и операционным усилителем [3]. На рис. 1 приведена упрощенная структурная схема такого электрометра вместе с источником тока I_x,

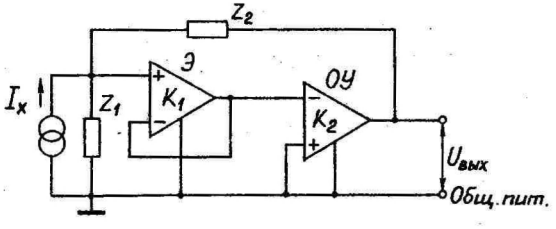

Рис. 1. Структурная схема электрометрического усилителя тока с повторителем на входе.

суммарным импедансом на входе Z_1 и импедансом преобразователя тока в напряжение Z_2 в цепи параллельной отрицательной обратной связи. В импеданс Z_1 входят собственная входная емкость

усилителя Э, емкость источника сигнала, а также емкость соединительного кабеля и другие конструктивные паразитные емкости, и все сопротивления утечек, шунтирующие вход.

Передаточная функция W такого электрометра может быть представлена в виде формулы [2]:

$$W = \varphi \cdot Z_2 ,$$

где φ - коэффициент поправки, характеризующий неидеальность усилителя, обусловленную конечностью коэффициентов усиления K_1 и K_2 усилителей Э и ОУ, а также наличием входного импеданса $Z_1 \neq \infty$.

В идеальном случае ($\varphi = 1$) передаточная функция W не зависит от Z_1, т.е. от емкости на входе. Реально же коэффициент поправки имеет вид:

$$\varphi = \frac{1}{1 + (1+K_1)/\alpha K_1 K_2} ,$$

где

$$\alpha = Z_1/(Z_1+Z_2) .$$

С помощью разности реального ($\varphi \neq 1$) и идеального ($\varphi = 1$) коэффициентов поправки можно оценить влияние входного импеданса Z_1 (через коэффициент α) на передаточную функцию, а вместе с тем на динамическую погрешность электрометра:

$$|\varphi - 1| = (1 + K_1)/(\alpha K_1 K_2 + K_1 + 1).$$

Если $K_1 >> 1$, то оценка $\varphi - 1$ принимает вид:

$$|\varphi - 1| \approx 1/\alpha K_2 . \qquad (1)$$

Передаточная функция W электрометрического усилителя значительно изменяется, если общую для входа и выхода электрометра низкоомную клемму отсоединить от общей клеммы питания и подсоединить ко входу электрометрического повторителя Э, как показано на рис. 2. Для этой схемы получим коэффициент поправки в виде формулы

$$\varphi = \frac{1}{1 + 1/\alpha K_1 (K_2+1)} ,$$

а оценку динамической погрешности

$$|\varphi - 1| = 1/[\alpha K_1 (K_2+1) + 1].$$

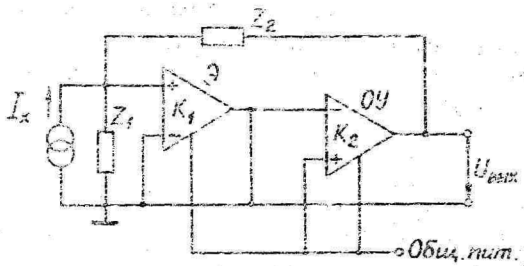

Рис. 2. Структурная схема электрометрического усилителя тока с уменьшенной зависимостью быстродействия от емкости на входе.

При $K_1, K_2 >> 1$ имеем:

$$\left| \beta - 1 \right| \approx 1/K_1 K_2 \ . \qquad (2)$$

Сравнивая выражения (1) и (2) убеждаемся, что во втором случае влияние α_1 а тем самым входной емкости (в составе Z_1), на передаточную функцию в K_1 раз слабее по сравнению со схемой на рис. 1. Расчет эффективных входных импедансов при больших K_1 и K_2 даст для схемы по рис.1 соотношение:

$$Z_{вх.1} \approx Z_2/K_2 \ ,$$

а для схемы по рис. 2

$$Z_{вх.2} \approx Z_2/K_1 K_2 .$$

Таким образом, вторая схема и здесь более выгодна, так как для идеального измерителя тока $Z_{вх.}$ --> 0.

Учитывая вышеприведенные результаты, за основу структуры быстродействующего электрометра УТ-9003 принята схема по рис. 2. При подключении ко входу устройства емкости до 1000 пФ быстродействие практически не меняется.

Блок-схема электрометра УТ-9003 представлена на рис. 3. Прибор состоит из двух блоков - основного и выносного. Малогабаритный (20 x 26 x 90 мм^3) выносной блок позволяет во многих случаях соедининть вход электрометра с объектом измерения непосредственно (без входного кабеля), благодаря чему уменьшается емкость на входе и снижается уровень шумов на выходе прибора.

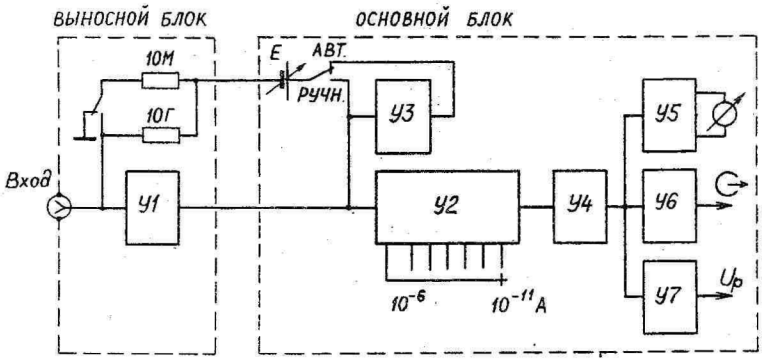

Рис. 3. Блок-схема быстродействующего измерителя малого тока УТ-8003: У1 - электрометрический усилитель; У2 - масштабный усилитель; У3 - блок автоматической компенсации постоянной составляющей сигнала; У4 - усилитель частотной коррекции; У5 - согласующий усилитель; У6 - выходной усилитель (инвертор); У7 - измеритель размаха.

В выносном блоке расположены измерительные резисторы, реле для их переключения и плата с электрометрическим усилителем У1 (входной повторитель и последующий операционный усилитель). Диапазон измеряемых токов 10^{-13} - 10^{-8} А перекрывается двумя измерительными резисторами 10 ГОм и 10 МОм. В качестве входного элемента применен сдвоенный полевой транзистор с *p-n* переходом КПС 104.

Для ручной компенсации смещения нуля и/или постоянной составляющей измеряемого тока используется регулируемый источник напряжения Е (рис. 3), а для автоматической компенсации - блок У3, с помощью которого постоянная составляющая входного сигнала подавляется примерно в 100 раз.

Измерительный резистор (10 ГОм или 10 МОм) включается в цепь параллельной отрицательной обратной связи электрометрического усилителя У1. С помощью масштабного усилителя У2 весь диапазон измерения разбит на поддиапазоны с пределами $\pm(10^{-11}, 10^{-10}, 10^{-9}, 10^{-8}, 10^{-7}, 10^{-6})$ А.

Быстродействие прибора (время нарастания фронта выходного сигнала от 10% до 90% установившегося значения при воздейст-

вии на входе прямоугольного импульса тока) переключаемое и составляет 1 мс или 10 мс. На измерительном резисторе 10 ГОм быстродействие 1 мс реализуется только при коррекции частотной характеристики электрометра. Для этого используется каскад У4, содержащий частотно-зависимые цепи. Коррекция осуществляется вне цепи общей отрицательной обратной связи электрометра по методу, изложенному в [4].

С целью ограничения полосы пропускания встроен переключаемый фильтр нижних частот, определяющий быстродействие 1 мс или 10 мс.

Выходной сигнал в виде напряжения на выходе усилителя У6 регистрируется с помощью внешнего осциллографа или вольтметра. Для установку нуля и оценки уровня постоянной составляющей сигнала может быть использован стрелочный индикатор на лицевой панели прибора, подключенный к выходу согласующего усилителя У5.

Особенностью прибора УТ-8003 является возможность измеререния размаха переменного и импульсного токов. На выходе измерителя размаха У7 (рис. 3) с помощью вольтметра постоянного напряжения можно измерять удвоенную амплитуду синусоидального тока или размах периодического несинусоидального (например, импульсного) тока.

Литература

1. Ансо М.Х. Интегратор-дифференциатор с автоматической компенсацией постоянной составляющей входного тока // Измер. техника.- 1985.- No. 8.- С. 51.

2. Ансо М.Х. Согласование быстродействующего измерителя малых токов с объектом измерения // Измер. техника.- 1982.- No. 10.- С. 35-36.

3. Куксов А.Г. Электрометрический усилитель на полевых транзисторах с *p-n* переходом // ПТЭ.- 1987.- No.3.- С. 132-133.

4. Anso, M., Kärner, L., Roos, M., Saks, O. Dynamic qualities of electrometers // J. of Electrostatics.- 1989.- V. 23.- P. 273-282.

FAST PICOAMMETER UT-8003

M. Roos, O. Saks

A b s t r a c t

The paper contains theoretical considerations about a special circuit design of a picoammeter $\pm(10^{-13}...10^{-8})$A with the measurement rate independent of the source and input cable capacitance.

The picoammeter consists of the mainframe and the remote head. The small-size remote head can be connected directly to the signal source. In this way, the noise level decreases due to smaller capacitance at the picoammeter's input.

The picoammeter is equipped with a built-in device for measuring the amplitude values of AC or periodical current pulses. The rise time from 10 % to 90 % (adjustable 1 ms or 10 ms) does not depend on the source capacitance up to 1000 pF.

MEASUREMENT OF DISTURBANCES CAUSED BY THE OPERATION OF THE NEEDLE-CONTACT ON ELECTROMETER INPUT

O. Saks, J. Hämmalov

In the operation of electrometers various commutation elements are needed in their input circuits. Evidently these elements do not essentially decrease the metrological characteristics of electrometers. In high-sensitivity electrometers the needle-contact elements for commutations are preferred for their low-level operational disturbances. In previous research the parasitic charge induced at the electrometer input [1] has been pointed out as the main and perhaps the only source of disturbances. This parasitic charge arising by the opening of the contact is determined by the work function difference between contact surfaces and by the open contact capacity. This circumstance is the main reason for the application of needle-contacts.

For the first time other kinds of disturbances arising in the operation of the needle-contact were reported recently [2]. The disturbances consist in a rise of fluctuational disturbances and of the level of the parasitic current for a certain time after the operation (shutting or opening) of the needle-contact. For a certain time these phenomena decrease the metrological parameters of the electrometer.

Experimental. This paper presents the results of a more detailed investigation of the above disturbances. The possible causes of the disturbances could be the following : the phenomena at contacting surfaces (the spoiling of the adsorption-desorption balance, structural changes), emission of charged particles (electrons) from contacting surfaces, e.g. exoemission of electrons. Our investigations were based on the presumption that the above causes of disturbances would be eliminated (or diminished) by placing the contacting surfaces inside the chamber modelling thus a Faraday cage arrangement. The needle-contact arrangement based on the above mentioned principle is presented in Fig. 1. The arrangement is attached to the input of the electrometer UT-6801 : the body 2 is located upon the guard electrode 3 and the cylinder 7 upon the input electrode 8 of the electrometer. The cylinder 7 has a cavity in its upper end. This cavity can be covered with the circular lid 6 or 12, whereas the lid 6 has

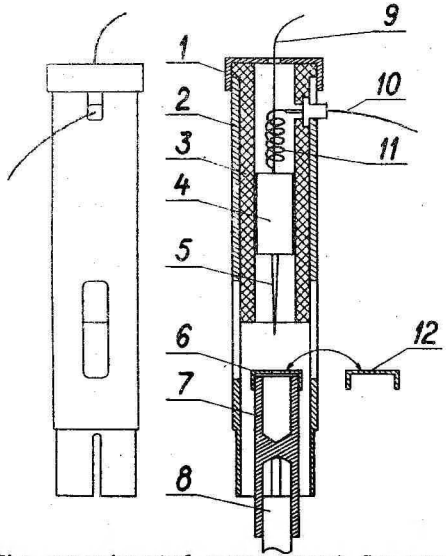

Fig. 1. The experimental arrangement for measurements of the needle-contact disturbances.
1 - the screen-lid; 2 - the body; 3 - the insulating cylinder; 4 - the needle-holder; 5 - the needle; 6 and 12 - the lids; 7 - the cylinder; 8 - the input terminal of the electrometer UT-6801; 9 - the thread for needle--driving; 10 and 11 - the wires for the connection of the needle into the electrometer feedback circuit.

a hole in its center and the lid 12 has no hole. The contact-needle 5 together with the needle-holder 4 are placed inside the insulating cylinder 3 and will be set into upward motion by the thread 9, they move downward due to their weight. The spiral wire 11 and the wire 10 connect the contact-needle into the electrometer feedback circuit.

The cavity in the cylinder 7 covered with the lid 6 models the Faraday cage where the needle 5 moving downward through the hole in the lid 6 makes contact with the electrometer input on the bottom of the cavity. In the other case when the cavity is covered with the lid 12, which does not have a hole in it, the contact between the needle 5 and the electrometer input is obtained on the surface of the lid 12. Thus in this case the Faraday cage model will not be realized and the proposed sources of disturbances will not be removed. In both cases the measurements were carried out.

The results of measurements were registered on a diagram paper of the recorder connected to the electrometer output.

Results and discussion. 1. The cylinder 7 was covered with the lid 6 , the contact occured on the bottom of the cavity.

a) The needle was driven into contact once or many times successively. In the final state the needle remained in the cavity in contact with the electrometer input which means the closed electrometer input. In this case no change was registered at the fluctuational noise level of the electrometer. All the time this noise was at the level of 16 μV (p-p) in the frequency range from $5 \cdot 10^{-4}$ to $5 \cdot 10^{-1}$ Hz.

b) The measurements identical to those in pos. 1, a. In the final state the needle was taken out of the cavity and fixed at a distance of some centimeters above the electrometer input. Thus the electrometer operated in the open input regime or in the so-called current-measuring regime. In this case no change in the fluctuational noise level was registered, either. Naturally the stationary noise level of the electrometer operating in the open input regime was now higher [4] : 31-32 μV (p-p) in the same frequency region.

In the open input regime the electrometers were characterized by a level of parasitic background current. Now after contacting operations a noticeable change in the background current level having a relaxation character was registered. Such a relaxation background current arising after five-fold

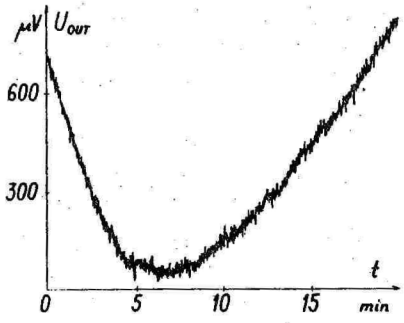

Fig. 2. The change in electrometer output-voltage in its open-input regime after five-fold contacts of the needle-contact inside the Faraday cage.

contacts is depicted in Fig. 2. The run of the curve in Fig. 2 is typical for these measurements. At the same time the value of relaxation current and the position of the curve

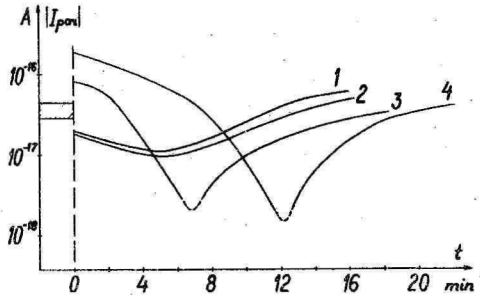

Fig. 3. Absolute values of electrometer parasitic currents resulting from various numbers of contact operations inside the Faraday cage: 1 - one-fold contact; 2 - two-fold contact; 3 - five-fold contact; 4 - 15-fold contact.

minimum on the time coordinate were dependent on the number of contacts made, they both rose with the increasing number of contacts. In Fig. 3 absolute values of generated relaxation current in dependence on time are depicted after the numbers of contacts. Before the measurements the background current level of the electrometer was located in the striped region in Fig. 3. The zero point of time in Fig. 3 coincided with the last contact moment of the needle.

2. The cylinder 7 was covered with the lid 12: the contact occurred on the surface of the lid.

a) The measurements idential to those in pos. 1,a. In the final state the needle remained in contact with the surface of the lid 12.

In this case, differently from the measurements in pos. 1,a, the level of fluctuational noises did not remain unchanged. After the one-fold contact the noise level increased during the first 5-10 minutes up to the level 20-24 μV (p-p) (before the measurements the stationary level was 16 μV (p-p)).

After manyfold contacts the noise level rose up to 32-35 μV (p-p) remaining at this level longer, the number of contacts was larger.

b) The measurements identical to those in pos. 1,b. Here a relaxation parasitic current rose, as in pos. 1,b. But now its time-dependent run was somewhat different. Fig.4 presents the run of measurements with 20 contacts. The difference between the curves in Figs. 2 and 4 appears at the initial moments of time. In Fig. 4 the curve runs through the maximum value repeating afterwards qualitatively the run of the curve in Fig. 2. Consequently the processes involved in the origin of the relaxation current in this case are more complicated than in pos. 1,b. Fig. 5 represents the curves characterising the time-dependence of the absolute level of the

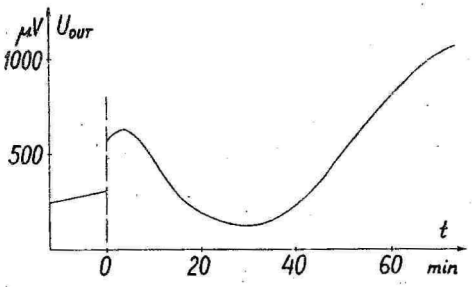

Fig. 4. The electrometer parasitic current run resulting from 20-fold contacts of the needle outside the Faraday cage.

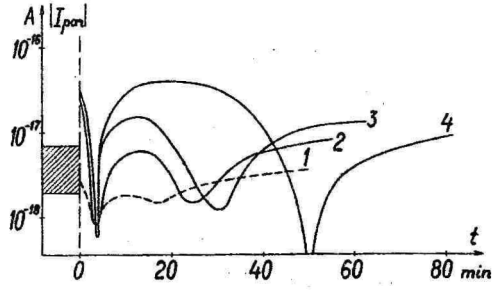

Fig. 5. Absolute values of electrometer parasitic currents resulting in various numbers of contacts outside the Faraday cage: 1 - one-fold contact; 2 - seven-fold contact; 3 - 20-fold contact; 4 - 40-fold contact.

relaxation current after one-fold or manyfold contacts. The striped region in Fig. 5 denotes the background current level of the electrometer before the measurements.

Differently from the measurements in pos. 1,b the fluctuational noise level here rises after contacts. After one-fold contact this level rises up to the level 68-70 μV (*p-p*) and only after 30-35 minutes stabilizes on the previous stationary level (31-32 μV (*p-p*)).

After manyfold contacts the time of increased noise level lengthens, e.g. after 40 contacts it is about 120-140 minutes. In the same case also the maximum noise level increases, but it never exceeds 110-120 μV (*p-p*) (i.e. less than four times above the stationary level).

The results of the measurements lead to the conclusion that by making contact inside the Faraday cage additional fluctuation noise can be eliminated; this does not happen in other cases of contact (cf. also [2]). At the same time it was impossible to get rid of the relaxation parasitic current in this way in spite of its certain variation depending on the measurement conditions.

The manipulations of the needle-contact can cause some distortions in the support-insulator on the electrometer input which in its turn could be the source of some kind of parasitic currents. To be sure that the rise of relaxation current is not connected with various relaxation processes in the insulator the relevant possibilities were thoroughly investigated. For this cylinder 7 (Fig.1), previously from stainless steel, was replaced by an iron one. Then the approach of the permanent magnet to the measuring device (Fig. 1) could be the reason for distoritons in the support--insulator. The measurements gave negative results: no noticeable disturbances occured. Thus the mechanism of the rise of the relaxation parasitic current after our experiments is not clear. Evidently the surface phenomena, e.g. the adsorption of molecules in the case of Faraday cage cannot be used to account for the possible mechanism. Probably the mechanism based on the exoelectron emission can after all occur regardless of the modelling by means of the Faraday cage.

References

1. Сакс О.В., Шуличенко Е.И. О применимости магнитоуправляющих и игольчатых контактов в электрометрических устройствах // Уч. зап. Тарт. ун-та.- 1985.- Вып. 707.- С. 140-148.

2. Хяммалов Ю.А. Помеха, вызванная игольчатым контактом в электрометрах // "Автоматизация электрометрических измерений" - Тез. докл. республ. н.-т. сем.- Тарту.- 1988.- С. 55-56.

3. Кайтса Э.К., Кирсс Ю.Э., Мадисе Т.В., Рээбен В.А., Сакс О.В. Высокочувствительный электрометр типа УТ-6801 с динамическим конденсатором // Тр. ВНИИФТРИ.- 1973.- Вып. 10 (40).- С. 18-26.

4. Хяммалов Ю.А. Об источниках флуктуационных помех динамического электрометра // Уч. зап. Тарт. ун-та.- 1988.- Вып. 824.- С. 153-161.

ИССЛЕДОВАНИЕ ПОМЕХ, ВЫЗВАННЫХ ДЕЙСТВИЕМ ИГОЛЬЧАТОГО КОНТАКТА НА ВХОДЕ ЭЛЕКТРОМЕТРА

О.В. Сакс, Ю.А. Хяммалов

Р е з ю м е

В статье представлены результаты исследования помех от действия коммутационного игольчатого контакта на входе электрометра. Для этого было сконструировано специальное измерительное устройство, конструкция которого приводится.

DEPENDENCE OF SURFACE NOISE ON THE NUMBER OF ADSORBED GAS MOLECULES

J. Hämmalov

Research of the surface work function fluctuations (surface noise) needs the solution of the problem about the dependence of their spectral density on the surface area or on the number of adsorbing molecules. On the one hand it is known that adsorption of gas molecules on the surface induces a change in work function linearly connected with the number of molecules adsorbed on the unit surface area. Then the level of work function fluctuations increases with the number of molecules taking part in adsorption or, in other words, with an increase of the surface area. On the other hand, we have got some relevant experimental data to make a comparison. Fig. 1 presents the spectral densities of surface fluctuations measured by two different methods and on two substantially different surface areas. Into the striped region A in Fig. 1 fall the results of the spectral density measurements taken from [1] carried out with the measuring apparatus described in detail in [2]. The well-known dynamic capacitor method has been used. The surfaces of circular stainless-steel electrodes (diameter 14 mm) of the dynamic capacitor were coated with a thin layer of gold applying the vacuum sputtering method. In these measurements the work function fluctuations caused by the adsorption of air molecules on the gold surface were investigated.

The striped region B in Fig. 1 repeats the results of measurements presented in papers [3, 4]. A field emission microprojector was used as the measuring apparatus. The work function fluctuations were brought on by the adsorption of different gas molecules on a very small surface located at the electrode tip.

Thus the regions A and B in Fig. 1 represent the spectral densities of surface work function fluctuations measured on essentially different surfaces, i.e. essentially different number of gas molecules taking part in the fluctuational process. Certainly the comparison of these results must not be taken as absolute, since experimental conditions of both measurements were essentially different: in one case the adsorption of air molecules on gold surface by normal gas pressures

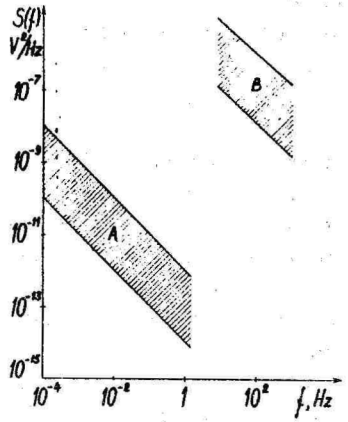

Fig. 1. Results of spectral density measurements of surface work function fluctuations. Region A from [1] and region B from [3, 4].

and in the other case - the adsorption of the rest of the gas molecules in high vacuum conditions were measured.

The other known fundamental fluctuation processes, namely shot noise and thermal noise, are connected with the number of particles taking part in fluctuation processes. In the case of shot noise the spectral density of current fluctuations is given by Shottky's equation:

$$S_i(f) = 2qI_0,$$

where I_0 - the direct current; q - the charge of particles. As $I_0 = qn$, where n is the number of particles flowing in unit time through a unit surface perpendicular to the direction of current, then the relative fluctuations of current can be expressed as

$$\sqrt{S_i(f)}/I_0 = \sqrt{2q/I_0} \sim 1/\sqrt{n}.$$

In the case of thermal noise the spectral density of voltage fluctuations can be expressed by Nyquist relation

$$S_u(f) = 4kTR,$$

where R - the resistance of the measurable object, k - the Boltzmann constant and T - the temperature.

It is known that R in solid state objects depends on the number n of charge carrying particles in the unit volume

$R \sim 1/n$. Then

$$S_u(f) \sim 1/n,$$

the spectral density of voltage thermal fluctuations is inversely proportional to the number of particles taking part in the fluctuation process.

In both cases the probability theory law of great numbers [5] has an effect.

As for $1/f$-fluctuations, the third fundamental kind of fluctuations, the matter is more complicated. It is known that such kind of fluctuations arise in solid state objects, in most thoroughly investigated objects as a result of various structural changes in these objects [6]. The $1/f$--fluctuations are made detectable by a direct current flowing through the object. The structural changes in the object as if modulate the direct current through the object and so these fluctuations are made detectable. In other kind of objects, carrying $1/f$- fluctuations, the problems connected with these fluctuations are not so thoroughly investigated. Therefore it is the main cause for having no universal analytical relation of spectral density function of this kind of fluctuations. Still there is the so-called Hooge's empirical formula [6] that can be used in the case of solid state objects:

$$S_u(f) = \alpha U^2/Nf,$$

where U - the direct voltage on the object, N - the number of charge carriers in the object, α - proportionality factor.

In this formula N is just the number of particles "examining" the object but not the number of particles characterizing the structural changes in the object. The results of measurements by field-emission method, placed into the region B in Fig. 1, present just the current fluctuations modulated by the processes taking place on the surface of the tip. If any structural changes on the surface occur, for example due to adsorption, then it finds its expression in work function changes, which have an effect on the number of emitted electrons from the tip accordingly to the Fowler--Nordheim relation. Therefore the experimental conditions of the capacitor method including the dynamic capacitor method, are essentially different. Here the immediate information about the structural changes on the surface can be obtained

and there is no need for an examination of surfaces by any kind of "searching" particles. In this sense the capacitor method is unique as a rare method allowing such of measurements. Therefore the problem of the number of particles taking part in the fluctuational process can find a simpler explanation as the disturbing "searching" particles are missing.

Also in this case connecting the work function fluctuations with the number of adsorbing-desorbing molecules, we have to start from the version of the law of great numbers, from the central limiting theorem [5]. Besides, the normal distribution of amplitudes of work function fluctuations are to be taken into account indicating the stationarity of adsorption-desorption processes. As we know from earlier publications, e.g. [7], the spectral density of $1/f$-fluctuations is very closely connected with the relaxational time-dependent drift of the work function of the surface. It means that the mean value of amplitudes of work functions changes in time and therefore the conditions of the central limiting theorem are not satisfied. But still after the surface has been for a relatively long time in externally undisturbed conditions the work function drift is sufficiently low, and therefore the amplitude distribution function of fluctuations is nearly normal.

Let us have a surface with the number N adsorption places or $n = W/N$ adsorption places per unit area, where W is the surface overall area. Wishing to determinate the spectral density of the work function fluctuations we must treat the adsorption process a progressing in time. Then, steadily, in every single adsorption place a fluctuational process of the work function occurs. Thus we can characterize the work function fluctuations by a number of spectral density functions in connection with each individual adsorption place: $S_1(f)$, $S_2(f)$,..., $S_N(f)$. Then the spectral density of work function fluctuations of the total surface can be expressed as follows :

$$S(f) = S_1(f) + S_2(f) + \ldots + S_N(f) + Q, \qquad (1)$$

where Q is the function accounting for covariance and having a spectral densities dimensionality. Thus the function Q expresses the mutual influence of fluctuational processes of different adsorption places. Supposing the independence of

adsorption processes at every place which was the approach in our previous papers, e.g. [8], the function Q must be equal to zero ($Q = 0$). So the molecules adsorbing and desorbing on the surface cannot react with one another. Then

$$S(f) = S_1(f) + S_2(f) + \ldots + S_N(f). \qquad (2)$$

As it was said above, in nearly stationary conditions the distribution function of fluctuation amplitudes in every adsorption place is nearly normal. Then according to the central limiting theorem the total amplitude distribution function over the surface is also normal. This treatment corresponds to the measuring process where in all adsorption places the spectral densities have been measured. Then the total spectral density can be expressed by equation (2). If the individual spectral densities are equal $S_1(f) = S_2(f) = \ldots = S_N(f) = S_{eq}(f)$, then

$$S(f) = NS_{eq}(f) = n\bar{W}S_{eq}(f). \qquad (3)$$

The relation (3) shows that the increase in the number of adsorption places or equivalently of the surface area, gives rise to the spectral density of work function fluctuations. But this contradicts to the results of measurements given in Fig. 1.

Consequently, we have to change something in the preconditions. The starting-point of noninfluence of several molecules adsorbing and desorbing on the surface resulting in relations (2),(3) is appropriate to the analysis of the type of fluctuations on the surface [8] and perhaps is not useful in the solution of the problem dealt with in this paper. Really we are dealing with the surfaces having more than one adsorption place and then the work function is an integral characteristic quantity. It then follows that the fluctuations can be characterized only by the spectral density of the work function mean value. The process can be regarded as evolving in time as follows. In every moment the work function mean value of the surface can be measured. In succeeding moments this mean value of work function has different values and we can say that it fluctuates in time. It means in its turn that the spectral density $S(f)$ in equation (2) really presents an energetic characteristic of the mean value of work function fluctuations of the surface. It is equivalent to the statement about the nonequality of function Q ($Q \neq 0$)

to zero. Thus, the adsorbing or desorbing molecules can really be treated as noninfluencing one another, but the fluctuations of work function caused by them cannot any more be treated as noninfluencing quantities. Thus an analytic form of the function Q is to be found, which in its turn cannot be easily resolved.

To find a solution to the problem of the dependence of the spectral density of work function fluctuations on the number of fluctuating molecules, we can proceed from the above-mentioned fact that in stationary conditions the amplitude distribution of work function fluctuations is nearly normal. It means the normal distribution of the mean value of work function fluctuations. In this case an analysis of normal distribution function known in mathematical statistics and used in the theory of measurement errors may be helpful [9]. We may have an amount of n independent quantities having the dispersion δ^2. Furthermore, there can be series consisting of N mentioned independent quantities, it means that every element of the series N contains n independent quantities. We can average mathematically every element of series N and find out the dispersion of these element mean values, denoting it as $\delta_{\overline{N}}{}^2$. Then an analysis of mathematical statistics gives in the case of great values of n and $N(n \longrightarrow \infty$, $N \longrightarrow \infty)$ the normal distribution function :

$$\delta_{\overline{N}}{}^2 = \delta^2/n. \qquad (4)$$

Returning to the problem of surface processes the process may be regarded as follows. At the surface each adsorption place has in every moment of time a certain value of work function which over the total surface fluctuates having the mean value $\overline{\varphi}$ and the dispersion δ^2. In successive moments of time the mean value of the work function of the total surface fluctuates having a dispersion denoted as $\delta^2_{\overline{\varphi}}$. If then the number of adsorption places is relatively great and the fluctuation process is observed during a relatively long time, we can write on the grounds of the relation (4):

$$\delta^2_{\overline{\varphi}} = \delta^2/N, \qquad (5)$$

where N is the number of adsorption places.

It is known that both the dispersion and the spectral density of fluctuations are values characterizing the power of fluctuations and therefore they are closely connected [10].

since the spectral density is a frequency dependent function, it may often be interpreted as a distribution of mean square values $\overline{\Psi}^2$ of the fluctuation amplitudes over a frequency range, it can be taken as the change of mean square value in dependence on frequency :

$$\overline{\Psi}^2 = \int_{f_1}^{f_2} S(f)\mathrm{d}f. \qquad (6)$$

In the case of centered moments the mean square value of fluctuations is equal to the dispersion, $\overline{\Psi}^2 = \delta^2$ [10]. In measurements of the spectral density of the work functions it means an elimination of the mean value $\overline{\varphi}$ of the work function. In such a way the measurements are usually carried out.

On the grounds of relations (5) and (6) the dependence of the spectral density of work function fluctuations on the number of molecules taking part in the fluctuation process can be written as follows:

$$S(f) = S_0(f)/N. \qquad (7)$$

Here $S_0(f)$ expresses the spectral density of fluctuations on the adsorption place in the sense of the concept introduced in earlier publications [7, 8, 11, 12]. Thus on the grounds of relations (5) in [12] and (7) in this paper, the spectral density function $S_N(f)$ for the fluctuating quantity of molecules can be written as follows:

$$S_N(f) = L^2\overline{\Delta N^2}/(fN), \qquad (8)$$

where $L = \sqrt{\dfrac{1}{\ln \tau_b/(\tau_a c)}}$, where τ_a and τ_b are the shortest and the longest life-time of molecules in adsorbed states on the surface accordingly, c is the Euler-Masceroni constant.

The spectral density function $S(f)$ for the fluctuations of the work function using relation (1) in [11] has a form:

$$S_\varphi(f) = L^2\mu^2\overline{\Delta N^2}/(\varepsilon_0^2 fN), \qquad (9)$$

where μ - the dipole moment between the adsorbed molecules and surface atoms, ε_0 - the electric constant.

So we have found the analytic formulas (8) and (9) for the spectral density function, where the number N of adsorption places on the surface under the conditions of sta-

tionarity of processes has been taken into account. Thus the number of adsorption places N is linearly connected with the surface area W, $N = \beta W$ (β denotes the number of adsorbed molecules on the unit surface), the spectral density functions (8) and (9) can be expressed in another way :

$$S_N(f) = L^2\overline{\Delta N^2}/(\beta f W), \tag{10}$$

$$S(f) = L^2\mu^2\overline{\Delta N^2}/(\varepsilon_0{}^2\beta f W). \tag{11}$$

In conclusion it is reasonable to compare the measurement results of regions A and B in Fig. 1 proposing the equality of the quantities L, μ, β and $\overline{\Delta N^2}$ in both cases. Then

$$S_\varphi^B(f)/S_\varphi^A(f) \approx W_A/W_B,$$

where the indexes A and B refer to the previously given quantities in regions A and B .

In both cases the surfaces of electrodes are circular with radii r_A and r_B, where r_A = 7 mm and $r_B \approx$ 1000-2000A [13], then

$$S_\varphi^B(f)/S_\varphi^A(f) \approx r_A{}^2/r_B{}^2 \approx (1 - 5)\cdot 10^9. \tag{12}$$

Fig. 1 presents an interval of $10^8 - 10^{10}$ for the relation $S_\varphi^B(f)/S_\varphi^A(f)$. Thus the evaluation result (12) is in accordance with the measurements given in Fig. 1.

References

1. Исследование шумов динамического конденсатора // Тарт. ун-т. - Отчет по НИР No. ГР 01.85.007872. - Тарту. - 1989.- 103 с.

2. Разработка и исследование вакуумированного входного устройства динамического электрометра // Тарт. ун-т.-Отчет по НИП No. ГР 73070840.- Тарту.- 1976.- 40 с.

3. Kleint Ch., Gasse H.-J. Schrot- und Funkelrauschen bei kalter Elektronen-Emission // Z. Naturforsch.- 1960.- B.15a.- H.1.- S. 89.

4. Kleint Ch. Die Temperaturabhängigkeit des Funkelrauschens bei Feldemission // Chechoslovak. J. Phys.- Sect.B. - 1964.- V. 14.- No. 4.- P. 256-266.

5. Феллер В. Введение в теорию вероятностей и ее приложения. - Т. I.- М., Мир, - 1984.- 528 с.

6. Hooge F.N., Kleinpenning T.G.M., Vandamme L.K.J. Experimental studies on 1/*f* noise // Rep. Progr. Phys.- 1981.- V. 44.- No. 5.- P. 479-532.

7. Хяммалов Ю.А. Исследование влияния поверхностных явлений на дрейф и паразитный ток электрометра // Уч. зап. Тарт. ун-та.- 1987.- Вып. 755.- С. 150-158.

8. Хяммалов Ю.А. Связь 1/*f*-флуктуаций с релаксационным дрейфом на основе адсорбционно-десорбционных процессов // "Флукт. явл. физ. сист." - Тез. докл. V Всесоюзн. конф.- Вильнюс.- 1988.- С. 150-152.

9. Кассандрова О.Н., Лебедев В.В. Обработка результатов наблюдений. - М., Наука, - 1970.- 104 с.

10. Бендат Дж., Пирсол А. Измерение и анализ случайных процессов. - М., Мир, - 1974.- 464 с.

11. Хяммалов Ю.А. О фликкер-шумах адсорбционных процессов на поверхности // Уч. зап. Тарт. ун-та. - 1984. - Вып. 669.- С. 85-93.

12. Хяммалов Ю.А. Исследование адсорбционно-десорбционных помех при электрометрических измерениях и разработка первичных преобразователей с улучшенными метрологическими характеристиками на базе динамического конденсатора.- Автореф. дисс. к.т.н. - Ленинград. - 1989. - 16 с.

13. Swanson L.W., Davis P.R. Work function measurements // Methods of experimental physics.- 1985.- V. 22.- P.1-22.

ЗАВИСИМОСТЬ ПОВЕРХНОСТНОГО ШУМА ОТ ЧИСЛА АДСОРБИРУЕМЫХ НА ПОВЕРХНОСТЬ МОЛЕКУЛ ГАЗА

Ю.А. Хяммалов

Р е з ю м е

При исследовании флуктуационных процессов работы выхода поверхности (поверхностного шума) необходимо установить зависимость их спектральной плотности от числа адсорбируемых на поверхность молекул газа. Установлено, что спектральная плотность флуктуаций работы выхода зависит обратно пропорционально от числа адсорбирующих мест на поверхности.

Tartu Ülikooli toimetised
Vihik 950
METHODS OF STUDY OF ELECTRICAL PROCESSES
IN GASES AND AEROSOLS
Ionization, aerosols, electrometry
Tartu Ülikool
EE2400 Tartu, Ülikooli 18
Vastutav toimetaja T.-E. Parts
8.24.8.75.T.381.300
TÜ trukikoda. EE2400 Tartu, Tiigi 78